REACTIONS OF SILICON WITH SULFATE-BASED OXIDISERS USED IN PYROTECHNIC TIME DELAY COMPOSITIONS

By

Shepherd Masimba Tichapondwa

Thesis submitted in partial fulfilment of the requirements for the degree of

Doctor of Philosophy

In

Chemical Engineering

In the Faculty of Engineering, Built Environment and Information Technology

University of Pretoria

Pretoria

August 2015

DECLARATION

I, **Shepherd Masimba Tichapondwa**, **student No. 29718092**, do hereby declare that this research is my original work and that to the best of my knowledge and belief, it has not been previously in its entirety or in part been submitted and is not currently being submitted either in whole or in part at any university for a degree or diploma, and that all references are acknowledged.

SIGNED on this —————— day of ——————————————2015.

Shepherd M. Tichapondwa

i

REACTIONS OF SILICON WITH SULFATE-BASED OXIDISERS USED IN PYROTECHNIC TIME DELAY COMPOSITIONS

Author: Shepherd Masimba Tichapondwa

Supervisor: Prof. Walter W. Focke

Department: Chemical Engineering

Degree: PhD (Chemical Engineering)

ABSTRACT

Chemical time delay detonators are used to control blasting operations in mines and quarries. Slow-burning Si-BaSO$_4$ pyrotechnic delay compositions are employed for long time delays. However, soluble barium compounds may pose environmental and health risks. Hence it is necessary to consider replacing the barium sulfate with an alternative "green" oxidant that has similar burn properties. Anhydrous calcium sulfate was identified as a suitable, inexpensive alternative "green" oxidant. The initial part of the investigation focused on characterising the burn properties of the Si-CaSO$_4$, as well as proposing a viable reaction mechanism for this composition. Thermochemical calculations indicated that stoichiometry corresponds to a composition that contains ca. 30 wt.% silicon (Si). Combustion was only supported in the range 30–70 wt.% Si. In this range the bomb calorimeter data and burn tests indicate that the reaction rate and energy output decrease with increasing silicon content. The compositions were filled into rigid aluminium elements and assembled into full detonators. Burn rates ranged from 6.9 to 12.5 mm s^{-1}. The reaction product was a complex mixture that contained crystalline phases in addition to an amorphous calcium silicate phase. A reaction mechanism consistent with these observations is proposed.

Slow-burning Si-BaSO$_4$ pyrotechnic delay compositions are employed commercially for intermediate to long time delays. However, there is very little information on this composition available in the open literature. The reactivity of this composition was therefore characterised and compared with that of Si-CaSO$_4$. The Si-BaSO$_4$ composition supported combustion in the range of 20 to 60 wt.% Si in the bomb calorimeter. However, burning was only sustained between 20 and 40 wt.% Si in rigid aluminium tubes. The burn rates varied between 8.4 and 16 mm s^{-1}. These values are comparable to those for the Si-CaSO$_4$ system (6.9–12.5 mm s^{-1}). However, the CaSO$_4$-based formulations tended to have a higher energy output and produced a more pronounced transient pressure response than the barium sulfate compositions.

Both the calcium sulfate- and barium sulfate-based formulations were insensitive to impact, friction and electrostatic discharge stimuli. The reaction products were a complex mixture that contained crystalline phases in addition to an amorphous phase. Although barium sulfate is insoluble in water and decidedly non-toxic, the reaction products produced by the Si-BaSO$_4$ compositions were found to contain water-soluble barium compounds. This ranged from 50 to 140 mg Ba per gram of barium sulfate reacted.

The burn rates of delay compositions used in detonators can be modified by varying a range of parameters in addition to the stoichiometry. With this in mind, the effect of additives and fuel particle size distribution on the burn rate of the silicon-calcium sulfate pyrotechnic delay compositions was investigated. The burn rate decreased with increase in fuel particle size, while the enthalpy remained constant. The addition of fuels to a base composition of 30 wt.% Si-CaSO$_4$ increased the burn rate, with an increase from 12.5 mm s^{-1} to 43 mm s^{-1} being recorded on the addition of 10 wt.% Al. Ternary mixtures of silicon, calcium sulfate and an additional oxidiser generally decreased the burn rate. The exception was bismuth trioxide which increased it. The Si-CaSO$_4$ formulation was found to be sensitive to the presence of inert material as the addition of as little as 1 wt.% of fumed silica stifled combustion in the aluminium tubes.

Keywords: Silicon, Calcium sulfate, Barium sulfate, Pyrotechnics, Time delay, Additives

DEDICATION

Dedicated to

Celine, Danielle, Ethan and Sean

ACKNOWLEDGEMENTS

Last but not least I would like to thank my fellow engineer, researcher and soul mate, Mercy, for holding the fort at home, exercising extreme patience, exchanging ideas and her unending support during the course of these studies.

TABLE OF CONTENTS

LIST OF FIGURES

LIST OF TABLES

LIST OF SCHEMES

ABBREVIATIONS

AH	Calcium sulfate anhydrite
ARM	Arrested reactive mixing
BET	Brunauer-Emmett-Teller
DH	Calcium sulfate dihydrate
DSC	Differential scanning calorimetry
DTA	Differential analysis
ESD	Electrostatic discharge
HH	Calcium sulfate hemihydrate
ICP/ICP-OES	Inductively coupled plasma optical emission spectrometer
IR	Infrared spectroscopy
MCL	Maximum contaminant level
PETN	Pentaerithritol tetranitrate
PSD	Particle size distribution
SEM.	Scanning electron microscopy
SHS	Self-propagating high-temperature synthesis
TG/TGA	Thermogravimetric analysis
TMD	Theoretical maximum density
UN	United Nations
XRD	X-ray diffraction
XRF	X-ray fluorescence

LIST OF SYMBOLS

Theory relating burn rate to the physical properties of the mixture

v burn rate [m s^{-1}]

λ thermal conductivity [Wm^{-1} K^{-1}]

R gas constant [8.314 J mol^{-1} K^{-1}]

T_c maximum temperature of the burning column [K]

E Apparent Arrhenius activation energy [J mol^{-1}]

P density [kg m^{-3}]

ΔH_R heat of reaction [J kg^{-1}]

k rate constant [s^{-1}]

k_o pre-exponential factor [s^{-1}]

$g(n)$ a weak function of the reaction order n. It varies between 1 and 2.

Propagation inequality

ΔH_R heat of reaction [J kg^{-1}]

E Apparent Arrhenius activation energy [J mol^{-1}]

F_{fb} fraction of the energy that will be fed forward [-]

CHAPTER 1   INTRODUCTION

1.1   Introduction

Delay detonators are extensively employed in mining, quarrying and other blasting operations. They are used to facilitate sequential initiation of explosive charges in a pattern of boreholes (Beck and Flanagan, 1992; Aubé, 2011). The timing of the sequential initiation events is carefully chosen in order to control the fragmentation and throw of the rock being blasted. This approach also reduces ground vibration and air blast noise (Beck and Flanagan, 1992; Davitt and Yuill, 1983). Both chemical and electronic time delay detonators are used to achieve the required time delays. The simplicity, ruggedness and low cost of pyrotechnic delays make them particularly attractive for high-volume mining applications.

Pyrotechnic compositions generally consist of one or more oxidisers in combination with one or more fuels (McLain, 1980; Berger, 2005; Danali *et al*., 2010). Pyrotechnic reactions are self-sustaining and are capable of igniting and propagating in the absence of atmospheric oxygen (Ellern, 1968; Kosanke *et al*., 2012). In these reactions the oxidisers may release oxygen to the reducing fuel via lattice destabilisation, melting, sublimation and thermal decomposition (McLain, 1980; Conkling, 1985; Laye and Charsley, 1987). The selection of an oxidiser for a given fuel is dependent on the desired energy output, reaction rate and the physical state of the reaction products (Conkling, 2001). Slow-burning pyrotechnic reactions are usually obtained when the oxidiser releases oxygen at high temperatures and undergoes endothermic decomposition (McLain, 1980; Conkling, 2001). This is exemplified by the oxidizer barium sulfate in slow-burning silicon-based pyrotechnic delay compositions (Stern and Weise, 1966; Davitt and Yuill, 1983; Beck and Flanagan, 1992). Some of the more common oxidisers used in pyrotechnic compositions include oxides and oxy salts of alkali, alkali earth or transition metals. The oxy salts are classified according to relevant anions, i.e. chlorates, perchlorates, nitrates, chromates and sulfates (McLain, 1980; Steinhauser and Klapötke, 2008).

Although the amount of pyrotechnic charge in the majority of initiators is relatively small, there are growing health and safety legislative requirements that the charges should not contain toxic substances (Wilharm *et al*., 2013; Steinhauser and Klapötke, 2008; Cramer, 2012). This is in order to avoid problems during manufacture, to reduce emissions and also to lessen the problem of exposure at the point of end-use (Boberg *et al*., 1997). Some commercial pyrotechnic

compositions contain heavy metal-based or water-soluble oxidisers, e.g. lead, barium and chromate compounds (Wilharm *et al*., 2013; Poret *et al*., 2013). Such compounds are deemed environmentally unfriendly and pose a potential health hazard as they leach into underground water sources (Poret *et al*., 2013). This has led to concerted efforts to find "green" replacements for traditional compositions. The development of stringent legislation towards compliance with green chemistry has influenced the manner in which pyrotechnics development has progressed over the years. The environmental law power curve shown by Cramer (2012) relates well to the manner in which energetic materials have developed over the years. The general progression in the development of energetic materials with time is summarised in Figure 1-1.

Si-Pb_3O_4 and Si-$BaSO_4$ are currently commercially employed for short-time and long-time delays, respectively. Although Si-$BaSO_4$ pyrotechnic delay compositions are extensively used, very little information on this composition and its reaction products is available in the open literature, although patents by Davitt and Yuill (1983), Beck and Flanagan (1992) and Aubé (2011) are available. Rugunanan (1992) carried out an extensive study on silicon-fueled pyrotechnic composition. In his preliminary studies he also considered the Si-$BaSO_4$ composition, but this composition was not evaluated further. Due to their health and environmental effects, both lead and barium-based oxidants have been earmarked for replacement. Despite the fact that barium sulfate is insoluble and relatively non-toxic, some of its potential reaction products are soluble barium compounds that are toxic to humans (Moffett *et al*., 2007). The maximum contaminant level (MCL) of barium in drinking water is 2 mg L^{-1} (WHO, 2004). Acute exposure at levels above this can potentially cause gastrointestinal disturbances and muscular weakness. Long-term exposure results in hypokalemia, which can result in ventricular tachycardia, hypertension and/or hypotension, muscle weakness and paralysis (Jacobs *et al*., 2002).

19th Century ⟹ **20th Century** ⟹ **21st Century**

Ordnance Technology	Flash Powders Explosives Gun ammunition Projectiles	Pyrotechnics initiators Plastic Bonded Explosives High impulse propellants Strategic & Tactical Missiles	Urban Combat Army BCT Navy DDG Destroyer Range Sustainment
Energetic Materials	Mercury Fulminate Lead Azide TNT Nitrocellulose Nitroglycerine	Mg/PTFE AP/Al RDX/TNT RDX/HTPB HMX/NG	AP Replacements Energetic Nanomaterials High-Nitrogen Compounds Reclaimed Materials Solventless Processing

Early Chemistry — *Classical Organic Chemistry*

Brown Chemistry — *Materials Replacement Reduced Waste Reduced Emissions*

Green Chemistry — *New Materials Nanotechnology Biotechnology*

Environmental Impact	Toxic Ingredients Polluting Reactions Batch Process Carcinogenic Solvents Volatile Emissions Hazardous Waste	Toxic Materials replacements Solventless Processing Continuous Processing Risk Assessment Risk Management	Eliminate Toxic Ingredients Renewable Resources Aqueous Solvents Clean Manufacturing

Figure 1-1   Time evolution of energetics chemistry from the 19th century to the 21st century (adopted from Cramer, 2012)

1.2   Aims and Objectives

The aim of the present study was to search for a "green", inexpensive and readily available alternative oxidant to replace barium sulfate in slow-burning silicon-fuelled pyrotechnic delay compositions. The resulting formulation should provide burn rates similar to those of the presently used Si-BaSO$_4$.

After anhydrous calcium sulfate had been identified as a potential candidate to replace barium sulfate, the initial part of the investigation focused on characterising the burn properties of the Si-CaSO$_4$ composition and elucidating its reaction mechanism.

Since very little information on the Si-BaSO$_4$ system is available in the open literature, the second part of the study characterised the reactivity of this composition. McLain (1980) states that the crystal form and crystal defects present in pyrotechnic reagents influence the reactivity of pyrotechnic compositions. Barium sulfate and calcium sulfate both have orthorhombic crystal structures (Caspari, 1936). The reactivity of pyrotechnic compositions utilising an oxy salt oxidiser is known to depend primarily on the nature of the anion (Conkling, 1985).

3

However, the cation potentially also plays a role (Spice and Staveley, 1949). In the present study this was investigated by comparing the performance of Si-CaSO$_4$ with that of Si-BaSO$_4$.

The burn behaviour of pyrotechnic delay compositions is influenced by a wide range of parameters (Kosanke *et al*., 2004; Yoganarasimhan and Josyulu, 2014). Parameters such as the nature of the fuel and the oxidant, the mixture stoichiometry, particle size distributions, the presence of additives and the quality of mixing are regarded as the most important (McLain, 1980). These should be considered when designing a new delay composition. Each of these parameters acts by affecting one or more of the activation energy, heat of reaction or efficiency of energy feedback (Kosanke *et al*., 2004). In order to produce the desired pyrotechnic effects, these variables must be optimised and held constant from batch to batch so as to attain reproducible behaviour. With this in mind, the final part of the study investigated the use of fuel with varying particle sizes and the addition of inert or chemically active additives as a means of modifying the burn rates of Si-CaSO$_4$ pyrotechnic delay compositions.

1.3   Outline of Thesis

The thesis is structured in seven chapters. An outline of each of these chapters is given below.

Chapter 1 gives a brief background to the use of pyrotechnic compositions in mine detonators as a means of imparting time delays. It also explains that some of the compositions that are currently being used commercially have potential environmental and health hazards and are therefore targeted for replacement. The overall aim and objectives of the study are defined.

Chapter 2 presents the literature review of the study. Here a brief history on the use of pyrotechnics as a means of imparting delays in detonator set-ups is explored. This is followed by a general appreciation of the basic terms and principles used in pyrotechnic delay detonators. The conditions necessary for successful ignition and propagation of a composition, together with the factors affecting the burn rates, are discussed. A brief outline of several silicon-based formulations that have been previously studied is given and finally the use of calcium sulfate and barium sulfate as oxidisers in pyrotechnic formulations is reviewed.

Chapter 3 outlines the materials, experimental procedures and methods, as well as the characterisation techniques and specifications used in each of the three main sections of the study.

Chapter 4 presents the results and discussion of the work carried out on characterising and developing the reaction mechanism of the Si-CaSO$_4$ composition. This part of the investigation has been titled "Calcium Sulfate as a Possible Oxidant in 'Green' Silicon-Based Pyrotechnic Time Delay Compositions"**.**

Chapter 5 reports the findings of the characterisation of the Si-BaSO$_4$ composition. It goes on to compare these results with those of the calcium sulfate oxidised composition. The differences in the reactivity of the two formulations are discussed and their sensitivity to friction, impact and electrostatic discharge (ESD) is shown. The potential toxic nature of the reaction products is explained. This part of the investigation has been titled "A Comparative Study of Si-BaSO$_4$ and Si-CaSO$_4$ Pyrotechnic Time Delay Compositions".

Chapter 6 reports the effects of varying silicon fuel particle size and addition of inert or chemically active additives as a means of modifying the burn rates of Si-CaSO$_4$. The chapter is thus presented under the sub-heading "The Effect of Additives on the Burning Rate of the Silicon-Calcium Sulfate Pyrotechnic Delay Compositions".

Chapter 7 presents the overall conclusions of the study together with recommendations for possible future work.

CHAPTER 2   LITERATURE REVIEW

2.1   Introduction

Pyrotechnics is described as the science of using materials capable of undergoing self-contained and self-sustained exothermic chemical reactions in the absence of atmospheric oxygen producing heat, light, gas, smoke, sound or pressure depending on the choice of reactants (McLain, 1980). Pyrotechnic compositions are a subgroup of high-energy chemical compositions. High-energy materials are categorised into three subgroups based on the velocity at which the reaction takes place (Ellern, 1968; Fordham, 2013):

- *High explosives* –detonate at speeds in the km s^{-1} range
- *Propellants* – deflagrate at speeds in the m s^{-1} range
- *Pyrotechnics* – burn in the mm s^{-1} range

Pyrotechnic compositions have numerous uses in both military and civilian applications, such as flares, fireworks, tracers, smokes, gas generators, ignition sources and time delays (Ellern, 1968; McLain, 1980; Danali *et al*., 2010). In time delay applications the compositions are used to impart delays in blasting caps, fuses and initiators of various types, such as squibs, detonators and primers. To generate these effects, most pyrotechnic compositions contain at a minimum one fuel (reducing agent) and one oxidiser that are capable of producing a highly exothermic, self-propagating oxidation–reduction reaction. Complementary ingredients such as binders, burn rate modifiers, colorants and processing aids may also be used (Conkling, 1985; Berger, 2005). The pyrotechnic redox reactions take place in one or a combination of the following reaction states: solid–solid, solid–liquid or solid–gaseous producing solid, liquid and gaseous reaction products (McLain, 1980; Berger, 2005; Kosanke *et al*., 2004).

2.1.1   Delay Detonators

In many explosive applications, such as mining, quarrying and other blasting operations, it is advantageous if the detonators are fired in a predetermined order rather than being fired simultaneously. This sequential timing and initiation of the explosive charges controls the fragmentation and throw of the rock being blasted. This approach also reduces ground vibration and air blast noise (Beck and Flanagan, 1992) and ultimately leads to greater effectiveness of the blast (Ellern, 1968). This effect is achieved by the use of delay detonators which provide a specified delay between actuation of the charge and the final detonation of the main charge.

There are two main classifications of detonators, i.e. *electronic* and *pyrotechnic*. Electronic detonators achieve the desired time delay by use of wiring circuits or a programmed microchip with a timing circuit which is placed within the detonator. Electronic devices are generally more precise and more accurate than chemical pyrotechnic delays but they are considerably more expensive (Rugunanan, 1992; Beck and Flanagan, 1992; Ricco *et al*., 2004). Pyrotechnic detonators, on the other hand, use a pyrotechnic composition packed into a column to provide a time delay. This packed column is known as a *delay element*. Pyrotechnic detonators are generally simpler, more rugged, cheaper and do not require a power source. They also feature a higher degree of inherent safety compared with electronic elements (Kosanke *et al*., 2004; Danali *et al*., 2010).

Delay detonators consist of a metallic shell which is closed at one end and contains the following sequence of material starting from the delivery end: a base charge of a detonating high explosive such as pentaerithritol tetranitrate (PETN), followed by a primer charge of heat-sensitive detonable material such as lead azide or lead styphnate, and then the delay element. The time taken for the composition in the element to burn from one end to the other provides the desired time delay (Davitt and Yuill, 1983; Beck and Flanagan, 1992). The delay composition in the detonator can be ignited by one of the following mechanisms: impact, an electrically heated bridge wire, or by the heat and flame of a low-energy detonating cord or shock tube (Davitt and Yuill, 1983; Beck and Flanagan, 1992). More recently, lasers have been used as a source of ignition in some applications (Trunov *et al*., 2005). Figure 2-1 shows the typical detonator construction.
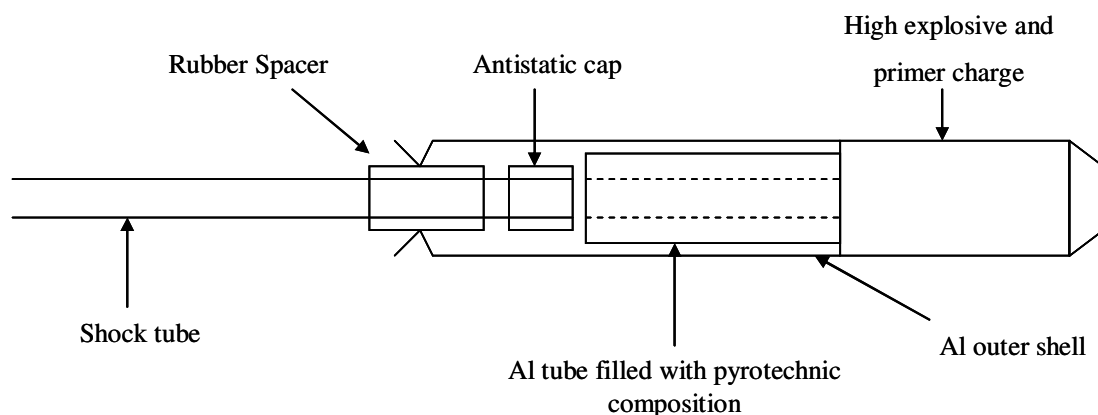
Figure 2-1   Typical detonator construction (Ricco *et al*., 2004)

2.1.2 Delay Compositions

Pyrotechnic compositions used in delay elements generally consist of one or more oxidisers in combination with one or more fuels (McLain, 1980; Berger, 2005; Fordham, 2013). These compositions react as redox reactions where the fuel is oxidised by the oxidiser. The reactions take place in the form of solid–solid, solid–liquid or solid–gaseous reactions producing solid, liquid and gaseous reaction products (McLain, 1980; Berger, 2005; Kosanke *et al*., 2004). Often the reagents used are fine powders of metals or metalloids, together with an oxy-salt or an easily reduced metal oxide powder (Steinhauser and Klapötke, 2008; Fordham, 2013). Table 2-1 shows some of the fuels and oxidisers commonly used in pyrotechnic systems. Ideally, the delay composition reaction should be "gasless", i.e. it should burn without the production of gaseous products. Typically, a composition is regarded as gasless if the volume of gas produced is less than 10 cm^3 g^{-1} (Charsley *et al*., 1980). In time delay applications, gas production is deemed to be a problem as it causes variability in the burn rate of sealed assemblies (McLain, 1980; Kosanke *et al*., 2004).

Table 2-1   Fuels and oxidants commonly used in pyrotechnic mixtures (Rugunanan, 1992)

Fuels	Oxidants
Metals:	
Aluminium	Chlorates
Chromium	Chromates
Iron	Dichromates
Magnesium	Iodates
Manganese	Nitrates
Molybdenum	Oxides
Titanium	Perchlorates
Tungsten	Peroxides
Zirconium	Permanganates
	Sulfates
Non-metals:	
Boron	
Phosphorus	
Carbon	
Selenium	
Silicon	
Sulphur	

8

Black powder was the first form of pyrotechnic time delay to be used as early as the 6th and 7th centuries (McLain, 1980). It consists primarily of charcoal, sulphur and potassium nitrate (KNO_3). Chinese artisans used it to make fuses for fireworks by wrapping the powder in tissue paper. The use of black powder continued as the prime time delay composition throughout World War I and the initial stages of the World War II (McLain, 1980). Up to this point the manufacture of pyrotechnics was an empirical art, and system modification was by trial and error (Yoganarasimhan and Josyulu, 2014). However, the development of modern weaponry, which requires high levels of performance reliability, reproducibility and safety under a wide range of environmental conditions, necessitated a scientifically based approach in the design of pyrotechnics. This approach resulted in the development of a multiplicity of gasless delay compositions. Notable early publications based on this approach were from Spice and Staveley (1949), who developed the $Fe-BaO_2$ and $Fe-K_2Cr_2O_7$ compositions, Dubin (1949), who developed the $Ni–KClO_4$ composition, and McLain and Ruble (1953), who developed a mixture of Pb_3O_4 with Mn and Si. These formulations became the basis for the development of a large number of delay compositions over the past half-century.

The combustion process of a pyrotechnic composition can be used to provide a time interval ranging from a few milliseconds to several minutes between successive mechanical, electric or explosive events, depending on the composition and length of the delay column (Kosanke *et al*., 2004). The speed at which the burning front progresses through the element is influenced by a wide range of factors (Yoganarasimhan and Josyulu, 2014; Kosanke *et al*., 2004). These factors are related to the properties of the composition itself and to other stimuli both internal and external to the system (Kosanke *et al*., 2004). The cumulative effect of these factors results in a measured burn time for a particular column length – the *delay interval* (Kosanke *et al*., 2004).

The relationship between the burn rate of a given element and the numerous parameters that affect burn rate has been subject of study by a number of researchers. Their attempts have resulted in a wide range of models being developed (Khaikin and Merzhanov, 1966; Aldushin and Khaykin, 1975; Boddington *et al*., 1975; Dunmead *et al*., 1989). Khaikin and Merzhanov (1966) proposed the simplest theory relating burn rate to the physical properties of the mixture. The theory assumes physical properties independent of composition and temperature, a thin reaction zone and a gasless exothermic n^{th} order solid-state reaction:

$$\frac{dx}{dt} = k(1-x)^n$$

2-1

The nth order solid-state reaction has an Arrhenius-type temperature dependence for the rate constant:

$$k = k_0 e^{E/RT}$$

2-2

The resulting relationship of the burn velocity to the physical properties of the system is shown in Equation 2-3.

$$v = \sqrt{\frac{\lambda k_o R T_c^2}{\rho E \Delta H_R \, g(n)} \exp(E/RT_c)}$$

2-3

where
v = burn rate (m s^{-1})

λ = thermal conductivity (Wm^{-1} K^{-1})

R = gas constant (8.314 J mol^{-1} K^{-1})

T_c = maximum temperature of the burning column (K)

E = apparent Arrhenius activation energy (J mol^{-1})

ρ = density (kg m^{-3})

ΔH_R = heat of reaction (J kg^{-1})

k = rate constant (s^{-1})

k_o = pre-exponential factor (s^{-1})

$g(n)$ = a weak function of the reaction order n. It varies between 1 and 2.

2.2   Ignition and Propagation of Pyrotechnic Compositions

Kosanke *et al*. (2004) provided a detailed review of the ignition and propagation of pyrotechnic delay elements. They described ignition as the process of stimulating a pyrotechnic composition to release its internal energy. Pickard (2002) defines the ignition temperature as the minimum temperature to which a pyrotechnic composition must be heated in order to induce thermal runaway. To accomplish ignition, external energy has to be supplied. This energy increases the internal energy of the composition until it overcomes the minimum energy barrier (activation energy) and causes the release of the stored chemical energy in the composition (heat of reaction). It should be noted that although the ignition source increases

10

the internal energy, the overall system also experiences thermal loss. In order for effective ignition to occur, the rate of heat generation within the material should exceed the rate at which heat is lost by radiation, convection and conduction to the surroundings. The rate of heat loss depends on the thermal diffusivity of the composition, the degree of packing, the convective heat loss coefficient, the geometry of the detonator and the difference in temperature between the composition and ambient temperature (Kosanke *et al*., 2004). Frank-Kamenetzky (1931), quoted by Merzhanov and Averson (1971), described the conditions necessary for ignition and propagation to occur; these were summarised using the graph shown in Figure 2-2. The diagram shows the relationship between heat generation and heat loss curves and the point where they intersect. At these intersection points the rate of heat generation is equal to the rate of heat loss. Point A corresponds to the low-temperature oxidation of the fuel, while point C represents the equilibrium combustion temperature. At point B the system is unstable and at temperatures slightly lower than T_B, the rate of heat loss exceeds the rate of heat generation, resulting in the cooling of the material to T_A. At temperatures slightly higher than T_B, the exothermic heat generated will exceed the heat loss and the temperature of the composition will increase spontaneously to the steady-state flame temperature T_C. Therefore, T_B defines the lowest temperature at which the composition must be heated for it to ignite spontaneously (Merzhanov and Averson, 1971; Kalombo, 2005).
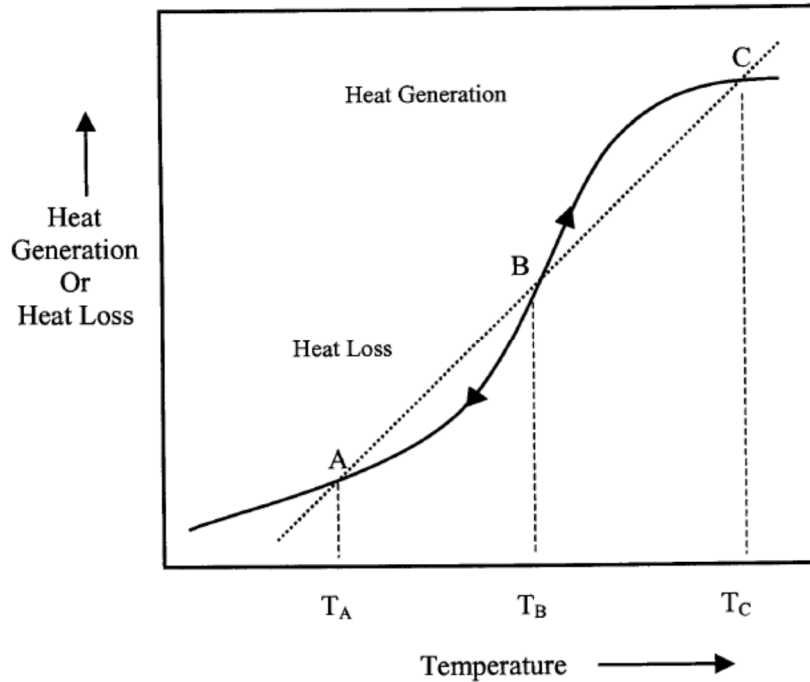
Figure 2-2 Frank-Kamenetzky plot of heat generation and heat loss versus temperature (Merzhanov and Averson, 1971; Kosanke *et al*., 2004; Kalombo, 2005)

Successful ignition of a pyrotechnic composition does not guarantee propagation of the reaction. The application of an external stimulus, such as a flame, typically provides thermal energy to only a small portion of the composition, and the ignition stimulus is usually of relatively short duration. After the application of the stimulus, the pyrotechnic combustion reaction will continue to propagate through the composition only if the pyrotechnic reaction itself provides sufficient energy to the unreacted composition. Figure 2-3 shows a schematic of the propagation of a rod of pyrotechnic composition. Heat is produced by the burning composition (ΔH_R) (reacting material). Some of this heat is lost to the surroundings. However, some fraction of the energy (F_{fb}) will be fed forward from the reacting layer to the pre-reacting layer. The actual amount of energy fed forward is the product of the heat of reaction and the fraction that is fed forward (i.e. $\Delta H_R \cdot F_{fb}$). Propagation will occur if more energy is fed forward than is required for ignition of the pre-reacting disc of the composition. The conditions necessary for propagation can be expressed using the so-called *propagation inequality* (Kosanke *et al*., 2004):

Energy fed forward> Activation energy (E)   **2-4**

Energy fed forward = $\Delta H_R \bullet F_{fb}$ **2-5**

12

Thus propagation inequality is:

$$\Delta H_R \bullet F_{fb} > E_a \qquad\qquad\qquad \textbf{2-6}$$

As long as this relationship holds true, propagation will continue.

The probability of successful propagation can therefore be enhanced by the following:

- Increasing the energy output of the composition
- Decreasing the activation energy
- Increasing the fraction of energy being fed forward to the pre-reacting material
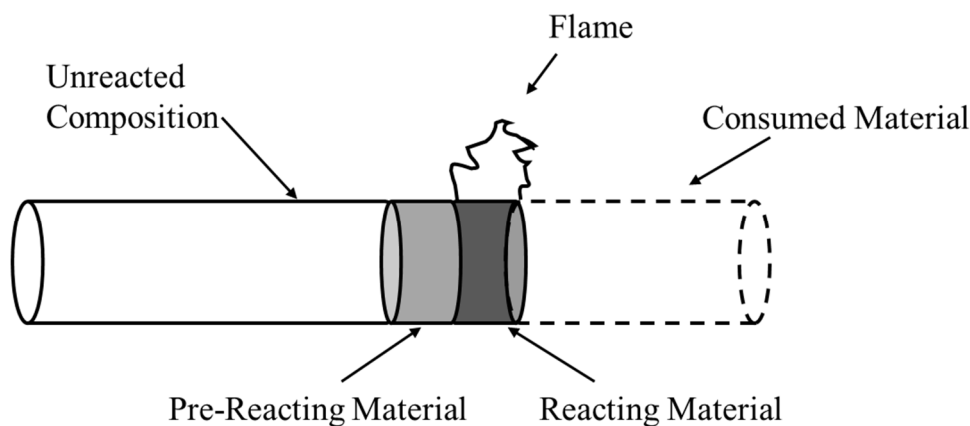
Figure 2-3   Schematic of the propagation of a rod of pyrotechnic composition (Kosanke *et al*., 2004)

2.3   Factors Affecting the Burn Rate

Yoganarasimhan and Josyulu (2014), Kosanke *et al*. (2004) and Berger (2005) have all presented an exhaustive list of the parameters influencing burn behaviour that should be considered when designing a delay composition. They mention around 15 parameters, which is quite a formidable list of parameters for quantification. There is not a single pyrotechnic device for which all the parameters have been fully defined (Kosanke *et al*., 2004). In most cases only qualitative trends have been identified. For each parameter, the change in burn rate is produced by chemical effects, physical effects, or both. In terms of the propagation inequality (Equation 2-6), each parameter will act by affecting one or more of the following: the activation

energy (E_a), the heat of reaction (ΔH_R) or the efficiency of energy feedback (F_{fb}) (Kosanke *et al*., 2004). A brief discussion on some selected factors follows.

2.3.1 Choice of Fuel and Oxidiser

The choice of fuel(s) and oxidiser(s) significantly affects the activation energy, the heat of reaction and the efficiency of energy feedback. Meyerriecks and Kosanke (2003) illustrated the effect of oxidiser type by reporting the variations in heat of reaction and burn rates observed for boron- and zirconium-fuelled compositions reacted with different oxidisers. Berger (2005) showed the variability in energy output and burn rate when boron, titanium and zirconium are coupled with $KClO_4$. The effect of the choice of reactants on the activation energy can be explained in terms of the amount of energy required for an oxidant to make its oxygen available to react with fuel. These oxidisers may release oxygen to the reducing fuel via lattice destabilisation, melting, sublimation and thermal decomposition (McLain, 1980; Conkling, 1985; Laye and Charsley, 1987). Some oxidisers require the input of a large amount of energy, while others actually produce energy in the process of releasing their oxygen. Potassium nitrate, for example, requires energy for it to decompose, while $KClO_3$ produces energy when it decomposes. Therefore, if a similar fuel is used, the KNO_3 composition would have a higher activation energy compared with the $KClO_3$ composition (Shidlovskiy, 1997).

Since burning propagates by re-ignition from layer to layer along the burn path and the efficiency of energy feedback from reacting to unreacted material is influenced by conduction, convection and radiation, the choice of chemicals can affect the efficiency of all three feedback mechanisms. Mixtures prepared from metal fuels have a higher conductivity compared non-metals and thus they have better conductive feedback (Hill *et al*., 1950; Khaikin and Merzhanov, 1966; McLain, 1980; Kosanke *et al*., 2004, Yoganarasimhan and Josyulu, 2014). Gas-producing fuels and oxidisers increase convective energy transfer, while dark-coloured fuels, such as charcoal, can increase the absorption of radiant thermal energy (Kosanke *et al*., 2004).

In summary, if a fast burn rate is desired, a metallic fuel with a high heat output per gram should be selected, together with an oxidiser with a low decomposition temperature. For slow-burning compositions, a fuel with a low heat output per gram should be used, together with

oxidisers with high decomposition temperatures and more endothermic heats of decomposition (Conkling, 1985).

2.3.2 Fuel to Oxidiser Ratio

In any pyrotechnic composition there exists an optimal stoichiometric composition that gives rise to the highest energy output. This often corresponds to the situation where the reaction will be essentially complete, with little fuel or oxidiser remaining after the reaction (Kosanke *et al.*, 2004; Berger, 2005). Deviation from this optimum value leads to reduced energy outputs. In such situations the excess fuel or oxidiser acts as an inert diluent. Although a decrease in energy output is usually accompanied by a decrease in the burn rate, in compositions where metal fuels are used it is not uncommon for the maximum energy output and the highest burn rates to occur at different ratios. This is because metal fuels have a higher thermal conductivity and diffusivity than solid oxidisers (Yen and Wang, 2012). Thus when more metal is added, the efficiency of energy feedback and ultimately the burn rate increase (Ellern, 1968; McLain, 1980; Conkling, 1985). Changes in the fuel to oxidiser ratio can also influence the product spectrum for a given pyrotechnic system. The Si-PbO_2 system was used by McLain (1980) to illustrate this effect and the results are presented in Table 2-2.

Table 2-2 Effect of changes in the fuel to oxidiser ratio on the products obtained for reactions of Si and PbO_2 (McLain, 1980; Kalombo, 2005). The reactions were revised and the Si content corrected.

Si, wt.%	Reactants	Products
2.9	$Si + 4PbO_2$	$Pb_4SiO_6 + O_2$
3.8	$Si + 3PbO_2$	$SiO_2 + 3PbO + 1/2\ O_2$
5.5	$Si + 2PbO_2$	Pb_2SiO_4
7.3	$2Si + 3PbO_2$	$2PbSiO_3 + Pb$
10.5	$Si + PbO_2$	$SiO_2 + Pb$
15.0	$3Si + 2PbO_2$	$SiO_2 + 2SiO + 2Pb$
19.0	$2Si + PbO_2$	$2SiO + Pb$
26.0	$3Si + PbO_2$	$Pb + Si + 2SiO$

2.3.3 Degree of Mixing

The effect of mixing plays a very critical role in the burn rate of pyrotechnic compositions. Since these compositions are primarily mixtures of powders, situations can arise where the entire volume of a poorly mixed pyrotechnic composition may have the optimum fuel to oxidiser ratio, but there will be many small regions where the fuel to oxidiser ratio is far from optimum (Kosanke *et al*., 2004). When burning takes place, the burn rate will be determined by the fuel to oxidiser ratio at each of those small regions rather than by that of the bulk. Poorly mixed compositions will therefore have slower burn rates compared with well-mixed, homogeneous mixtures. Kosanke *et al*. (2004) demonstrated this using black powder which was processed by different methods, resulting in varying degrees of mixing. One sample was dry mixed by passing it several times through a 60-mesh screen and burned at a rate of 0.2 g s^{-1}. For another sample the charcoal and sulphur were dry ball-milled for 4 hours, followed by the addition of the potassium nitrate and wet ball-milled for 8 hours. Finally, the sample was dried and crushed to –100 mesh with a mortar and pestle. This sample had a burn rate of approximately 0.5 g s^{-1}. Several methods of improving the homogeneity of pyrotechnics are currently in use. These include ultrasonics, resonant acoustic mixing, arrested reactive mixing (ARM) and spray drying (Umbrajkar *et al*., 2006; Morgan and Rimmington, 2012; Osorio and Muzzio, 2015).

2.3.4 Effect of Particle Size and Surface Area

The influence of particle size on the reactivity of gas–solid or liquid–solid chemical reactions is well documented (Peacock and Richardson, 2012; Levenspiel, 1999). Similarly, this effect applies to solid–solid reactions in general and pyrotechnic reactions in particular (McLain, 1980; Pantoya and Granier, 2005; Piercey and Klapoetke, 2010). In the case of the burn rate, the general trend is that a decrease in particle size of either the fuel or the oxidiser increases the burn rate (Rugunanan, 1992; Kosanke *et al*., 2004; Ricco *et al*., 2004; Kalombo *et al*., 2007). The particle size effect is brought about by a reduction in the effective activation energy of the system since smaller particles require less energy to be heated to the ignition temperature. Also, as the particle size decreases, the specific surface area increases and the number of contact points between the reactants also increases (Shimizu *et al*., 1990; Brown *et al*., 1998; Valliappan and Puszynski, 2003). The homogeneity of a two-component system also increases as the particle size of at least one of the components decreases (Conkling, 1985; Oh *et al*.,

1998; Dreizin, 2009; Yetter *et al*., 2009). The particle size effect is reported to be more pronounced in the fuel particles rather than the oxidiser (Brown *et al*., 1998; Berger *et al*., 1996; Kosanke *et al*., 2004). This is because most oxidisers melt or decompose at temperatures at or below the ignition temperature of the pyrotechnic composition (Ellern, 1968; Kosanke *et al*., 2004). Berger (2005) reports that the particle size of a reducing agent does not influence the heat of reaction. However, Bernard *et al*. (1980) reported changes in the reaction enthalpy with particle size possibly reflecting the effect of incomplete combustion or variations in the oxide content contributed by the passive surface layer on the fuel particles.

2.3.5   Effect of Additives

The burn rates of a binary system can be modified by conversion to a ternary system through the incorporation of additives (Beck and Brown, 1986; Rugunanan and Brown, 1993a). These additives can be either inert or chemically active. They can function as processing aids, fluxing agents, heat sinks, thermal insulators, sensitisers or catalysts within the main pyrotechnic composition. The presence of additives influences any of the activation energy, heat of reaction or efficiency of energy feedback in a given composition (Kosanke *et al*., 2004). Since burning propagates by re-ignition from layer to layer along the burn path, the thermal diffusivity of the mixture plays a significant role in the burn rate (Hill *et al*., 1950; Khaikin and Merzhanov, 1966). The addition of inert materials may alter the thermal properties of the system, leading to a reduction in the rate of heat transfer through the mix, thus slowing the reaction. McLain (1980) noted that the addition of inert materials with low thermal conductivities, such as kaolin, reduces the burn rate, while thermally conductive fine Cu and Ag powders increase it. Inert material may also act by reducing the contact between fuel and oxidant (Beck and Brown, 1986). Fluxing agents are metals or metal compounds that melt at temperatures lower than the burning temperature of the base composition. The molten phase increases the contact points, resulting in faster burn rates and fewer failures upon ignition (Beck and Brown, 1986; Beck and Flanagan, 1992). Catalysts are sometimes used in pyrotechnic compositions. These act by lowering the decomposition temperature of the oxidiser which in turn lowers the ignition temperature of the composition (Beck and Flanagan, 1992; Kosanke *et al*., 2004). Sensitisers are often added to compositions with a high ignition temperature. These act by reacting before the main reaction and providing heat which then initiates the main reaction (Ilunga *et al*., 2011).

2.3.6   Crystal Effects

Most of the materials used in pyrotechnic compositions are crystalline in nature. The smallest repeat unit or building block of these crystalline materials is referred to as a *unit cell* and the orderly array of points in space with which the atom groups can be associated is called the *crystal lattice* (McLain, 1980; Callister and Rethwisch, 2007). Crystalline solids are generally categorised according to the nature of the chemical bonds that hold the crystals together, i.e. covalent, ionic metallic or intermolecular crystals. The physical properties of solids, such as melting or decomposition temperatures and conductivity, depend greatly on the nature of the crystal bonding forces. The properties of crystals also depend on the specific crystal structure since the same atoms may link together in several different configurations. Crystal structures are characterised by the geometric symmetries of the unit cell repeated throughout the lattice and by the closeness of their packing. The relation between the physical properties of the solid and the chemical and geometric crystal classification is far from exact since crystals are not perfect and contain a variety of crystal defects. Besides altering the physical properties of crystal structures, the presence of defects greatly influences the reactivity (Callister and Rethwisch, 2007). At crystal decomposition temperature, material is first lost at the edges, corners or high-energy grain boundaries.

McLain (1980) states that the crystal form and crystal defects present in pyrotechnic reagents influence the reactivity of pyrotechnic compositions. The oxidisers used in high-energy mixtures are generally ionic solids and the looseness of the ionic lattice is quite important in determining their reactivity (McLain, 1980; Conkling, 1985). A crystalline lattice has vibrational motions that increase in amplitude about their average lattice position with increase in temperature. Tamman (1925), quoted by McLain (1980), and Kosanke *et al.* (2004) used the ratio of the temperature of the solid to its melting temperature as a rough measure of lattice loosening. Ionic surface mobility is said to become effective at a T/T_m ratio of 0.3, while lattice diffusion takes place at ratios of 0.5 (McLain, 1980). These phenomena result in the ignition temperature of solid-solid pyrotechnic reactions occurring well below the melting or decomposition temperatures of the constituent reactants.

Although only a few of the factors affecting the burn rate have been discussed in some detail, a summary of all the parameters affecting the burn rate and their relationship to heat of reaction, activation energy and the efficiency of energy feedback is shown in Table 2-3.

Table 2-3 Factors influencing the burn rate of pyrotechnic reactions and their relations to activation energy (E_a), heat of reaction (ΔH_R) and efficiency of energy feedback (F_{fb}) (Kosanke *et al*., 2004)

Controlling factor	E_a	ΔH_R	F_{fb}
Choice of oxidiser or fuel	X	X	X
Fuel to oxidiser ratio	-	X	-
Degree of mixing	-	X	-
Particle size	X	-	-
Particle shape	X	-	-
Presence of additives	X	X	X
Presence of catalysts	X	-	-
Ambient temperature	X	-	-
Local pressure	-	-	X
Degree of confinement	-	-	X
Physical form	-	-	X
Degree of consolidation	-	-	X
Geometry	-	-	X
Crystal effects	X	-	X
Environmental effects	X	X	X

"X" indicates the major control mechanisms

2.4 Reaction Mechanisms

Besides having a good understanding of the factors that affect the burn rates in delay composition applications, one of the other major requirements in pyrotechnics development is having a good appreciation of the ignition and reaction mechanisms for a given composition (Al-Kazraji and Rees, 1979a; Laye and Charsley, 1987; Brown, 2001). Considerable success in determining the mechanisms of some pyrotechnic compositions has been achieved through the use of thermal analysis techniques (Al-Kazraji and Rees, 1979a; Charsley *et al*., 1980; Laye and Charsley, 1987; Tuukkanen *et al*., 2006; Nakahara, 1961). These include differential thermal analysis (DTA), differential scanning calorimetry (DSC), thermogravimetric analysis (TGA) and bomb calorimetry. Although the conditions under which thermal analysis takes place are controlled and do not accurately depict the high-temperature reactions occurring during the actual reaction, the analyses still give insights into the actual reactions. The controlled conditions allow for the occurrence of phase changes and slow reactions, as well as the escape of the evolved gases (Beardell and Kirshenbaum, 1974; Boddington *et al*., 1982)

and the instruments can detect all these stages. Under conditions that lead to ignition, the ignition temperature can be accurately determined.

Thermal analysis is usually complemented by a variety of phase analysis techniques that aid in identifying the intermediate and final reaction products of a given formulation. These techniques include X-ray diffraction (XRD), X-ray fluorescence (XRF), infrared spectroscopy (IR), and optical and scanning electron microscopy (SEM) (Laye and Charsley, 1987). It should, however, be noted that in pyrotechnics applications, these phase identification techniques have a few drawbacks which one should be aware of when interpreting the results. These include (Tribelhorn, 1995):

- Pyrotechnic reaction products are formed at high temperatures, but can only be examined after cooling. The phases produced at these temperatures during the reaction may not necessarily be present or stable at room temperature. Hence the product spectrum obtained by the analyses might be markedly different from high-temperature phases.
- The rapid cooling that usually takes place immediately after the reaction can result in the solidification of phases that are X-ray amorphous.
- Reaction of product phases with the surrounding atmosphere is difficult to prevent.

2.5   Theoretical Predictions

McLain (1980) pointed out that the number of potential binary fuel–oxidant combinations is of the order of 4 020 and this increases to about 250 000 when ternary combinations are considered. The design and development of new pyrotechnic systems is usually based on specific performance requirements. A new pyrotechnic system must be able to produce a specified effect for a given time within defined spatial constraints. Ensuring that these objectives are met is often difficult, time-consuming and costly, especially when the constraints are new and untried (Barton *et al*., 1982). It is therefore important to be able to "design" a pyrotechnic composition with the minimal experimentation. To aid the designer, the application of computer programs is becoming more popular. These programs are capable of calculating the reaction products and their compositions, together with the thermodynamic properties of pyrotechnic formulations (Conkling, 1985; Webb, 2004). The use of simulations also aids in determining the reaction mechanism for a given composition. The thermodynamic codes generally work on the principle of finding a chemical equilibrium composition from the

20

given reactants by minimisation of Gibbs free energy. A number of pyrotechnics thermodynamics codes have been developed. However, the reliability of the results remains a point of discussion (Webb, 2004). Some of the most common include ICT code, EKVI code, NASA Lewis, Cheetah, HSC and PROPEP (Webb, 2004). According to Webb (2004), most of these thermodynamic models are not suited for pyrotechnic compositions that produce a relatively high proportion of solid species upon combustion. This is because the programs tend to "hang" as they will not be able to converge to a solution for equilibrium. The EKVI code is, however, not prone to this and has fewer problems converging.

2.6 Sensitivity

Although most of the factors highlighted in pyrotechnics research focus on tuning the burn rates for given compositions, one other key aspect in pyrotechnics composition design is the sensitivity of the material to external stimuli. In pyrotechnic compositions *sensitivity* is defined as a measure of a composition's response to mechanical stimuli (impact and friction) and to electrostatic discharge (ESD) (Kosanke *et al*., 2004). Other authors include thermal sensitivity in this definition (Conkling, 1985). Sensitivity is a very important aspect as it has safety implications during the processing, handling, transporting and final application of the composition. McIntyre (1978) and Bayley *et al*. (1992) published surveys on accidents in the USA and UK pyrotechnics industries, respectively. They found that the majority of ignitions were attributed to the application of friction to the materials. Table 2-4 presents a summary of their findings.

Table 2-4   Causal stimuli for accidental ignition of pyrotechnics

Stimulus	Number of ignitions caused by stimulus (%)	
	McIntyre (1978) (USA)	Bayley *et al*. (1992) (UK)
Friction	64	66
Impact	13	6
Electrostatic discharge (ESD)	11	5
Other	12	23

The United Nations (2007) developed a set of regulations and recommendations on the transportation of dangerous goods. In these regulations they consider the impact and friction sensitivity of explosives, propellants and pyrotechnics in ascertaining their safety in

21

transportation. These safety characteristics were evaluated using standard procedures from military standard MIL-STD-1751A (2001) developed by the US Department of Defense.

The sensitivity to an ignition stimulus is said to be influenced mainly by the heat output of the fuel upon oxidation (Conkling, 1985). The sensitivity generally increases as the heat of combustion increases. Hence mixtures containing Mg, Al or charcoal are quite sensitive to thermal and static stimuli. The sensitivity of a composition is also determined by the thermal stability of the oxidiser (Laye and Charsley, 1987). Oxidisers that decompose exothermally tend to be more sensitive than those that require heat to decompose. No simple correlation between ignition temperature, friction, impact or static sensitivity has been proposed (Conkling, 1985).

The general classifications of sensitivity to friction and impact are shown in Table 2-5 (Piercey and Klapoetke, 2010). Electrostatic discharge measurements are carried out in order to make sure that the sensitivity of the material to static discharge is below the static potential developed by the human body (5–20 mJ) (Piercey and Klapoetke, 2010).

Table 2-5   Friction and impact sensitivity classes (Piercey and Klapoetke, 2010)

Stimuli	Experimental sensitivity	Sensitivity class
Friction	>360 N	Insensitive
	80–360 N	Moderately sensitive
	10–80 N	Sensitive
	<10 N	Very sensitive
Impact	>40 J	Insensitive
	35–40 J	Moderately sensitive
	4–35 J	Sensitive
	<4 J	Very sensitive

2.7   Previous Work on Selected Pyrotechnic Compositions

2.7.1   Silicon as a Fuel in Pyrotechnics

Silicon is one of the most widely used fuels in pyrotechnic time delay compositions for blasting applications. It is also used in primer compositions, near-infrared illuminants and smoke formulations (Koch and Clement, 2007). Silicon powders of different grades and particle sizes

22

may be used, with the burn rate being generally controlled by the choice of oxidant. A wide range of binary and ternary silicon-fuelled compositions has been researched and reported in varying degrees of depth in the literature. A summary of some of these compositions is presented in Table 2-6.

Silicon is chemically abundant on the Earth's surface and is found mainly as silica (SiO_2) in the form of quartz or sand. Pure silicon is obtained by the chemical reduction of silane or by the electrolytic decomposition of molten mixtures of K_2SiF_6–LiF–KF or SiO_2–Na_3AlF_6 (Rugunanan, 1992). It can also be obtained by the reduction of SiO_2 with coal (Koch and Clement, 2007). Silicon has a melting point of 1410 °C, and its oxidation in oxygen atmosphere occurs in the temperature range 990–1200 °C with the formation of amorphous silicon dioxide (SiO_2) (Mott, 1993). This exothermic reaction takes place according to Scheme I and has a standard enthalpy of formation of -911 kJmol^{-1}. The rate of silicon oxidation is faster in wet oxygen atmospheres than in dry oxygen atmospheres (Deal and Grove, 1965). In both cases the oxidation kinetics are a function of the partial pressures of H_2O and O_2.

$$Si + O_2 \rightarrow SiO_2 \qquad\qquad \Delta H^o_f = -911 \text{kJ mol}^{-1}$$

Scheme I   Oxidation of silicon in an oxygen atmosphere

Although the reaction of silicon with oxygen is exothermic, its high melting temperature tends to make it more difficult to oxidise compared with other pyrotechnic fuels such Al and Mg (Smit *et al*., 1995). At low temperatures, silicon tends to react sluggishly and this hinders its application in some pyrotechnic compositions (Smit *et al*., 1995). The typical combustion products of silicon in pyrotechnic reactions are silicon dioxide and silicates. These possess high phase-change temperatures, which are ideal media to accomplish heat transfer via conduction and radiation (Koch and Clement, 2007). Under certain conditions at high temperature, gaseous SiO can also form (Ellern, 1968; Smit *et al*., 1995).

Table 2-6 Some binary and ternary silicon-based pyrotechnic compositions reported in the literature

Binary compositions		Ternary compositions	
Composition	**References**	**Composition**	**References**
$Si-Pb_3O_4$	Hale, 1931 Nakahara & Hikita, 1960 Al-Kazraji *et al*., 1980 Moghaddam & Rees, 1981 Hedger, 1983 Jakubko, 1999	$Si-Bi_2O_3-MnO$	Boberg *et al*., 1997
$Si-PbO$	Al-Kazraji & Rees, 1979a Moghaddam & Rees, 1981 Goodfield and Rees, 1985	$Si-Bi_2O_3-SiO_2$	Boberg *et al*., 1997
$Si-PbO_2$	Ripley & Lipscomb, 1968 McLain, 1980 Al-Kazraji, 1982	$Si-Fe_2O_3-Sb_2O_3$	Rugunanan & Brown, 1994
$Si-SnO_2$	Davitt & Yuill, 1983 Goodfield & Rees, 1985	$Si-Fe_2O_3-Pb_3O_4$	Yoganarasimhan & Josyulu, 2014
$Si-KNO_3$	Krishnamohan *et al*., 1982 Rugunanan & Brown, 1994	$Si-BaSO_4-V_2O_5$	Beck & Flanagan, 1992
$Si-Fe_2O_3$	Goldschmidt, 1908 Spector *et al*., 1968	$Si-Sb_6O_{13}$-fumed silica	Kalombo *et al*., 2007
$Si-PbCrO_4$	Hale, 1931 Rugunanan, 1992 Ricco *et al*., 2004	$Si-PbCrO_4-SiO_2$	Ricco *et al*., 2004

Binary compositions		Ternary compositions	
Composition	References	Composition	References
Si-Bi$_2$O$_3$	Boberg *et al*., 1997 Brammer *et al*., 1996 Kalombo *et al*., 2007	Si-Al-Sb$_2$O$_3$	Ricco *et al*., 2004
Si-Sb$_2$O$_3$	Rugunanan, 1992 Rugunanan & Brown, 1993b Rugunanan & Brown, 1994 Ricco *et al*., 2004	Si-CuSb$_2$O$_4$-SiO$_2$	Ricco *et al*., 2004
Si-CuSb$_2$O$_4$	Ricco *et al*., 2004	Si-Bi$_2$O$_3$-B$_2$O$_3$	Kalombo, 2005
Si-Sb$_6$O$_{13}$	Kalombo *et al*., 2007	Si-B-Bi$_2$O$_3$	Kalombo, 2005
Si-BaSO$_4$	Davitt & Yuill, 1983 Beck, 1989 Beck & Flanagan, 1992	Si-Bi$_2$O$_3$-KMnO$_4$	Ricco *et al*., 2004
Si-MnO$_2$	Rugunanan, 1992	Si-BaSO$_4$-Pb$_3$O$_4$	Davitt & Yuill, 1983 Aubé, 2011

2.7.2   Silicon-based Pyrotechnic Delay Compositions

2.7.2.1 Silicon-Lead Oxide Systems

The silicon-lead oxide mixtures i.e. Si-PbO, Si-PbO$_2$ and Si-Pb$_3$O$_4$, are among the most extensively studied pyrotechnic systems. Hale (1931) reported the first use of these compounds in a composition consisting of 14.85 wt.% Si, 84.4 wt.% Pb$_3$O$_4$ and 0.8 wt.% glycerine binder. This composition was used to make fuses for projectiles used at high altitudes. Studies carried out on these systems can be classified as either thermal analysis studies or burn rate studies. The thermal analysis studies aid in establishing the combustion mechanism of the compositions.

Thermal Analysis Studies

Al-Kazraji & Rees (1978, 1979a) and Moghaddam & Rees (1981) carried out differential thermal analysis (DTA) and differential scanning calorimetry (DSC) studies on silicon and lead oxide mixtures.

Si-PbO System

A composition of 30% Si-PbO was analysed using DTA. The composition was initially tested in air with the temperature being raised to 900 °C at 6 °C min^{-1}. This mixture gave rise to two main exothermic peaks. The first peak appeared as a shoulder at 540 °C and then eventually reached a maximum at 590 °C. The second exotherm peaked at 665 °C. The shoulder and two peaks were attributed to the reactions shown in Scheme II:

$$6PbO \; + \; O_2 \; \xrightleftharpoons{350-540 \; ℃} \; 2\,Pb_3O_4$$

$$2Pb_3O_4 + \; Si \; \xrightarrow{590 \; ℃} SiO_2 + 6PbO$$

$$PbO + Si + \; {^1\!/_2}\,O_2(from\;air) \xrightarrow{665 \; ℃} Pb + \; SiO_2$$
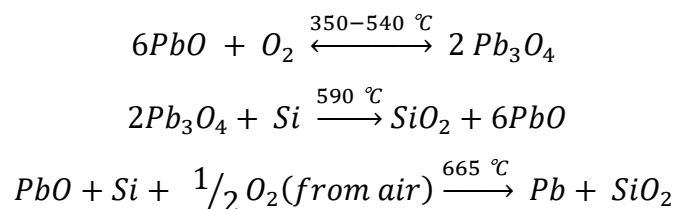
Scheme II   Step-wise thermal decomposition of PbO

The 30% Si-PbO composition is fuel rich and the reactions shown in Scheme II were thought to be surface reactions. However, the second exothermic reaction which took place at higher temperatures favours the movement of reactants so that they penetrate the product layer. When the same composition was run in nitrogen atmosphere, the area under the second peak decreased. This signified that the reaction was less violent due to the absence of atmospheric oxygen.

Moghaddam and Rees (1981) also carried out DSC measurements on the Si-PbO system at compositions ranging between 5 and 50 wt.% Si. Their results showed two exothermic peaks. The first one started at 548 °C and reached a maximum at 637 °C, and then terminated at 667 °C. This temperature also marked the start of the second peak. The maximum of the second peak was 709 °C and it terminated at 726 °C. X-ray analysis was carried out on the products produced at the end of each peak. Unreacted Si and PbO, together with trace amounts of Pb and SiO_2, were detected in the temperature range of the first peak. This peak was thought to

have arisen from the surface reaction of the reactants. The reaction products at the end of the second peak were SiO_2 and Pb only. The peak was thus attributed to the bulk reaction of Si and PbO where the silicon atoms penetrate the PbO crystal lattice.

Si-PbO₂ System

Al-Kazraji (1982) conducted DTA studies on the Si-PbO₂ system. His results showed that PbO₂ in inert nitrogen atmosphere produced five endotherms. The first four were attributed to the step-wise decomposition of PbO₂ which occurs according to Scheme III. The fifth endotherm was observed at 876 °C and was attributed to the melting of PbO. DSC analysis of the Si-PbO₂ composition in a nitrogen atmosphere showed a sharp exotherm at 500 °C which became sharper at high oxidant concentrations. The position of the exotherm represented the ignition temperature of the composition, whilst the increase in the sharpness of the endotherm represented faster more energetic burning as the composition approached stoichiometry.

$$PbO_2 \xrightarrow{435\ ^\circ C} PbO_{1.56} \xrightarrow{465\ ^\circ C} PbO_{1.43} \xrightarrow{495\ ^\circ C} Pb_3O_4 \xrightarrow{573\ ^\circ C} PbO$$
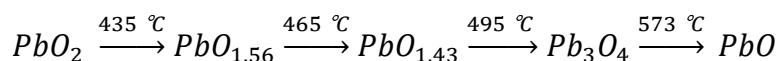
Scheme III   Step-wise thermal decomposition of PbO₂

Pb₃O₄ System

Al-Kazraji and Rees (1978) carried out DTA studies on Pb₃O₄ in air. They reported a response that was characterised by two endothermic peaks at 590 and 868 °C, respectively. The first peak related to the decomposition of Pb₃O₄ to PbO and O₂, while the second peak was associated with the melting of PbO. DTA studies were also carried out on Si-Pb₃O₄ compositions in inert and oxidising atmospheres. The inert nitrogen atmosphere resulted in a response with two exothermic peaks, the first being a shoulder at 540 °C and the second a peak at 590 °C. The second peak coincided with the endothermic decomposition of Pb₃O₄. Thus the peak arises from the simultaneous decomposition of Pb₃O₄ and the oxidation of Si according to Scheme IV.

$$2Pb_3O_4 \xrightarrow{590\ ^\circ C} 6PbO + O_2$$
$$Si + O_2 \rightarrow SiO_2$$
$$Si + 2PbO \rightarrow SiO_2 + 2Pb$$
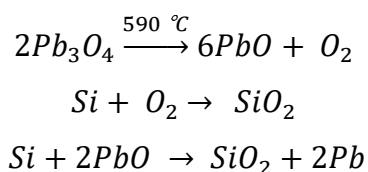
Scheme IV   Reaction mechanism of Si with Pb₃O₄

27

In an oxidising atmosphere three exothermic peaks were observed in the fuel-rich compositions. The first two occurred over temperature ranges similar to those in nitrogen, but the second peak was considerably more energetic. This was because the Pb formed reacts further with atmospheric oxygen to form PbO, which in turn reacts with excess silicon at 665 °C. This reaction produces sufficient heat to raise the temperature for further reaction to take place in the bulk, following diffusion through the reaction products layer. The third exotherm occurred between 755 and 788°C and was present only in the fuel-rich compositions. This peak arose from the reaction between PbO and $PbSiO_2$ through migration of the PbO into the $PbSiO_2$ lattice at its melting point (Mellor, 1924; Al-Kazraji and Rees, 1979b).

Combustion studies

McLain (1980) showed that energy output and the product spectrum of the $Si-PbO_2$ reaction are highly dependent on the fuel to oxidiser ratio (see Table 2-2). The maximum energy output corresponding to the stoichiometric reaction occurred at 10 wt.% Si. This corresponds to the reaction shown in Scheme V:

$$Si + PbO_2 \rightarrow SiO_2 + Pb$$
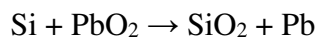
Scheme V   Stoichiometric reaction of the $Si-PbO_2$ composition which results in the maximum energy output

Ripley and Lipscomb (1968) reported mass burn rates of $Si-PbO_2$ compositions that ranged between 2.97 and 5.19 g s^{-1}, with the maximum burn rate recorded at 35 wt.% Si. Burning was sustained for compositions with a silicon content of up to 60 wt.%. Their tests also revealed that the rate of combustion decreased with an increase in the particle size of both fuel and oxidiser. The burn rates were also shown to be dependent on the source of the PbO_2.

The $Si-Pb_3O_4$ composition is fast burning, with burn rates of up to 300 mm s^{-1}. Al-Kazraji and Rees (1979b) studied the heats of reaction and burn rates of this composition. They determined the experimental heats of reaction using bomb calorimetry and compared these values with the theoretical energy outputs that were calculated after having assumed that the overall reaction proceeds according to Scheme VI.

$$2Si + Pb_3O_4 \rightarrow 3Pb + 2SiO_2$$
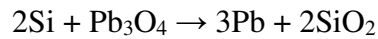
Scheme VI   Stoichiometric reaction of silicon and red lead

The relationship between energy output and composition resulted in a convex-type curve covering a fuel range of 5–50% Si. The maximum of this curve occurred at 10% Si and had a value of 1300 J g^{-1}. Compositions were prepared using silicon powders with average d_{50} particle sizes of 1.9, 3.9 and 5 µm. All three sets of compositions generally had similar energy outputs, although the composition prepared from the 1.9 µm particles had slightly higher outputs in the 20–50% Si region. The shape of the calculated theoretical energy output curve was similar to the experimental results, although the calculated values were higher.

The relationship between burn rate and composition was similar to that of the energy outputs. However, the maximum burn rates occurred at different compositions, depending on the fuel particle size. The composition prepared using fine 1.9 µm silicon had a maximum burn rate of 257.4 mm s^{-1} occurring at 15% Si, while the composition prepared with 5 µm had a maximum combustion rate of 114.8 mm s^{-1} at 30% Si. Hedger (1983) also found that the maximum burn rate occurred at 30% Si; however, he recorded a combustion speed of 300 mm s^{-1}. Furthermore, he studied the effect of fuel surface area on the burn rate and found that an increase in fuel surface area increases the burn rate up to a certain point, after which further increases in surface area have no additional effect.

2.7.2.2 Silicon-Bismuth (III) Oxide (Si-Bi$_2$O$_3$) System

Boberg *et al*. (1997) patented the use of Si-Bi$_2$O$_3$ in slow (3–15 mm s^{-1}) to fast (20–200 mm s^{-1}) delay compositions, depending on the stoichiometry of the composition, as well as the type and amount of additives used. Both Si and Bi$_2$O$_3$ are chemically stable, non-toxic reagents and their reaction takes place with minimal gas evolution, forming stable residue products. Kalombo (2005) and Kalombo *et al*. (2007) also reported on the Si-Bi$_2$O$_3$ delay composition using Bi$_2$O$_3$ synthesised from bismuth subcarbonate (Bi$_2$O$_2$CO$_3$). Compositions were prepared using silicon with specific surface areas of 2.5, 6.3 and 10.1 m^2g^{-1}. Those with the higher surface areas supported combustion in the range 5–40% Si, while the coarser 2.5 m^2g^{-1} composition burnt from 20 to 40%. The maximum burn rate of 150 mm s^{-1} was observed from the composition prepared with the 10.1 m^2g^{-1} surface area silicon at 20% silicon content.

Both Boberg *et al*. (1997) and Kalombo (2005) investigated the effect of additives on the burn rate of the composition. Kalombo (2005) studied the effect of adding varying amounts of boric oxide, boron and potassium permanganate on the burn rate of a 25% Si-Bi_2O_3 composition that initially had a combustion speed of 100 mm s^{-1}. Addition of 7% boric oxide reduced the burn rate to approximately 80 mm s^{-1}, while a similar amount of $KMnO_4$ increased it to 110 mm s^{-1}. Boron fuel decreased the burn rate slightly to 90 mm s^{-1}. Boberg *et al*. (1997) incorporated a number of additives into the Si-Bi_2O_3 composition at different ratios in order to modify the burn rate. Table 2-7 summarises their results.

Table 2-7   Summary of the Si-Bi_2O_3 formulations reported by Boberg *et al*. (1997)

Formulation	Burn rate (mms^{-1})
40% Si – 60% Bi_2O_3	35
3% Si – 97% Bi_2O_3	5
28% Si – 5% Zr – 67% Bi_2O_3	76
30% Si –20% Zr – 50% Bi_2O_3	100
30% Si –20% MnO – 50% Bi_2O_3	20
32% Si –60% Bi_2O_3 – 8% SiO_2	11
3% Si – 10% Zr – 60%Bi_2O_3 – 27% TiO_2	9

2.7.2.3 Silicon-Antimony Trioxide (Si-Sb_2O_3) System

Rugunanan and Brown (1993b, 1994) and Brown *et al*. (1998) carried out comprehensive studies on the Si-Sb_2O_3 system, among others. They examined the thermal behaviour of the individual constituents and of the binary mixtures using TG and DSC analysis. These tests were carried out in nitrogen, air and oxygen atmospheres. DSC analysis on the silicon showed no significant thermal event up to 720 °C. TGA showed the onset of oxidation at around 550 °C in both air and oxygen atmospheres. In a nitrogen atmosphere, mass gain was noted beyond 720 °C. Rugunanan (1992) attributed this reaction to oxidation with trace oxygen rather than nitridation which occurs at temperatures above 1200 °C. Antimony trioxide placed in open crucibles and heated in nitrogen showed 92% mass loss between 500 and 620 °C. This indicated that sublimation takes place before the system reaches its melting temperature of 656 °C. The DSC curve of Sb_2O_3 had three endotherms. The first was a broad endotherm between 300 and 580°C and was due to sublimation. This was followed by one at 624 °C due to crystal transition

30

from the cubic to the orthorhombic structure, and the last endotherm at 681 °C was attributed to the melting of any residual Sb_2O_3. In an air atmosphere, sublimation started at 510 °C, resulting in a mass loss of 63%. The remaining portion was oxidised to Sb_2O_4. Further mass loss occurred at 910 °C, which corresponds to the decomposition of Sb_2O_4.

DSC analysis of a 40% Si-Sb_2O_3 composition yielded an exotherm between 590 and 615 °C with an associated enthalpy change of -0.53 kJ g^{-1} in nitrogen atmosphere. A similar exotherm amounting to an energy output of -0.74 kJ g^{-1} appeared in air between 600 and 680 °C. Both exotherms occurred in the same temperature range as that of Sb_2O_3 sublimation. TG analysis in nitrogen showed that the reaction was not complete, with only 5% Si reacting when open crucibles are used and 20% for the closed ones, as opposed to a theoretically possible 46.5%.

Burning was sustained in the range of 20–50 wt.% Si, with burn rates between 1.6 and 8.7 mm s^{-1} obtained (Rugunanan, 1991; Rugunanan and Brown, 1994). The maximum combustion rate was obtained from the 35% Si composition. Temperature profiles recorded for these compositions showed maximum combustion temperatures in the range 1 056–1301 °C. These temperature profiles were also used to determine the kinetic parameters of the compositions using the Hill (Hill *et al*., 1950) and Leeds (Boddington *et al*., 1975) approaches. An analysis of the reaction products using XRD revealed the presence of Si, Sb_2O_3 and Sb, together with traces of an unidentified crystalline phase that was thought to be antimony silicate. Infrared spectroscopy showed intense SiO_2 absorption peaks. The lack of XRD patterns of SiO_2 means that it was present in the amorphous phase. The main reaction was proposed to proceed according to the Scheme VII.

$$3Si + 2Sb_2O_3 \rightarrow 3SiO_2 + 4Sb$$
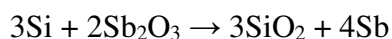
Scheme VII   Stoichiometric reaction of silicon with antimony oxide

The influence of silicon particle size and its specific surface area on the burn rate of a 40% Si-Sb_2O_3 composition was also investigated. Slight increases in burn rates with an increase in surface area were recorded. The addition of varying amounts of inert SiO_2 and Al_2O_3 to the 40% Si-Sb_2O_3 formulation showed decreases in burn rates with increases in the amount added. The burn rate of the standard 40% composition was 8 mm s^{-1} and addition of 5% SiO_2 and Al_2O_3 resulted in burn rates of 4.4 and 6.4 mm s^{-1}, respectively. Ternary compositions prepared

using active Fe_2O_3 oxidiser increased combustion rates to as much as 15.9 mm s^{-1} for a 40% Si-30% Fe_2O_3-30% Sb_2O_3 composition.

Ricco *et al*. (2004) also studied the Si-Sb_2O_3 composition and reported burn rates of 7, 11 and 14 mms^{-1} for compositions containing 25, 30 and 35% Si, respectively. They also investigated the effect of adding SiO_2 and Al to these compositions and found that both additives reduce the burn rate.

2.7.2.4 Compositions with the Same Fuel and Anion but Different Cations on the Oxidiser

The reactivity of pyrotechnic compositions utilising an oxy salt oxidiser depends primarily on the nature of the anion (Conkling and Mocella, 2010). However, the cation potentially also plays a role (Spice and Staveley, 1949; Drennan and Brown, 1992; Rugunanan, 1992). Spice and Staveley (1949) compared the burn rates and energy outputs of compositions of iron in combination with nitrates of Sr, Ba and Pb. Their results showed that the nature of the cation in combination with nitrate anions affected both the burn rates and energy outputs of the compositions. Drennan and Brown (1992) also illustrated similar effects using formulations of manganese mixed with either BaO_2 or SrO_2. The Mn-BaO_2 sustained combustion in the range 15–70 wt.% Mn and recorded a maximum burn rate of 11.7 mm s^{-1} at 20 wt.% Mn. The strontium peroxide oxidised reactions, on the other hand, sustained combustion in the 20–80 wt.% Mn range, with a maximum burn rate of 12.3 mm s^{-1} recorded at 75 wt.% Mn. A summary of some formulations that illustrate this effect is shown in Table 2-8.

Table 2-8 Comparison of compositions of a given reductant with two compounds that have the same oxidising anion coupled to different cations

Formulation	wt.% Fuel	Burn rate (mm s^{-1})	Energy output (kJg^{-1})	Reference
Fe-Sr(NO$_3$)$_2$	60	2.4	1.226	Spice and
Fe-Ba(NO$_3$)$_2$	60	1.6	1.305	Staveley, 1949
Fe-Pb(NO$_3$)$_2$	65	3.9	1.192	
Mn-BaO$_2$	40	6.7	1.42	Drennan and
Mn-SrO$_2$	40	7.5	1.52	Brown, 1992
Si-BaCrO$_4$	30	2.6	_	
Si-PbCrO$_4$	30	13.0	_	Rugunanan,
Si-K$_2$Cr$_2$O$_7$	40	14.2	_	1992
Si-Na$_2$Cr$_2$O$_7$	40	2.9	_	

Ellern (1968) used a commercial delay composition, D16, which consists of PbCrO$_4$, BaCrO$_4$ and Mn to compare the reaction of a given reductant with two compounds that have the same oxidising anion coupled to different cations. The burn rate of the D16 composition was shown to vary when the proportions in the compositions were changed (Table 2-9). An increase in BaCrO$_4$ at the expense of PbCrO$_4$ significantly slowed the burn rate. This was attributed to PbCrO$_4$ being less stable than BaCrO$_4$. The heat of formation of BaCrO$_4$ is 1398 kJmol^{-1} compared with 913 kJmol^{-1} for PbCrO$_4$. Lead chromate also has a lower melting point and undergoes transition at 707 °C, whereas BaCrO$_4$ has no transition (McLain, 1980).

Table 2-9 Burn rates for varying combinations of Mn with BaCrO$_4$ and PbCrO$_4$ (Ellern, 1968)

Mn, wt.%	44	39	37	33
BaCrO$_4$, wt.%	3	14	20	31
PbCrO$_4$, wt.%	53	47	43	36
Burning rate, mm s^{-1}	6.9	4.4	2.9	1.9

2.8   Silicon-Barium Sulfate (Si-BaSO$_4$) Composition

2.8.1   Barium Sulfate Oxidiser

2.8.1.1   Occurrence and Structure

Barium sulfate is found in nature in the form of high-density crystals referred to as barite (heavy spar). This naturally occurring form of barium sulfate is the most commonly used. Synthetically produced barium sulfate produced by precipitation is known as "permanent white" as it is normally used for applications that require very pure white colours. The barium sulfate crystals have orthorhombic unit cells and dipyramidal symmetry. Table 2-10 summarises the crystal properties of barium sulfate.

Table 2-10   Crystal properties of barite

Crystal:	Orthorhombic (2/m 2/m 2/m)
Symmetry:	Dipyramidal
Unit cell data:	
Space group:	Pnma
Dimensions:	A = 8.884(2); b = 5.457(3); c = 7.157(2); Z = 4
Crystal habit:	As crested to rosette-like aggregates of tabular individuals, concretionary, fibrous, nodular, stalactitic; may be banded; granular, earthy, massive

2.8.1.2   Toxicity

Barium sulfate is insoluble in water which makes it effectively non-toxic (Haarmann, 1985). There are also no known carcinogenic effects of barium sulfate exposure (Moffett *et al.*, 2007). It can be administered orally to humans as an X-ray contrast agent for improved imaging. Although barium sulfate is insoluble in water, most barium compounds, such as BaO and Ba(OH)$_2$, are soluble and toxic to humans. The U.S. Department of Health and Human Services, under the Public Health Service Agency for Toxic Substances and Disease Registry, indicate the hazards associated with exposure to various barium compounds (Moffett *et al.*, 2007).

2.8.1.3 Thermal Stability

The thermal decomposition of $BaSO_4$ takes place according to Schemes VIII or IX, depending on the partial pressures of SO_3, SO_2 and O_2 (Stern and Weise, 1966; Holt and Engelkemeir, 1970; Mohazzabi and Searcy, 1976). These authors report the decomposition temperature of the $BaSO_4$ to take place in the range 1125–1400 °C. The enthalpy of decomposition for $BaSO_4$ is 580 kJmol^{-1}.

$$BaSO_4\ (s) \rightarrow BaO\ (s) + SO_2\ (g) + \tfrac{1}{2}\ O_2\ (g)$$
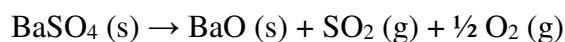
Scheme VIII Thermal decomposition of barium sulfate resulting in BaO (s) with a combination of SO_2 and O_2 as gaseous products

$$BaSO_4\ (s) \rightarrow BaO\ (s) + SO_3\ (g)$$

Scheme IX Thermal decomposition of barium sulfate resulting in BaO (s) with SO_3 as the only gaseous product

Studies by Yanagisawa and Sakai (1983) showed that the presence of V_2O_5 alone or a combination of V_2O_5 and SiO_2 reduces the decomposition temperature of $BaSO_4$ to as low as 700 °C. The V_2O_5 lowers the decomposition temperature primarily because V_2O_5 melts at 600 °C and acts as a flux, which dissolves $BaSO_4$ and yields products shown in the reaction in Scheme X. The mixture of $BaSO_4$ and SiO_2 did not show any appreciable reaction below 1400 °C. However, above this temperature the mixture reacts to form $BaSi_2O_5$ (Yanagisawa and Sakai, 1983).

$$BaSO_4\ (s) + 6\ V_2O_5\ (melt) \rightarrow BaV_{12}O_{30}\ (s) + SO_3\ (g) + \tfrac{1}{2}O_2\ (g)$$

Scheme X Reaction of barium sulfate with molten vanadium pentoxide

2.8.1.4 Reduction Reactions

Barium sulfate is thermally stable at temperatures below its crystal transition temperature of 1149 °C (Beck, 1989). In the presence of carbon or compounds containing carbon, barium sulfate can be reduced to BaS at temperatures as low as 720 °C. This reduction reaction is, however, relatively slow. The addition of small quantities of Na_2CO_3, NaCl or $CaCl_2$ has been reported to accelerate the process (Beck, 1989).

2.8.2   Barium Sulfate as an Oxidiser in Pyrotechnics

Silicon-barium sulfate delay compositions are used commercially to impart intermediate- to long-period delays. Davitt and Yuill (1983), Beck and Flanagan (1992) and Aubé (2011) patented the use of this system in combination with small amounts of Pb_3O_4 or V_2O_5. These worked as reaction-facilitating compounds which aid in reducing the number of misfires. In their patents they claim that the compositions are all non-toxic and have no known carcinogenic effects. This is due largely to the low solubility of $BaSO_4$ in water, as well as the low toxicity of both silicon and barium sulfate. However, not much emphasis was placed on the nature of the reaction products and their impact in terms of solubility and toxicity.

Beck (1989) carried DSC studies which showed that neither silicon nor barium sulfate undergoes transition below 1150 °C. A DSC scan of an intimate mixture of the two gave rise to a strong exothermic reaction at 850 °C. XRD analysis of the combustion products did not show the presence of any crystalline species other than residual silicon and weak reflections attributed to $BaSiS_4$, although this was not confirmed (Beck, 1989). The reaction between Si and $BaSO_4$ was thought to proceed according to any one of the pathways in Scheme XI.

$2\ BaSO_4\ (s) + Si\ (s) \rightarrow 2BaO\ (s) + SiO_2 + 2\ SO_2\ (g)$

$5\ BaSO_4\ (s) + 8Si\ (s) \rightarrow BaSiS_4\ (?) + 4BaO(s) + 7SiO_2(s) + SO_2\ (g)$
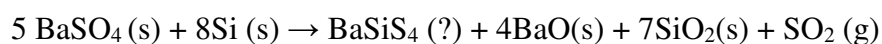
Scheme XI   Proposed reaction pathways for the combustion of silicon mixed with barium sulfate

Beck (1989) also ran a DSC analysis on a 45.5 wt.% Si composition doped with 10 wt.% V_2O_5. This reacted violently, which was attributed to the pre-ignition reaction between molten vanadium pentoxide (melting point 690 °C) and silicon. Temperature profiles of the Si-$BaSO_4$ reaction were also determined and a maximum temperature of 1400 °C was recorded for both the 30 wt.% Si and 45.5 wt.% Si compositions.

Si-$BaSO_4$ compositions were reported to propagate over a range of 30–55 wt.% Si with burn rates of 4–9 mm s^{-1} (Beck, 1989). Davitt and Yuill (1983) reported burn rates of between 3.1 and 7.5 mm s^{-1} for the same fuel range. For a given composition, the burn rate generally increased with an increase in the silicon surface area, with the source of the reactants also contributing to variations in the measured burn rates (Rugunanan, 1992). Impact, friction and

electrostatic discharge sensitivity tests carried out by Davitt and Yuill (1983) showed that the composition was insensitive to all these stimuli.

It was established that although the Si-BaSO$_4$ composition provides long time delays, it is often affected by the heat-sink effect of metal containment of the column of the delay composition (Davitt and Yuill, 1983; Beck and Flanagan, 1992; Aubé, 2011). This results in the quenching of the exothermic reaction before it propagates across the full length of the element. Beck and Flanagan (1992), however, showed that the addition of alkali metal salts such as NaCl, Na$_2$SO$_4$, and oxides such as PbO, Sb$_2$O$_3$, Sb$_2$O$_5$ or V$_2$O$_5$ significantly reduces the number of misfires without significant changes in the burn rate. Vanadium pentoxide in particular was shown to have virtually no influence on the burn rate, with compositions containing 1 and 10 wt.% V$_2$O$_5$ recording similar burn rates. These additives serve as a reaction-facilitating flux that forms a liquid phase at temperatures lower than the burning temperature of the silicon/oxidiser mixture, i.e. ca. 1400 °C in the case of BaSO$_4$. Davitt and Yuill (1983) and Aubé (2011) also patented the use of small amounts of Pb$_3$O$_4$ as the reaction-facilitating reagent in Si-BaSO$_4$ compositions.

2.9 Calcium Sulfate as a Candidate Replacement Oxidiser

2.9.1 Occurrence and Structure

Calcium sulfate occurs in three main forms: calcium sulfate dihydrate (DH) ($CaSO_4.2H_2O$), calcium sulfate hemihydrate (HH) ($CaSO_4.\frac{1}{2}H_2O$), and calcium sulfate anhydrite (AH) ($CaSO_4$). Calcium sulfate dihydrate occurs naturally as mineral gypsum in the following forms: selenite, satin-spar and alabaster. It is also the most common sulfate mineral (Hand, 1997). Calcium sulfate hemihydrate has the mineral name bassanite and is sometimes referred to as "Plaster of Paris". It occurs in two main forms: β-HH and α-HH. These two forms of HH have the same XRD pattern but different DSC characteristics (Caspari, 1936; Yang *et al*., 2009). The β-HH is usually used in the construction industry, while α-HH has applications in areas such as precision instrument moulds, ceramics, industrial arts and architecture due to its superior workability and high strength (Yang *et al*., 2009). Three distinct forms of anhydrous calcium sulfate are believed to be in existence: soluble AH (γ-anhydrite or AH III), insoluble AH (β-anhydrite or AH II), and high-temperature AH (α-AH or AH I) (Hand, 1997; Yang *et al*., 2009). Anhydrites II and III are retained at room temperature, but the soluble anhydrite III rehydrates readily to produce hemihydrate. The β-anhydrite is thermodynamically stable up to 1180 °C and occurs naturally as the mineral anhydrite. It may also be produced by high-temperature ($\approx$600 °C) calcinations of natural or by-product gypsum. Under ambient conditions, β-anhydrite reacts very slowly with water; this is sometimes referred to as "dead burnt gypsum" (Sievert *et al.*, 2005). The conversion of anhydrite II to anhydrite I is displacive and occurs at 1228 °C in air or at 1212 °C in an oxygen/sulphur dioxide atmosphere (Hand, 1997). Upon further heating, anhydrite I either melts or decomposes. Besides the naturally occurring calcium sulfate minerals, $CaSO_4$ is also produced in large quantities as a waste by-product of the chemical and fertiliser industries, and of various pollution-control systems. Table 2-11 summarises the various forms of calcium sulfate. The crystal properties of β-anhydrite/AH II are shown in Table 2-12.

38

Table 2-11 Commonly accepted calcium sulfate dihydrate, hemihydrates and anhydrites (Hand, 1997; Seufert *et al*., 2009)

Name	Formula	Alternative names	Modifications
Calcium sulfate dihydrate	$CaSO_4.2H_2O$	Gypsum	-
Calcium sulfate hemihydrate	$CaSO_4.\frac{1}{2}H_2O$	Plaster of Paris Bassanite Semihydrate	α,β
Anhydrite III	$CaSO_4$	Soluble anhydrite Dehydrated hemihydrate γ-anhydrite	α,β
Anhydrite II	$CaSO_4$	Insoluble anhydrite Dead burnt gypsum β-anhydrite	
Anhydrite I	$CaSO_4$	α-anhydrite	

Table 2-12 Crystal properties of β-anhydrite/AH II

Crystal:	Orthorhombic ($2/m^2/m^2/m$)
Symmetry:	Dipyramidal
Unit cell data:	
Space group:	Amma.
Dimensions:	A = 6.993(2); b = 6.995(2); c = 6.245(1); Z = 4
Crystal habit:	Massive – Fibrous – Distinctly fibrous fine-grained forms, Massive – Granular – Common texture observed in granite and other igneous rock Plumose – "Mica-like" minerals forming aggregates of plume-like forms

2.9.2 Thermal Stability

The thermal decomposition of $CaSO_4$ has been reported by a number of authors (Newman, 1941; Stern and Weise, 1966; Van der Merwe *et al*., 1999). Their TGA results showed that the onset temperature for the decomposition falls in the range 1080 to 1300 °C. Stern and Weise (1966) and Van der Merwe *et al*. (1999) state that, depending on the partial pressures of SO_3, SO_2 and O_2, the thermal decomposition of $CaSO_4$ takes place according to either Schemes XII or XIII.

39

$CaSO_4$ (s) → CaO (s) + SO_2 (g) + ½ O_2 (g)
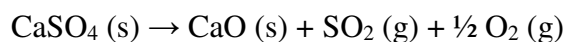
Scheme XII   Thermal decomposition of anhydrous calcium sulfate resulting in CaO (s) with a combination of SO_2 and O_2 as gaseous products

$CaSO_4$ (s) → CaO (s) + SO_3 (g)

Scheme XIII   Thermal decomposition of anhydrous calcium sulfate resulting in CaO (s) and SO_3 as the only gaseous product

2.9.3   Reduction Reactions

A considerable amount of research has been conducted towards understanding the reactions involved in the reductive decomposition of calcium sulfate in the presence of carbon (Mu and Zaremba, 1987; Zheng *et al*., 2013). The chemical reaction of calcium sulfate in the presence of solid carbon occurs according to one of the two mechanisms shown in Schemes XIV or XV. The first type of interpretation is based on a solid–solid reaction mechanism in which the reactions in Scheme XIV take place in an inert environment (Mu and Zaremba, 1987; Van der Merwe *et al*., 1999; Zheng *et al*., 2013).

$CaSO_4 + 2C → CaS + 2CO_2$ (1)

$3CaSO_4 + CaS → 4CaO + 4SO_2$ (2)

———

$2CaSO_4 + C → 2CaO + 2SO_2 + CO_2$ (3)
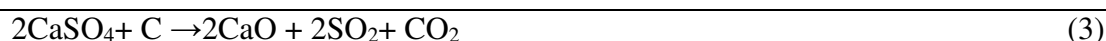
Scheme XIV   Solid–solid reaction mechanism for reduction of calcium sulfate in the presence of carbon

Reaction (1) of Scheme XIV takes place at low temperatures, while an increase in temperature favours reaction (2). The overall reaction is represented in reaction (3). The CaS in reactions (1) and (2) is an intermediate of the two-step reduction. The second mechanism involves gaseous carbon monoxide as an intermediate component. The resulting gas–solid reaction proceeds according to reactions (4) and (5). The overall reaction is shown in reaction (6).

$$2\text{ C} + 2\text{ CO}_2 \rightarrow 4\text{ CO} \tag{4}$$

$$\text{CaSO}_4 + 4\text{CO} \rightarrow \text{CaS} + 4\text{ CO}_2 \tag{5}$$

$$\text{CaSO}_4 + 2\text{ C} \rightarrow \text{CaS} + 2\text{ CO}_2 \tag{6}$$
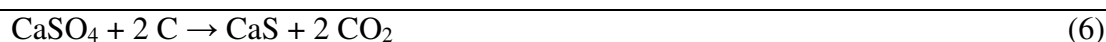
Scheme XV   Mechanism of the reduction of calcium sulfate in the presence of carbon by first forming gaseous carbon monoxide which acts as an intermediate component

2.9.4 $CaSO_4$ as an Oxidiser in Pyrotechnics

Sulfate-based oxidisers are attractive in pyrotechnics applications as their oxygen content compares favourably with that of traditionally used metal chlorates, perchlorates and nitrates. Table 2-13 shows a summary of the amount of oxygen available for various barium and calcium salts.

Table 2-13   Mass fraction of oxygen contained by various pyrotechnic oxidisers and sulfates

	Nitrate	Chlorate	Perchlorate	Sulfate
Barium	0.37	0.32	0.38	0.27
Calcium	0.58	0.46	0.41	0.47

However, one of the major disadvantages of using most sulfate compounds is that they are inherently hygroscopic due to their waters of hydration, therefore rendering them unusable in the real world (Haarmann, 1985). Although the extra oxygen atoms from the waters of hydration increase the total oxygen content, the extra oxygen is not available for productive work in the pyrotechnic reaction. Sulfate-based oxidisers also have fairly high melting and decomposition temperatures. Although this makes their compositions difficult to initiate and sustain a self-propagating reaction, it makes them highly suitable for slow-burning formulations (Haarmann, 1985).

The use of calcium sulfate as an oxidiser in pyrotechnics has been reported in several formulations for various applications. Ellern (1968) reported "white light" composition in

which $CaSO_4 \cdot \frac{1}{2}H_2O$ is used as an oxidiser in place of nitrates (Table 2-14). (White light is the composition of all of the spectrum of visible light.)

Table 2-14   White light compositions with calcium sulfate as oxidiser reported by Ellern (1968)

	Formulation 37	Formulation 38
	Weight %	Weight %
Magnesium/Aluminium alloy	41	-
Magnesium "Griess"	-	40
Sodium nitrate	11	13
Plaster of Paris ($CaSO_4 \cdot \frac{1}{2}H_2O$)	32	40
Water	1	7
Calcium carbonate	15	-

Incendiary mixtures based on thermite reactions of calcium sulfate with aluminium, titanium and magnesium have been reported (Linzell, 1947). These are used to produce heat of sufficient magnitude to melt or soften materials with a high melting point such as steel, stone or refractory materials. The stoichiometric reaction of an Al-$CaSO_4$ composition occurs at 35 wt.% Al and reacts according to Scheme XVI. This reaction had an energy output of 8.1 MJ kg^{-1}. This was much higher than the output of the traditional Al-Fe_2O_3 thermite composition which gives out 3.5 MJ kg^{-1} of heat at stoichiometry.

$$2\,Al + 3CaSO_4 \rightarrow Al_2O_3 + 3CaO + 3SO_2$$

Scheme XVI   Stoichiometric reaction of the Al-$CaSO_4$ composition

The reaction of silicon with calcium sulfate has been reported as a self-propagating high-temperature synthesis method for wollastonite (Gladun and Bashaeva, 1995). Self-propagating high-temperature synthesis (SHS) is a class of redox-type chemical reactions which, once initiated, are sufficiently exothermic to be self-propagating, producing useful products from the reagents, i.e. SHS places the emphasis on the nature of the product formed from pyrotechnic reactions (Subrahmanyam and Vijayakumar, 1992). Pure wollastonite has the chemical

formula $CaSiO_3$ and has three known modifications (α, β, γ). Wollastonite occurs naturally as a common constituent of a thermally metamorphosed impure limestone. In most cases it results from the reaction between calcite and silica, with the loss of carbon dioxide (Scheme XVII).

$CaCO_3 + SiO_2 \rightarrow CaSiO_3 + CO_2$
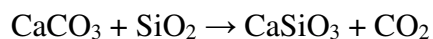
Scheme XVII   Natural wollastonite formation via the reaction of calcite and silica

Wollastonite can also be produced synthetically using high-temperature synthesis at temperatures in the range of 1000–1400 °C. An analysis of possible reactions of high-temperature wollastonite synthesis was reported by Gladun and Bashaeva (1995) (Table 2-15). They showed that a wide range of starting materials can be used to form high-temperature wollastonite. In some cases such as reaction 1, 2, 3 and 9 no gaseous products are formed.

Table 2-15   Possible reactions of high-temperature wollastonite synthesis (Gladun and Bashaeva, 1995)

N	Chemical reaction
1	$2Ca + 2Si + 3O_2 \rightarrow 2CaSiO_3$
2	$CaO + Si + O_2 \rightarrow CaSiO_3$
3	$CaO + SiO_2 \rightarrow CaSiO_3$
4	$CaCO_3 + Si + O_2 \rightarrow CaSiO_3 + CO_2$
5	$CaCO_3 + SiO_2 \rightarrow CaSiO_3 + CO_2$
6	$CaSO_4 + Si + \frac{1}{2}O_2 \rightarrow CaSiO_3 + SO_2$
7	$CaSO_4 + SiO_2 \rightarrow CaSiO_3 + SO_3$
8	$Ca(OH)_2 + Si + O_2 \rightarrow CaSiO_3 + H_2O$
9	$Ca + SiO_2 + \frac{1}{2}O_2 \rightarrow CaSiO_3$

CHAPTER 3   EXPERIMENTAL

3.1   Calcium Sulfate as a Possible Oxidant in "Green" Silicon-based Pyrotechnic Time Delay Compositions

3.1.1   Materials

Ball-milled Type 4 silicon was supplied by Millrox. The d_{50} particle size was 2.1 µm (Mastersizer Hydrosizer 2000) and the specific surface area was 11 m^2g^{-1} (Micrometrics Tristar II BET, N_2 at 77 K). Anhydrous calcium sulfate was supplied by Industrial Analytical. It had a d_{50} particle size of 3.8 µm (Mastersizer Hydrosizer 2000) and a specific surface area of 3.5 m^2g^{-1} (Micrometrics Tristar II BET, N_2 at 77 K). The X-ray diffraction (XRD) analysis of the silicon showed that it was a highly crystalline pure form, while that of the calcium sulfate showed that it was pure β-anhydrite or anhydrite II. This form of calcium sulfate was used in all the tests carried out during the course of this study.

3.1.2   Composition and Delay Element Preparation

The silicon fuel content in the $Si-CaSO_4$ pyrotechnic composition was varied from 20 to 80 wt.%. The powders were mixed by brushing them several times through a 75 µm sieve. The compositions were pressed into 25 mm-long aluminium tubes with an internal diameter of 3.6 mm and a wall thickness of 1.45 mm. The filling process started with two increments of a proprietary $Si-CuBi_2O_4$ starter composition pressed with a 100 kg load. Each increment weighed approximately 0.05 g and the starter accounted for between 5 and 6 mm of the total length of the tube. This was followed by repeated steps of adding two increments of the delay composition and pressing them with the same load until the tube was filled. The densities achieved were 57±3% of the theoretical maximum density (TMD).

3.1.3   Burn Rate Measurements

The burn rates were determined using commercial detonator assemblies. The detonators comprised an initiating shock tube coupled to a rigid aluminium time delay element contained in an aluminium shell. This outer shell contained increments of lead azide primary explosive and pentaerythritol tetranitrate (PETN) as the secondary explosive. The way the actual delay time was determined is illustrated by the scheme in Figure 3-1. The shock tube was ignited by the firing device and the resultant flash was recorded by the photoelectric cell. This signal was

© University of Pretoria

sent to the timer as the initiating signal. After detonation, the pressure transducer sent another signal to the timer which marked the end point of the timing sequence (Ilunga *et al*., 2011).
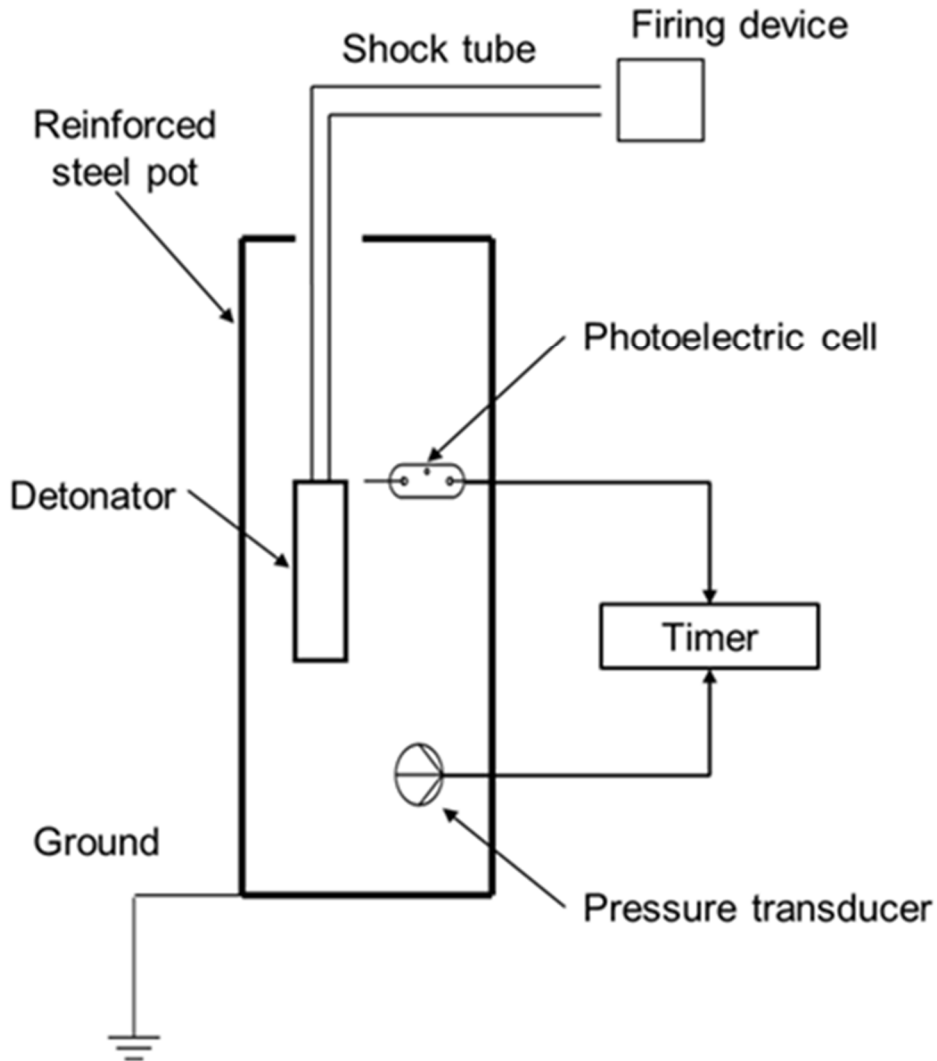
Figure 3-1   Firing and timing schematic used for burn rate measurements

3.1.4   Characterisation

The morphology of the Type 4 silicon and calcium sulfate powders used to prepare the various compositions was obtained using a JEOL JSM 5800 scanning electron microscope (SEM). The samples were coated five times with gold. A SEM auto-coating unit E2500 (Polaron Equipment Ltd) sputter coater was used.

Thermogravimetric analysis (TGA) was performed on a Mettler Toledo A851 TGA/SDTA using the dynamic method. About 15 mg of powder sample was placed in open 70 μL alumina pans. The temperature was scanned from 25 to 1300°C at a rate of 10°C min^{-1}, with nitrogen flowing at a rate of 50 mL min^{-1}. Three runs were carried out for each sample.

Enthalpy measurements were carried out using a Parr 6200 calorimeter utilising a 1104B 240 mL high-strength bomb. Tap-compacted test compositions (2 g) were initiated using 0.2 g of a proprietary Si-CuBi$_2$O$_4$ starter, which was ignited with an electrically heated 30 gauge nichrome wire. The tests were carried out in a 3.0 MPa helium atmosphere. The variation of pressure with time was followed using a National Instruments piezoelectric transducer. A Parr Dynamic Pressure Recording System was used for data collection. The recording frequency was 5 kHz and 30 000 data points were captured per test. Each composition was tested at least three times. The starter composition (0.2 g) was tested on its own and the reported experimental values were corrected for its contribution. Figure 3-2 shows the cross section of the combustion vessel used for the energy and pressure measurements
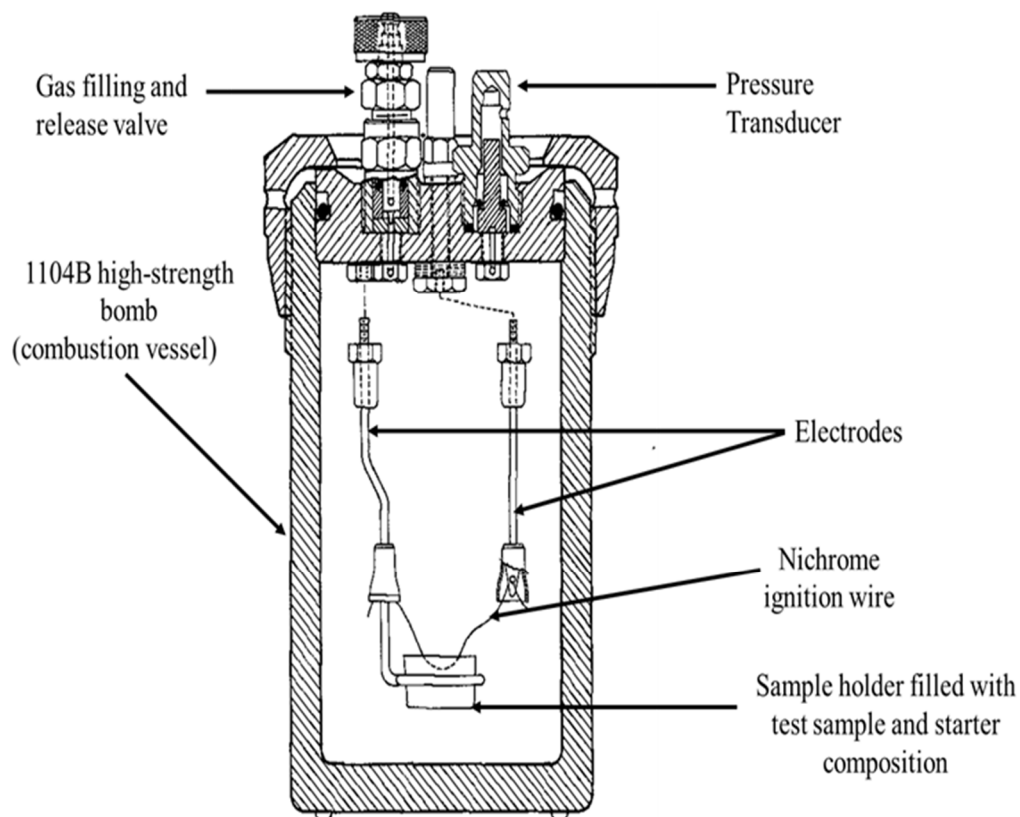
Figure 3-2   Cross sectional representation of the bomb calorimeter combustion vessel

XRD measurements were performed on a Bruker D8 Advance diffractometer with 2.2 kW CuKα radiation (λ=1.54060 nm) fitted with a LynxEye detector with a 3.7º active area. Samples were scanned in reflection mode in the angular range 2° to 70° 2θ at a rate of $0.01°$ s^{-1}. The generator settings were 40 kV and 40 mA. Data processing and analysis were carried out using the Bruker Diffrac^{Plus} EVA evaluation program. Quantitative XRD analyses were performed according to the Rietveld method using Diffrac^{Plus} TOPAS software. The powdered residues were spiked with known proportions of corundum, a highly crystalline material. This made it possible to determine the amorphous content from the recorded diffractograms using the Rietveld method, as discussed by Ward and French (2006).

Single-point sulphur analyses were performed on an Eltra CS 800 double dual-range carbon-sulphur analyser. Samples of the reaction products weighing ca. 0.2 g were milled and sieved to <75 µm. The samples were homogenised by slow rotation in a ceramic crucible with iron and tungsten chips. The instrument was calibrated using the Euronorm-CRM 484-1 Whiteheart malleable iron, Euronorm-CRM 058-2 sulphur steel and Euronorm-CRM 086-1 carbon steel standards. The instrument stability was monitored using the Council for Geoscience laboratory in-house soil reference standards. The sulphur detection limit was 0.009 wt.%.

3.2   A Comparative Study of Si-BaSO$_4$ and Si-CaSO$_4$ Pyrotechnic Time Delay Compositions

3.2.1   Materials

The properties of the materials used to prepare the different compositions are shown in Table 3-1. XRD analysis confirmed that all the raw materials were of high purity. The surface area was measured with a Micrometrics Tristar II BET. Laser diffraction particle sizing was performed with a Mastersizer Hydrosizer 2000 instrument using water as the dispersion medium.

Table 3-1 Standard enthalpy of formation (ΔH_f°), volume-based median particle size (D_{50}) and BET surface areas of the raw materials used

	Supplier (Grade)	ΔH_f° (kJ mol^{-1})	D_{50} (µm)	BET (m^2 g^{-1})
Barium sulfate	Sachtleben (Blank Fixe N)	- 1465	4.3	0.82
Calcium sulfate	Alfa Aesar	- 1433	4.1	3.8
Silicon	Millrox (Type 4)	-	1.9	11.0

3.2.2   Composition and Delay Element Preparation

The silicon fuel and $BaSO_4$ or $CaSO_4$ oxidants powders were mixed by brushing them several times through a 75 µm sieve. The compositions were pressed into 25 mm long aluminium tubes with an internal diameter of 3.6 mm and a wall thickness of 1.45 mm. The filling process started with two increments of a proprietary starter composition pressed with a 100 kg load. This was followed by repeated steps of adding two increments of the delay composition and pressing it with the same load until the tube was filled. The densities achieved were 57±3 % of the theoretical maximum density (TMD).

3.2.3   Burn Rate Measurements

The burn rates were determined using commercial detonator assemblies. The measurement method used was similar to the one outlined in section 3.1.2.

3.2.4   Determination of the Amount of Dissolved Barium

Approximately 2 g of solid reaction products obtained after combusting various Si-$BaSO_4$ compositions in inert helium atmosphere in the bomb calorimeter were contacted with 10 mL of de-ionised water. The mixture was agitated using an orbital shaker for 1 month and then filtered. The resultant solution was analysed for the barium using inductively coupled plasma optical emission spectroscopy (ICP-OES). Two grams of barium sulfate was also contacted with 10 mL of de-ionised water and the solution tested.

3.2.5   Characterisation

The SEM, TGA, enthalpy and pressure measurements, XRD analysis and single-point sulphur analysis were carried out using the same equipment and conditions as those described in **Section 3.1.4**.

A SPECTRO ARCOS ICP-OES was used to establish the amount of dissolved barium after the solid residue obtained from the combustion of Si-BaSO$_4$ compositions had been contacted with water. Calibration with a barium standard (ICP grade) was carried out before the leached samples were run. Each sample was measured three times and the average ICP value was recorded.

Sensitivity testing was performed on 30 wt.% silicon compositions using the standard procedures described in military standard MIL-STD-1751A (2001) developed by the US Department of Defense. The impact and friction sensitivities were determined with an OZM Research BFH-10 BAM fall hammer impact sensitivity tester and an OZM Research FSKM 50-20K BAM friction tester, respectively. An OZM Research ESD 2008A small-scale electrostatic spark sensitivity tester was used for electrostatic discharge (ESD) sensitivity. The nominal ignition thresholds were determined using the Bruceton 50% method as described in MIL-STD-1751A (2001).

3.3   The Effect of Additives on the Burn Rate of the Silicon-Calcium Sulfate Pyrotechnic Delay Compositions

3.3.1   Materials

Table 3-2 shows the median volume-based particle size and the Brunauer, Emmett and Teller (BET) surface area of the material used to determine the effect of fuel particle size and use of additives on a base Si-CaSO$_4$ composition. These properties were determined using a Mastersizer Hydrosizer 2000 and a Micrometrics Tristar II BET machine, respectively. XRD analysis was carried out on all the raw materials used in the experiments and they were confirmed to be of high purity.

Table 3-2   Volume-based median particle size (d_{50}) and BET surface area properties of the materials used to prepare a variety of compositions

Reagents		Particle size d_{50}, (μm)	BET surface area (m^2g^{-1})
Base reagents			
Silicon Type 2	(Si)	15.8	4.0
Silicon Type 3		5.0	10.5
Silicon Type 4		1.9	11.0
Calcium sulfate	($CaSO_4$)	4.1	3.5
Fuel		**25% Si + 5% Fuel + 70% CaSO₄**	
Aluminium	(Al)	10.2	0.14
Manganese	(Mn)	23.4	0.27
Boron	(B)	2.1	6.65
Tungsten	(W)	6.3	0.19
Sulphur	(S)	-	4.24
Carbon	(C)	10.8	76.0
Oxidisers		**30% Si + 5% Oxidiser + 65% CaSO₄**	
Vanadium pentoxide	(V_2O_5)	101.0	5.52
Bismuth trioxide	(Bi_2O_3)	8.8	0.78
Antimony trioxide	(Sb_2O_3)	0.9	2.42
Copper antimonite	($CuSb_2O_4$)	9.3	1.10
Copper(II) oxide	(CuO)	12.7	1.61
Manganese dioxide	(MnO_2)	8.3	13.57
Inert		**30% Si + 70% CaSO₄ + 5% Inert**	
Silica		9.7	1.26
Fumed silica		-	-
Attapulgite		9.7	72.9
Wollastonite		115	0.11

50

Reagents	Particle size d_{50}, (µm)	BET surface area (m^2g^{-1})
Vermiculite	10.7	15.8

3.3.2 Composition and Delay Element Preparation

Compositions of silicon and calcium sulfate were prepared in the fuel range of 30 to 70 wt.%, using three different silicon powders of varying particle size. Further Si-CaSO$_4$ compositions were prepared by addition of additives. Table 3-2 lists the additive materials used in the initial part of the investigation. Here 5 wt.% of additive was either substituted or added to a base composition of 30 wt.% Si. Type 4 silicon was used in these compositions. Based on the results obtained from the initial 5 wt.% additive tests, selected additives were used to prepare compositions containing 1, 2, 5, 7.5 and 10 wt.% additive concentrations. Another set of compositions was also prepared in which 5 wt.% of Si was substituted with an equivalent amount of aluminium for compositions in the fuel range of 30 to 70 wt.%. All these powders were mixed by brushing them several times through a 75 µm sieve.

The compositions were pressed into 25 mm-long aluminium tubes with an internal diameter of 3.6 mm and a wall thickness of 1.45 mm. The filling process started with two increments of a proprietary starter composition pressed with a 100 kg load. This was followed by repeated steps of adding two increments of the delay composition and pressing them with the same load until the tube was filled. The densities achieved were 57±8% of the TMD.

3.3.3 Burn Rate Measurements

The burn rates were determined using commercial detonator assemblies. The measurement method used was similar to the one outlined in **Section 3.1.2.**

3.3.4 Characterisation

TGA for the silicon powders with different particle sizes was performed on a Mettler Toledo A851 TGA/SDTA using the dynamic method. About 15 mg of powder sample was placed in open 70 µL alumina pans. The temperature was scanned from 25 to 1300°C at a rate of 10 °C min^{-1} with nitrogen flowing at a rate of 50 mL min^{-1}. Three runs were carried out for each sample.

The enthalpy and pressure measurements were carried out using the same equipment and conditions as those described in **Section 3.1.4.**

3.4 EKVI Combustion Modelling

All EKVI simulations were carried out using constraints that mimicked the conditions described in the bomb calorimetry experiments. These include a volume of 240 mL filled with helium at 30 bar pressure. The program was set to determine the maximum adiabatic temperature achieved by the reaction. The reaction products were not predetermined; rather, the simulation was set so that it automatically selects the products that best fit the thermodynamic conditions present for each of the individual systems.

CHAPTER 4   RESULTS: CALCIUM SULFATE AS A POSSIBLE OXIDANT IN "GREEN" SILICON-BASED PYROTECHNIC TIME DELAY COMPOSITIONS

4.1   Characterisation of Reactants

Figure 4-1 and Table 4-1 report the particle size distribution (PSD) of the silicon and calcium sulfate used in this part of the investigation. Figure 4-2 shows SEM images of these reactants.
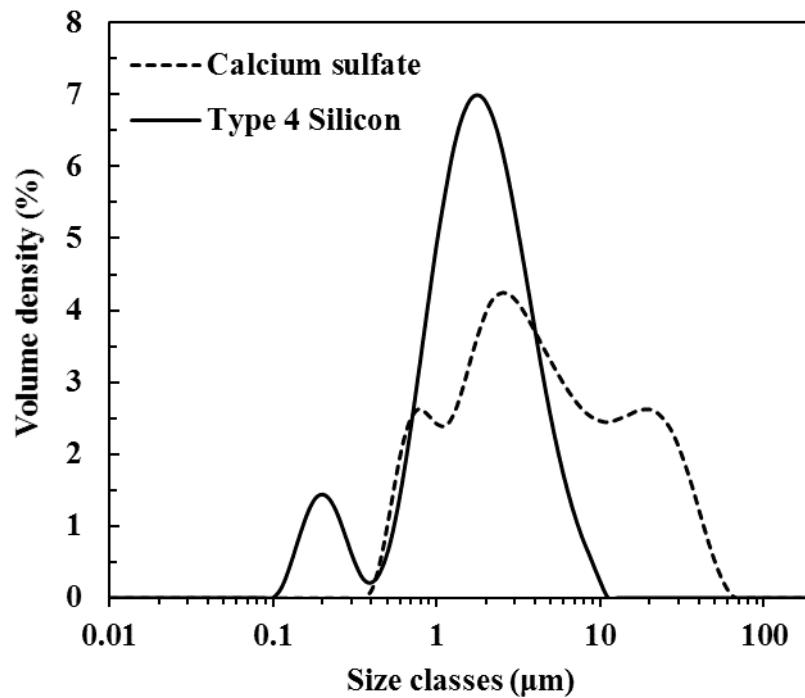
Figure 4-1   Particle size distribution of the Type 4 silicon and calcium sulfate used in this investigation

Table 4-1   Volume-based particle size distribution and BET surface areas of the raw materials used

	D_{10} (µm)	D_{50} (µm)	D_{90} (µm)	BET ($m^2\ g^{-1}$)
Type 4 Silicon	0.61	1.85	4.58	11.03
Calcium sulfate	0.91	4.05	25.3	3.78

53
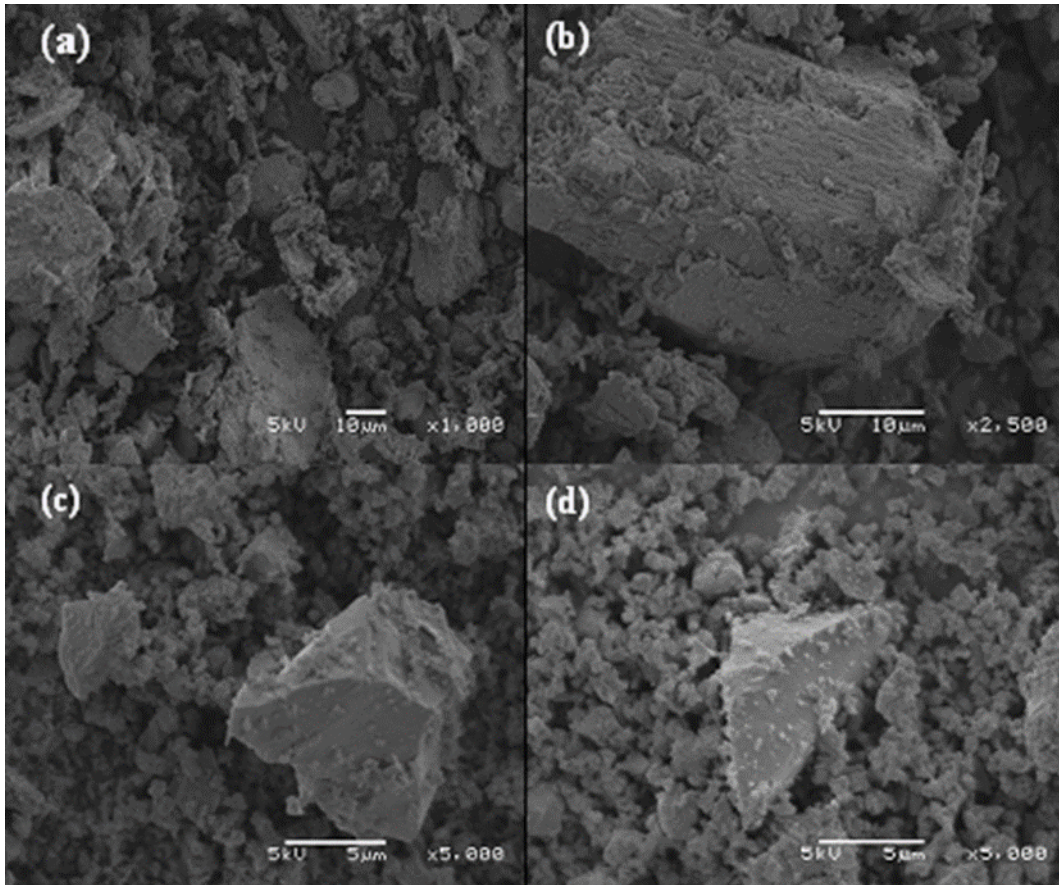
Figure 4-2   SEM images of: (a) and (b) calcium sulfate; (c) and (d) silicon

4.2   Thermal Stability of Reactants

Figure 4-3 shows the thermal stability of the silicon and calcium sulfate in a nitrogen atmosphere. The silicon showed no significant changes in mass between 25 and 600 °C. However, a mass increase associated with the formation of silicon nitride was noted above 600 °C. The anhydrous $CaSO_4$ was stable beyond 1 000 °C, with the onset of decomposition above 1100 °C. Previous TGA results indicate that the onset temperature for decomposition falls in the range 1080 to 1300 °C (Newman, 1941; Van der Merwe *et al*.; 1999). Depending on the partial pressures of SO_3, SO_2 and O_2, the thermal decomposition of $CaSO_4$ takes place according to either Scheme XII or Scheme XIII (Stern and Weise, 1966). Complete decomposition to CaO results in a theoretical mass loss of 59%.
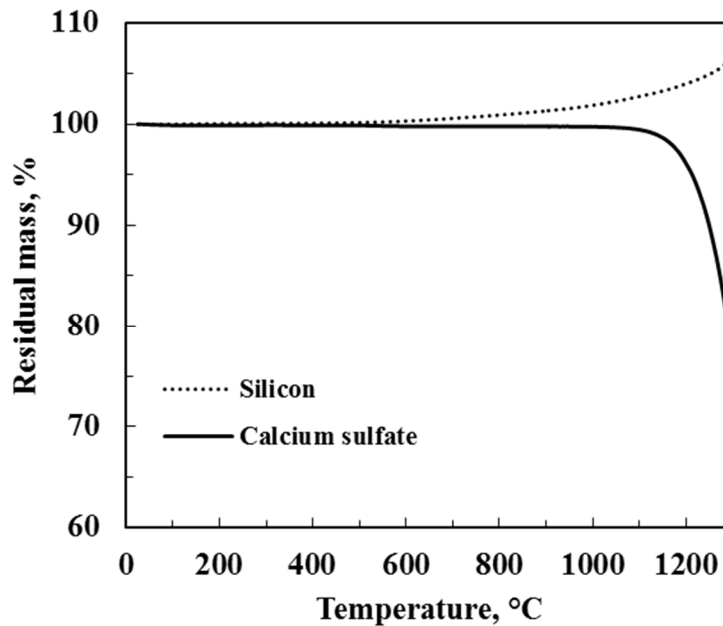
Figure 4-3   TGA results for silicon and calcium sulfate recorded in a nitrogen atmosphere

4.3   Experimental and Theoretical Energy Output Measurements

The effect of the fuel content on the energy output of the Si-CaSO$_4$ formulations is shown in Figure 4-4. Ignition and propagation were only sustained in the range of 30 to 70 wt.% silicon. Compositions containing 20 or 80 wt.% silicon failed to propagate. The energy output decreased approximately linearly with increasing silicon content. The outputs ranged from 3.87 to 1.97 MJ kg^{-1}. The 30 wt.% silicon composition, which is the closest to stoichiometry, had the highest energy output (Berger, 2005). The proprietary starter that was used had an energy output of 1.5 MJ kg^{-1}. The reported enthalpy results have been normalised to exclude the influence of the starter. Thermochemical predictions made using the EKVI thermodynamic software package over the range 10 to 90 wt.% silicon are also shown in Figure 4-4. The calculated exothermicity values from the EKVI program agreed reasonably well with the measured values. This suggests that the metal-oxidant reaction proceeded to form the thermodynamically favoured products. Table 4-2 shows the constant-volume adiabatic reaction temperatures calculated with the EKVI code. There is a clear dependency of the adiabatic temperature on stoichiometry, with the 30 wt.% silicon composition predicted to have the highest reaction temperature of 1685 °C.
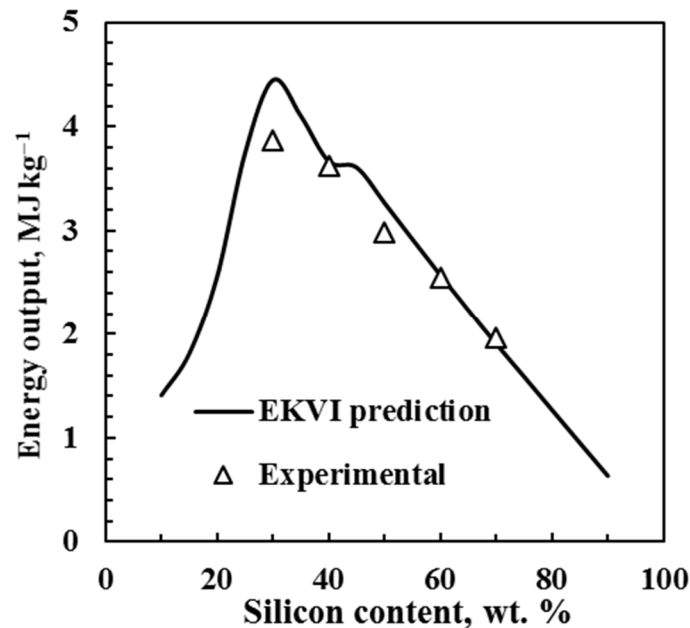
Figure 4-4 Comparison of experimental energy outputs obtained with the bomb calorimeter in a helium atmosphere with EKVI simulations for Si-CaSO$_4$ (isothermal reaction at 25°C)

4.4 Pressure–Time Analysis

Time-dependent changes in pressure, relative to the initially applied helium pressure of 3.0 MPa, are shown in Figure 4-5. A summary of the information extracted from the pressure–time relationships is presented in Table 4-2. There are clear trends with the rate of pressure rise, as well as the maximum peak pressure decreasing with increasing silicon content. This correlates with the observation of decreasing energy with increasing silicon content in this composition range. The data on the rate of pressure rise with time were obtained by fitting the experimental data using cubic spline interpolation, followed by calculating the first derivative of this fit. Figure 4-6 shows the resultant curves obtained after these calculations had been performed on the pressure–time curve for the 30 wt.% Si composition. The maximum rate of pressurisation for the composition shown in Figure 4-5 was found to be 4.45 MP s^{-1}. There was a noticeable time delay before the pressure rose. This time lag was almost independent of the fuel content of the composition. Figure 4-5 reveals higher residual pressure differences at the end of the six-second pressure test for the 30 and 40 wt.% silicon formulations compared with the other three compositions. This could be due either to a higher residual temperature caused by the higher energy outputs, or to the generation of more gas. The residual pressure differences, after cooling to room temperature, were calculated assuming a worst case scenario

56

where the entire calcium sulfate present in the test sample decomposed completely according to either Scheme XII or Scheme XIII (Table 4-3). Maximum pressure differences of 0.16 and 0.11 MPa, respectively, were found for the 30 wt.% composition. The maximum pressure difference was also calculated assuming that the Si-CaSO$_4$ composition reacts according to Scheme XVIII. The resultant maximum pressure differences were slightly lower than the worst case scenarios. In all the cases considered, the theoretical results were considerably lower than all the experimentally measured residual pressures after 6 seconds. This suggests that the higher differential pressures were caused by residual heating effects. The influence of the starter composition on the pressure–time curves is shown in Figure 4-7. The 0.2 g of starter that was used in the tests resulted in virtually no pressure rise. All the changes in pressure–time curves for the compositions were determined using 2 g of composition. With this in mind, tests were also carried out using 2 g of the starter. The pressure rises due to 2 g of starter was much lower than those recorded for the 30–50 wt.% silicon compositions.
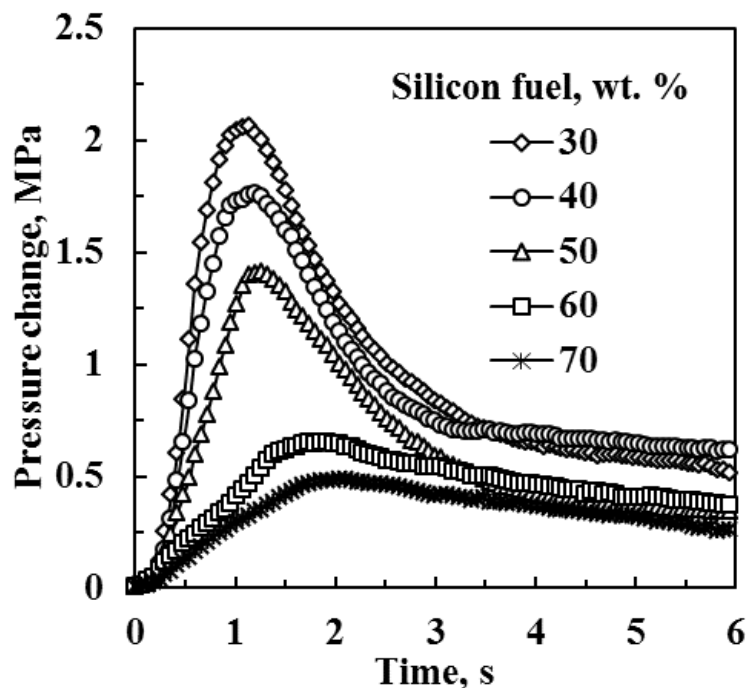
Figure 4-5   Pressure increase with time for different Si-CaSO$_4$ compositions during the bomb calorimetry experiments in a helium atmosphere

Table 4-2 Energy output and peak pressures, times to reach the peak pressure and the maximum pressurisation rates extracted from the relative pressure–time profiles measured in the bomb calorimeter

Si content (wt.%)	30	40	50	60	70
Energy output (MJ kg^{-1})	3.87	3.62	2.98	2.55	1.97
P_{max} (MPa)	2.06	1.76	1.41	0.65	0.49
t_{max} (s)	1.20	1.28	1.28	1.84	2.08
dP/dt_{max} (MPa s^{-1})	4.45	3.08	1.82	0.60	0.40

Table 4-3 Calculated maximum pressure differences assuming a worst case scenario where all the CaSO$_4$ in the samples placed in the bomb calorimeter decomposed according to either Scheme XII or Scheme XIII. The maximum pressure difference assuming that the reaction proceeds according to Scheme XVIII is also shown together with the adiabatic reaction temperatures predicted with the EKVI thermochemistry simulations

Si content (wt.%)	30	40	50	60	70
Scheme XII (MPa)	0.16	0.14	0.11	0.09	0.07
Scheme XIII (MPa)	0.11	0.09	0.08	0.06	0.05
Scheme XVIII (MPa)	0.10	0.08	0.07	0.06	0.04
Adiabatic reaction temperature (°C)	1684	1429	1300	1058	810
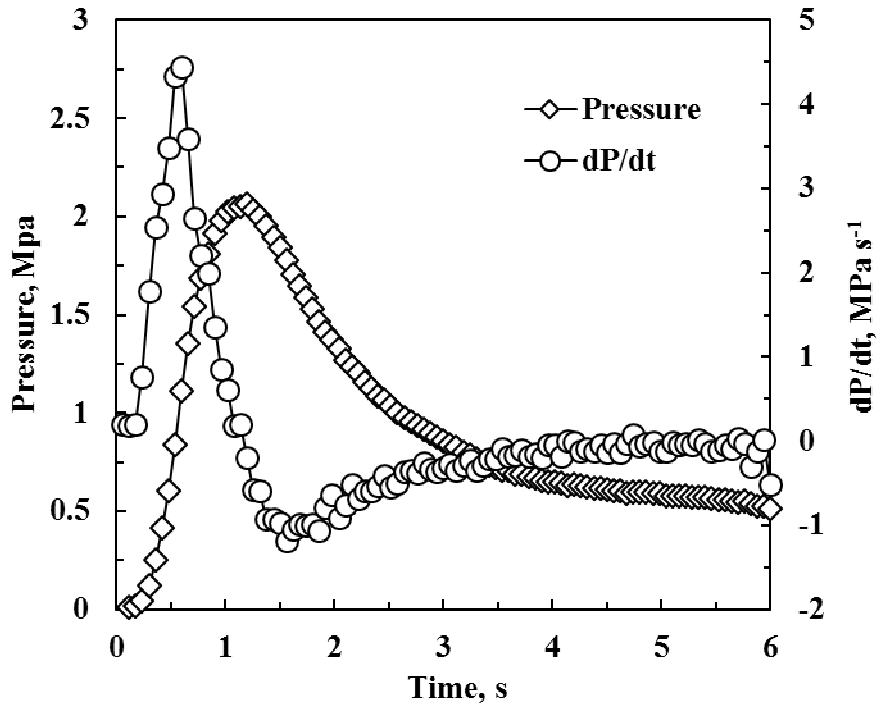
Figure 4-6 Change in pressure with time profile of 30 wt.% Si-CaSO$_4$ compositions and its associated first derivative obtained using cubic spline interpolation
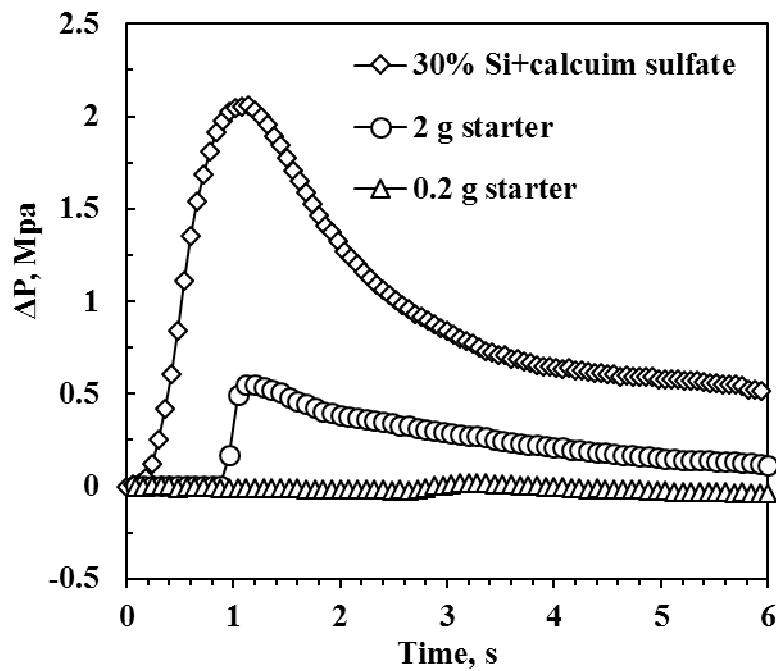
Figure 4-7 Comparison of pressure increase with time for the 30% Si-CaSO$_4$ composition with that of 2 g and 0.2 g starter during the bomb calorimetry experiments in a helium atmosphere

59

4.5   Burn Rates

Figure 4-8 shows the effect of stoichiometry on the burn rate of the Si-CaSO$_4$ system. The burn rate decreased with increasing silicon content. The composition containing 30 wt.% Si burned fastest (12.5 mm s^{-1}), while the 70 wt.% Si composition was the slowest (6.9 mm s^{-1}). This burn rate is similar to the burn rate of Si-BaSO$_4$ compositions (4–9 mm s^{-1}) (Beck, 1989), but is much slower than the range reported for Si-Pb$_3$O$_4$ compositions (40–257 mm s^{-1}) (Goodfield and Rees, 1981).

Figure 4-8 also shows that the burn rate and the energy output decrease in tandem as the fuel content increases. According to Khaikin and Merzhanov (1966), the burn rate varies inversely with the square root of the energy output. However, according to Hill *et al*. (1950), the burn rate should be directly proportional to the energy output and this is roughly the case for the present data.
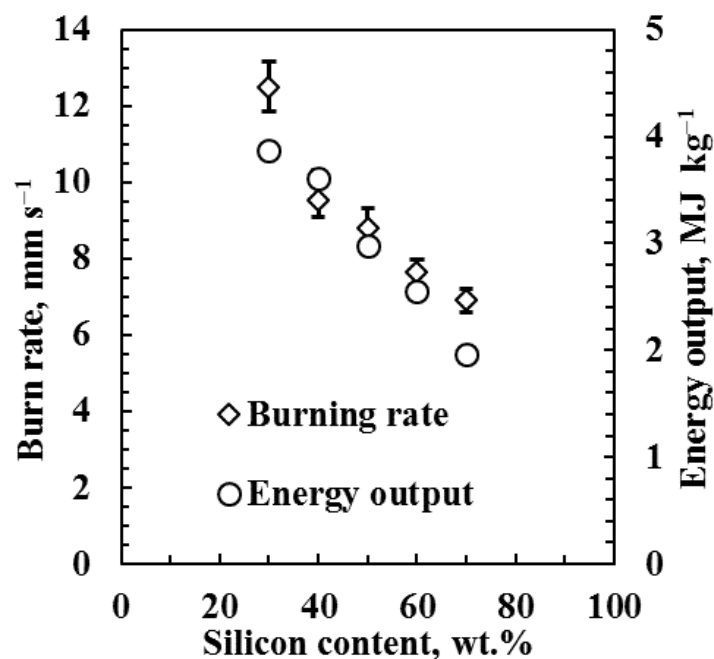
Figure 4-8   Effect of fuel content on the burn rate and energy output of Si-CaSO$_4$ compositions

4.6   XRD Analysis of Reaction Products

Quantitative XRD analysis was performed on the reaction products (see Table 4-4). This information was used to deduce a reaction mechanism and to establish whether the combustion

60

products were environmentally benign. The major crystalline products detected were calcium sulfide (CaS), pseudowollastonite ($Ca_3(SiO_3)_3$), quartz (SiO_2) and unreacted silicon. Trace amounts of bismuth metal and bismuthinite (Bi_2S_3) were also detected. These impurities derived from the proprietary bismuth oxide-based starter that was used to ignite the various formulations. These results also revealed the presence of a significant amount of an amorphous phase in the reaction products. No unreacted calcium sulfate was detected. This was expected since gypsum thermally degrades below the high pyrotechnic reaction temperatures.

Table 4-4 also reports the sulphur analysis of the solid reaction residues. Sulphur was essentially retained in the form of calcium sulfide, with minute amounts present in the amorphous phase. A sulphur mass balance enabled the determination of the amount of gas produced during the reaction, assuming no impurities in the reactants and that SO_2 is the only gas evolved. Depending on the stoichiometry, the gas evolved at standard temperature and pressure conditions ranged from 29.2 to 67.5 $cm^3 \, g^{-1}$. This is considerably higher than the 10 $cm^3 \, g^{-1}$ generally taken as the upper limit for classification as a gasless composition (Charsley *et al*., 1980).

Mass balances on the other elements were also carried out. In particular, the Si:Ca ratio in the amorphous phase exceeded 3 for all the compositions. This indicates that the amorphous phase was composed predominantly of silica (SiO_2). An example of the method and assumptions used to carry out the mass balances are shown in Appendix C.

Table 4-4 Sulphur content and XRD quantification of the reaction products for the Si-CaSO$_4$ pyrotechnic system

Phase	Formula	30	40	50	60	70
Silicon	Si	2.7	17.7	26.8	36.3	41.1
Quartz	SiO$_2$	2.6	4.0	4.9	1.1	1.2
Pseudowollastonite	Ca$_3$(SiO$_3$)$_3$	19.2	25.5	13.6	9.8	10.4
Calcium sulfide	CaS	9.2	14.4	13.6	10.7	1.9
Bismuth	Bi	0.6	2.4	1.3	1.5	1.7
Bismuthinite	Bi$_2$S$_3$	1.2	1.9	1.3	1.1	0.7
Amorphous[a]		64.5	34.1	38.5	39.5	43.1
Si:Ca ratios						
Reagents		2.08	3.23	4.84	7.27	11.3
Crystalline phase		1.04	2.19	3.77	5.99	13.6
Amorphous phase		3.02	6.64	7.47	10.2	9.15
Sulphur analysis	wt.%	9.9	5.5	5.3	4.0	3.1
CaS equivalent[b]		22.3	12.4	11.9	9.0	7.0
Gas evolved	cm^3 g^{-1}	57.5	67.5	50.9	41.5	29.2

[a]Mainly silica; [b]Estimated from sulfur content

Table 4-5   Major reaction products of the Si-CaSO$_4$ composition predicted using EKVI thermodynamics code under adiabatic conditions

Formula	10	20	30	40	50	60	70	80	90
SO$_2$ (g)	0.5	10.6	-	-	-	-	-	-	-
S$_2$ (g)	3.7	12.7	-	-	-	-	-	-	-
SiS(g)	-	-	3.7	0.3	-	-	-	-	-
Si (s)	-	-	0.1	15.2	29.4	43.5	57.6	71.8	85.9
SiO$_2$ (s)	12.2	19.5	57.5	52.6	44.1	35.3	26.5	17.7	8.8
CaS (s)	-	-	32.9	31.5	26.5	21.2	15.9	10.6	5.3
Ca$_3$Si$_2$O$_7$ (s)	24.3	57.2	5.9	0.5	0.1	-	-	-	-
CaSO$_4$ (s)	59.4	-	-	-	-	-	-	-	-
Total	**100**	**100**	**100**	**100**	**100**	**100**	**100**	**100**	**100**

Table 4-5, Figure 4-9 and Figure 4-10 provide details of the EKVI simulation results for the Si-CaSO$_4$ formulation. Figure 4-11 reports the silicon conversion predicted by the EKVI thermodynamics software compared to the apparent conversion based on the crystalline silicon phase estimated from the XRD of the reaction products. The conversions were similar for the 30–50 wt.% Si compositions. However, the remaining compositions showed higher conversions than those predicted by the EKVI thermochemistry simulations or are even physically possible. This discrepancy suggests that unreacted silicon must have been present in the amorphous phase.

The reaction product spectra predicted with the EKVI program were similar to those found experimentally. However, according to the EKVI simulation, all the test compositions essentially qualify as "gasless" since the predicted amount of gas produced was minimal. Exceptions were seen in the case of the formulations with low silicon content, i.e. 10 and 20 wt.% Si, where quantifiable amounts of SO$_2$ (g) and elemental S$_2$ (g) were predicted. In the case of the 30 wt.% silicon composition, SiS gas formation was predicted. The major solid phases predicted were SiO$_2$, CaS, Ca$_3$Si$_2$O$_7$ and unreacted silicon. The program predicted complete conversion of the CaSO$_4$ to CaS. However, Ca$_3$Si$_2$O$_7$ was prominent only in the 10

and 20 Si wt.% compositions. It should be noted that the EKVI database includes wollastonite $CaSiO_3$, but does not contain pseudowollastonite. Obviously this influenced the predictions made with the software.
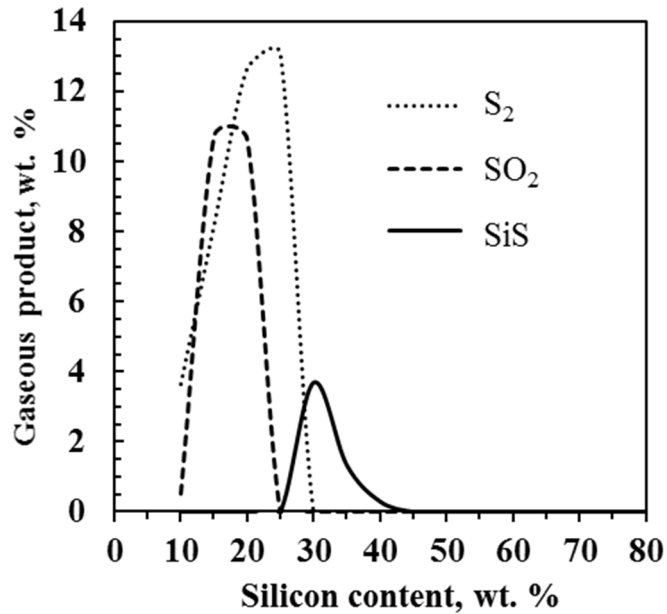
Figure 4-9 Gaseous products released during the combustion of the Si-CaSO$_4$ pyrotechnic composition predicted with the EKVI thermodynamics software
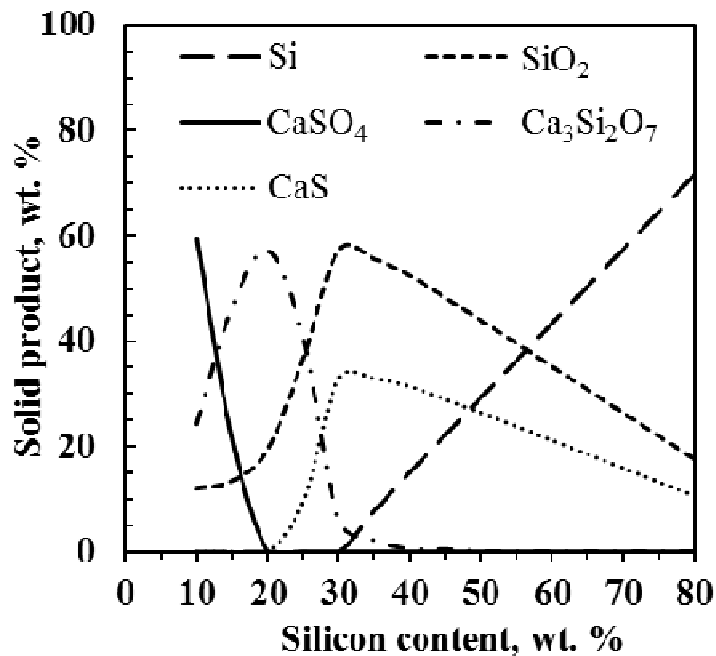
Figure 4-10 Solid products obtained during the combustion of the Si-CaSO$_4$ pyrotechnic composition predicted with the EKVI thermodynamics software
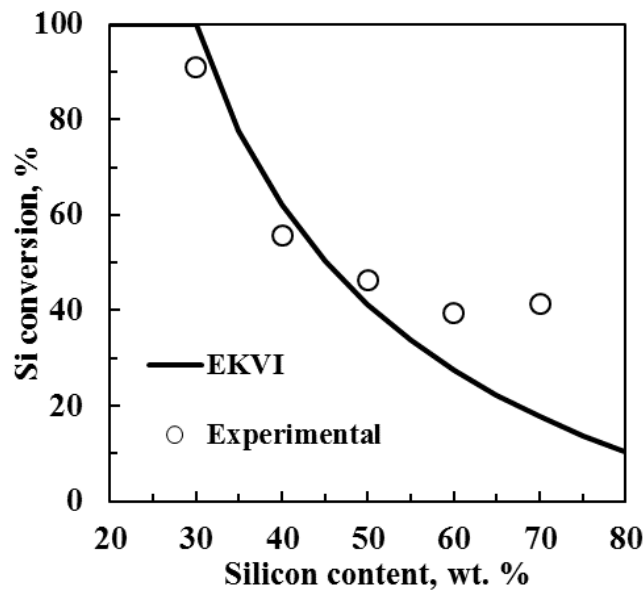
Figure 4-11   Silicon conversion   predicted by the EKVI thermodynamics software compared to the apparent conversion based on the crystalline silicon phase estimated from the XRD of the reaction products. The discrepancy suggests that unreacted silicon must be present in the amorphous phase.

4.7   Discussion

Pseudowollastonite and calcium sulphide were the dominant crystalline phases in the residue left by the Si-CaSO$_4$ reaction. The former is a high-temperature polymorph of wollastonite (CaSiO$_3$). Gladun and Bashaeva (1995) showed a range of possible reactions that can result in high-temperature synthesis of wollastonite. They found that it can be obtained in the temperature range 1000 to 1400 °C. Their results, the presented XRD and TGA data as well as the findings of Mu and Zaremba (1987) were combined and used to propose a possible reaction mechanism for the Si-CaSO$_4$ reaction. Scheme XVIII presents the resulting postulation. Reaction (1) was thought to be a solid-solid reaction which is driven above the Tamman temperature. The Tamman temperature refers to the ratio of the temperature of the solid to its melting temperature, it gives a rough measure of lattice loosening. Ionic surface mobility is said to become effective at a T/T$_m$ ratio of 0.3, while lattice diffusion takes place at ratios of 0.5 (McLain, 1980). These phenomena result in the ignition temperature of solid-solid pyrotechnic reactions occurring below the melting or decomposition temperatures of the constituent reactants. Based on the product spectra predicted by EKVI as well as the XRD results, reaction (1) is postulated to be the dominant reaction. The stoichiometry of reaction is

29.2 wt.% Si which corresponds to the value obtained from the EKVI simulations and suggested by the experimental results. Reaction (2) occurs when the reaction temperature has reached the $CaSO_4$ decomposition temperature as shown by the TGA results. The oxygen released by the decomposition reaction oxidises silicon according to reaction (3). Finally, the high reaction temperatures facilitate the occurrence of reaction (4). An overall reaction is shown in reaction (5).

$$CaSO_4 + 2Si \rightarrow CaS + 2SiO_2 \qquad\qquad (1)$$

$$2CaSO_4 \rightarrow 2CaO + 2SO_2 + O_2 \qquad\qquad (2)$$

$$Si + O_2 \rightarrow SiO_2 \qquad\qquad (3)$$

$$2SiO_2 + 2CaO \rightarrow 2CaSiO_3 \qquad\qquad (4)$$

$$\overline{3CaSO_4 + 3Si \rightarrow CaS + SiO_2 + 2SO_2 + 2CaSiO_3} \qquad\qquad (5)$$
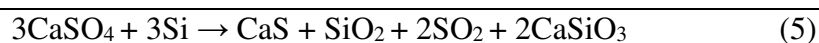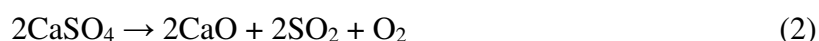
Scheme XVIII   Proposed reaction steps taking place in the reaction of the Si-$CaSO_4$ pyrotechnic composition

Figure 4-12 shows a CaO-SiO_2 phase diagram calculated using the MTDATA software developed by Davies *et al*. (2002). The phase diagram shows that several compounds or compound combinations are formed at different temperatures and CaO-SiO_2 ratios. A mass balance, which was carried out to establish the Si:Ca ratio, revealed that the amorphous phase is made up predominantly of SiO_2. Table 4-4 shows that the ratio of silicon to calcium in the amorphous phase of all the residues was much higher than the 1:1 ratio expected for wollastonite, varying from 3.02 to 10.2. These ratios correspond to the SiO_2 mol fractions of 0.75 to 0.91 in Figure 4-12. This means that the formation of the pseudowollastonite and the amorphous phase identified and quantified by XRD analysis can be attributed to a combination of reactions 3 and 4 of Scheme XVIII. It also implies that these phases were most likely fixed in the square temperature-composition region second from below and on the far right-hand side of the phase diagram in Figure 4-12. It is worth noting that the reported solid product analysis only provides an idea of the actual reaction products since the analysis was performed at room temperature whereas the theoretical adiabatic temperature can reach 1684 °C. Furthermore, the

cooling rate experienced by the residue may have influenced the distribution between the crystalline and the amorphous phases.
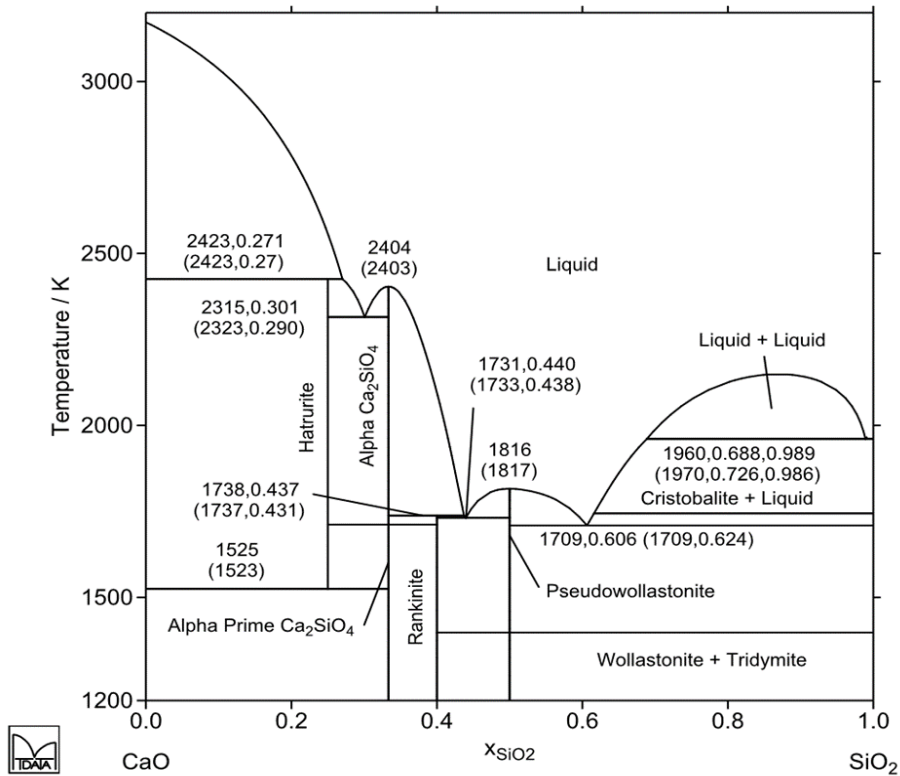
Figure 4-12   Phase diagram for the system CaO-SiO$_2$ (reproduced with permission from the authors – Davies *et al*., 2002).

CHAPTER 5   RESULTS: A COMPARATIVE STUDY OF Si-BaSO₄ AND Si+CaSO₄ PYROTECHNIC TIME DELAY COMPOSITIONS

5.1   Characterisation of Reactants

Figure 5-1 and Table 5-1 report the particle size distribution (PSD) of the silicon, calcium sulfate and barium sulfate used in this part of the investigation. Figure 5-2 shows scanning electron microscopy (SEM) images of the silicon and barium sulfate.
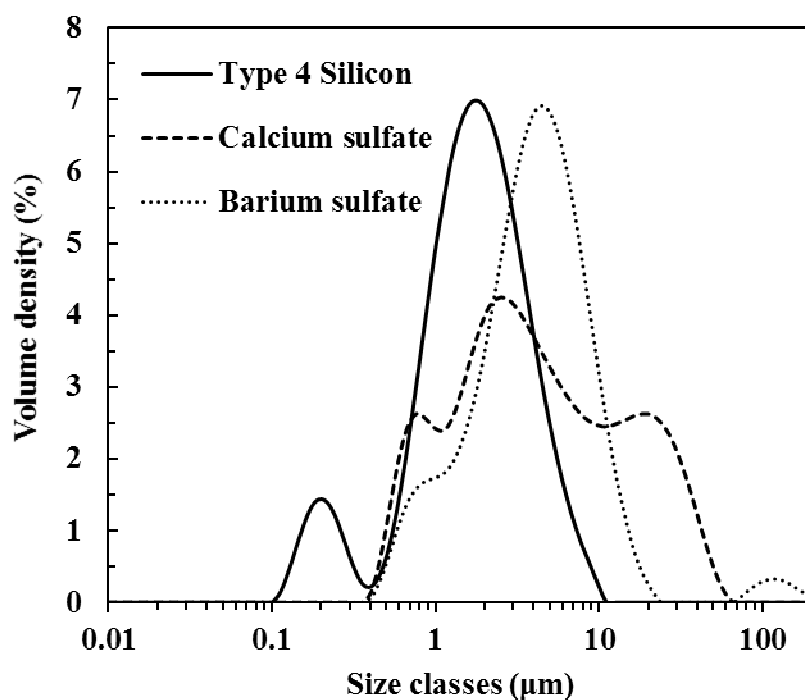
Figure 5-1   Particle size distribution of the Type 4 silicon, barium sulfate and calcium sulfate used in this investigation

Table 5-1   Volume-based particle size distribution and BET surface areas of the raw materials used

	D_{10} (µm)	D_{50} (µm)	D_{90} (µm)	BET (m² g⁻¹)	ΔH_f° (kJ mol⁻¹)
Barium sulfate	1.25	4.31	10.60	0.82	-1465
Calcium sulfate	0.61	4.05	25.30	3.78	-1433
Silicon	0.91	1.85	4.58	11.03	-

© University of Pretoria
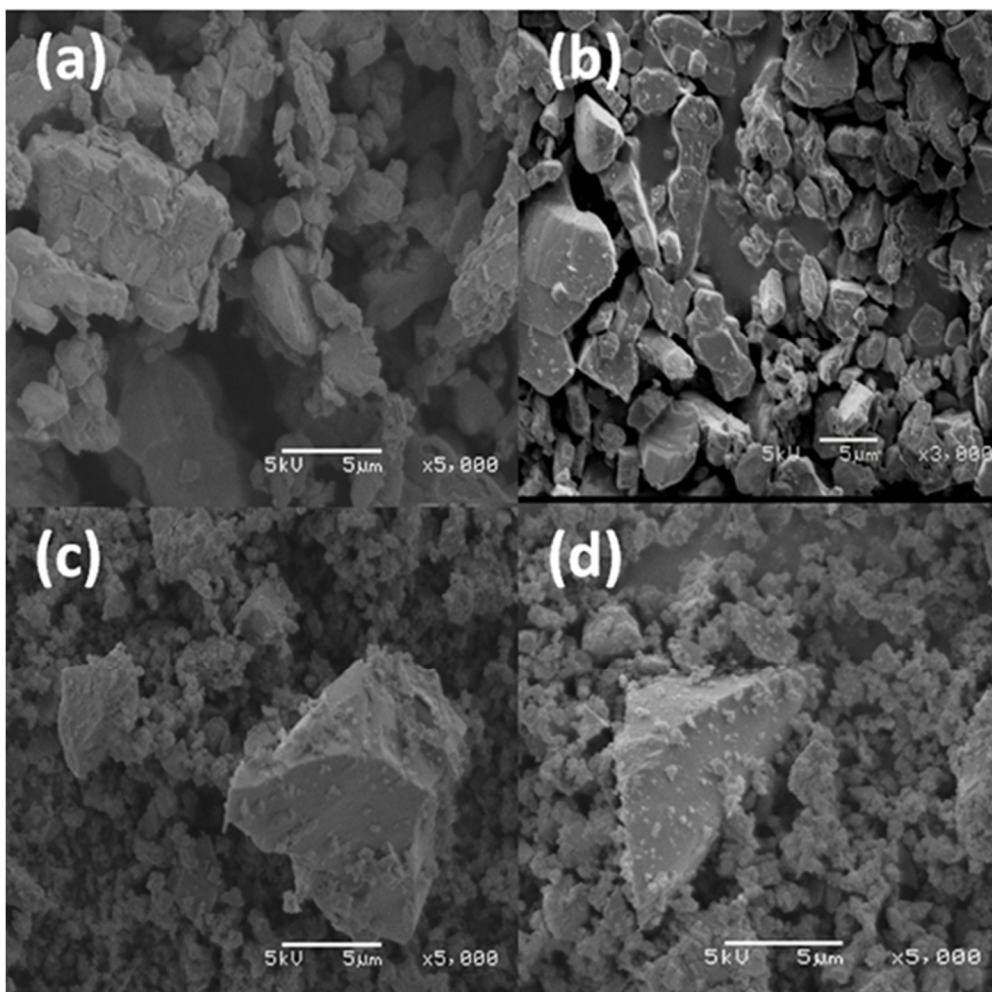
Figure 5-2   SEM images of: (a) and (b) barium sulfate; (c) and (d) silicon

5.2   Thermal Behaviour of Reactants in Nitrogen

Figure 5-3 shows the thermal behaviour of silicon, barium sulfate and calcium sulfate in a nitrogen atmosphere. The silicon showed no significant change in mass below 600 °C. However, a mass increase associated with the formation of silicon nitride was noted above 600 °C. Barium sulfate was stable in the temperature range tested, with only a slight mass decrease observed above 1200 °C. The thermal decomposition of $BaSO_4$ occurs in the temperature range 1125 to 1400 °C and takes place according to Scheme VIII or Scheme IX (Stern and Weise, 1966; Holt and Engelkemeir, 1970; Mohazzabi and Searcy, 1976). The ultimate theoretical mass loss is ca. 34.4%. The decomposition of anhydrous $CaSO_4$ proceeds in a similar manner in the range 1080 to 1300 °C (Newman, 1941; Stern and Weise, 1966; Tichapondwa et al., 2014).

The TGA results indicate that, although barium sulfate and calcium sulfate release the same molar amount of oxygen, barium sulfate releases it at a higher temperature, i.e. it is more thermally stable. This correlates with the standard enthalpy of formation values, where barium sulfate has higher enthalpy of formation (Table 5-1). Also, Stern and Weise (1966) state that the distortion and instability of sulfate salts increases with increasing polarising power of the cation. The polarising power of cations increases with increasing electronegativity and decreasing ionic radius. Therefore, salts with small highly charged cations are expected to be least stable. Since calcium ions have a smaller ionic radius than barium, it is expected that $CaSO_4$ would decompose at a lower temperature than $BaSO_4$.
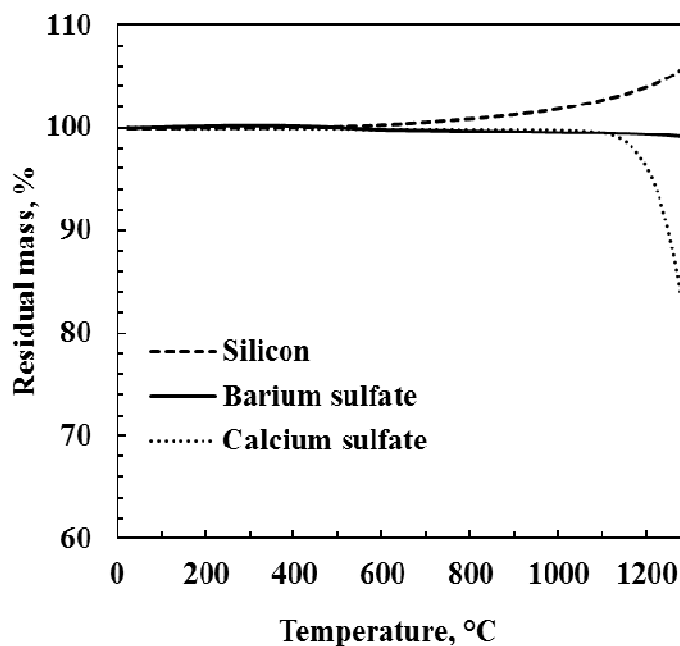
Figure 5-3   TGA results for silicon, barium sulfate and calcium sulfate recorded in a nitrogen atmosphere

5.3   Experimental and Theoretical Energy Output Measurements

Figure 5-4 compares the effect of fuel content on the energy output of the Si-BaSO$_4$ and Si-CaSO$_4$ formulations in a helium atmosphere. Whereas calcium sulfate supports combustion in the range of 30–70 wt.% silicon, barium sulfate only burns in the 20 to 60 wt.% silicon range. The energy outputs for both formulations decreased approximately linearly with increase in Si content. Compared with calcium sulfate, barium sulfate-based compositions had lower energy outputs (1.42–2.63 MJ kg^{-1}). The highest energy outputs were observed at 20 wt.% Si and 30

70

wt.% Si for the Si-BaSO$_4$ and Si-CaSO$_4$ systems, respectively. These compositions correspond to the ideal stoichiometry for both formulations and are similar to previously reported trends (Berger, 2005). Calculated exothermicity values from the EKVI program for both the Si-BaSO$_4$ and Si-CaSO$_4$ systems were in reasonable agreement with the measured heats of reaction recorded using the bomb calorimeter. The maximum deviation from the predicted value was 7% for the S-BaSO$_4$ system and 15% for the Si-CaSO$_4$ combination. This suggests that the metal–oxidant reactions proceeded via the thermodynamically favoured pathways. Figure 5-5 compares the predicted adiabatic reaction temperatures of the two systems. The Si-BaSO$_4$ compositions generated lower theoretical adiabatic temperatures compared with Si-CaSO$_4$. The highest temperatures were recorded at the stoichiometric composition for both formulations.
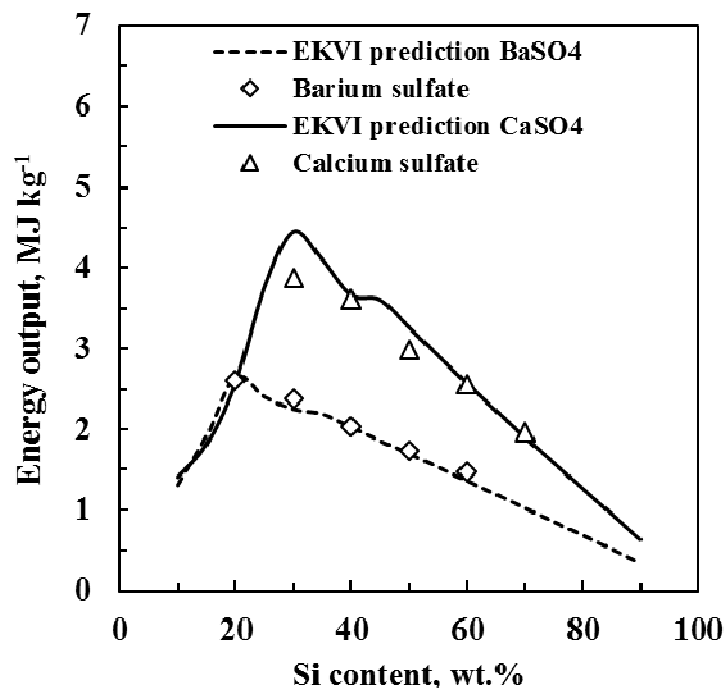
Figure 5-4   Comparison of energy outputs obtained from the bomb calorimeter measurements for the Si-CaSO$_4$ and Si-BaSO$_4$ systems, and EKVI simulations in a helium atmosphere (isothermal reaction at 25°C)
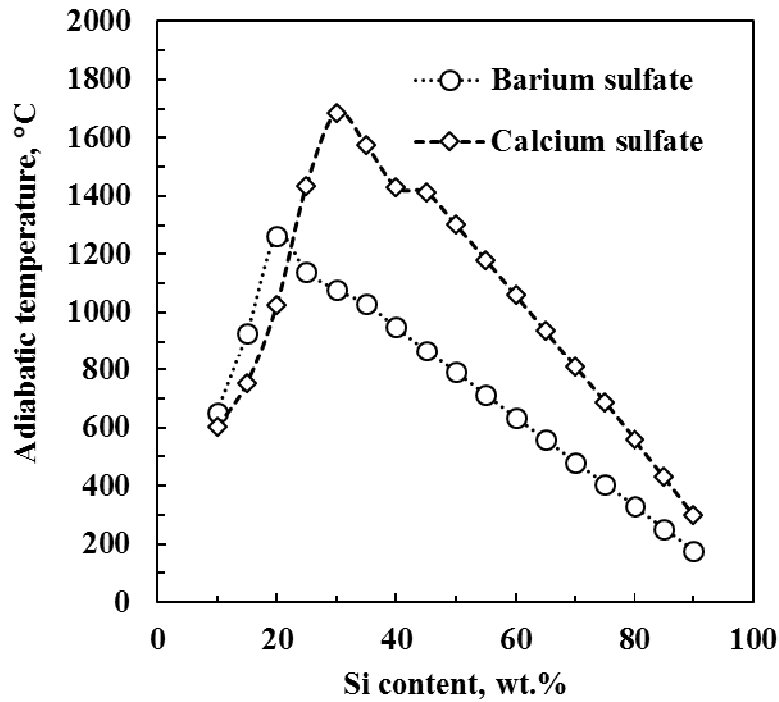
Figure 5-5 Comparison of the predicted adiabatic combustion temperature at different stoichiometries for both the Si-CaSO$_4$ and Si-BaSO$_4$ systems using EKVI software

5.4 Pressure–Time Analysis

Figure 5-6 and Table 5-2 report the pressure–time data obtained with bomb calorimetry. The indicated pressure readings are relative to the initial 3.0 MPa helium pressure. Above 30 wt.% silicon the rate of pressure rise, and the maximum peak pressure, decreased with increasing silicon content in accordance with the energy output trend. Based on the pressure–time parameters listed in Table 5-2, it can be concluded that Si-CaSO$_4$ is more reactive than corresponding Si-BaSO$_4$ formulations.
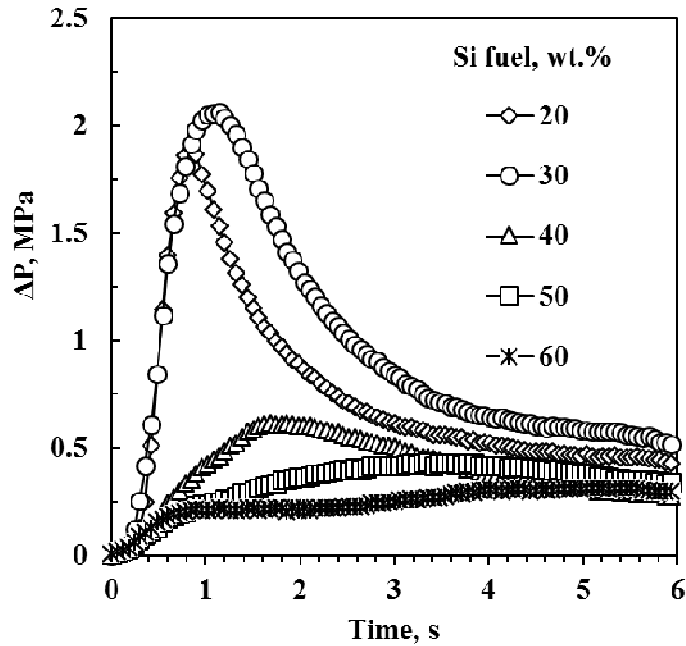
Figure 5-6 Pressure increase with time for different $Si-BaSO_4$ compositions during the bomb calorimetry experiments in a helium atmosphere

Table 5-2 Summary of the parameters extracted from pressure–time profiles of $Si-CaSO_4$ and $Si-BaSO_4$ compositions with varying silicon fuel content

Si content (wt.%)	Barium sulfate			Calcium sulfate		
	P_{max}(MPa)	t_{max} (s)	dP/dt_{max}(MPa s^{-1})	P_{max} (MPa)	t_{max}(s)	dP/dt_{max}(MPa s^{-1})
20	1.89	0.84	5.43	-	-	-
30	2.07	1.14	4.44	2.06	1.14	4.45
40	0.61	1.68	0.75	1.76	1.20	3.08
50	0.434	3.36	0.39	1.41	1.26	1.82
60	0.32	5.04	0.44	0.65	1.92	0.60
70	-	-	-	0.49	2.04	0.40

5.5 Burn Rates

The effect of stoichiometry on the burn rate for both the $Si-BaSO_4$ and $Si-CaSO_4$ systems is shown in Figure 5-7. Although combustion of the $Si-BaSO_4$ system was sustained in the range

of 20–60 wt.% Si in the inert atmosphere inside the bomb calorimeter, burning was only sustained in the range of 20–40 wt.% Si in the rigid aluminium tubes. This is attributed to higher heat losses experienced by compositions burning inside the tubes owing to more intimate contact with the conductive metal surface and a greater ratio of surface area to volume. In order to reduce such heat losses, Beck and Flanagan (1992) tested compositions compacted into thin-walled (1 mm) rectangular stainless steel channels with larger internal dimensions (6 mm × 10 mm). In this scenario compositions containing as much as 55 wt.% Si propagated. Calcium sulfate-based compositions had a wider burn range (30–70 wt.% Si). The burn rate decreased with increase in silicon content for both systems. The composition containing 20 wt.% Si-$BaSO_4$ burned fastest (16.0 mm s^{-1}), while the 40 wt.% Si was the slowest with a burn rate of 8.4 mm s^{-1}. These values are similar to those reported for the Si-$CaSO_4$ compositions (6.9–12.5 mm s^{-1}) (Tichapondwa *et al.*, 2015). It should be noted that the burn rates recorded for the Si-$BaSO_4$ compositions in these tests were higher than the literature values (4–9 mm s^{-1}) (Beck, 1989; Beck and Flanagan, 1992). Likely causes for the discrepancy include differences in the material of construction (Miklaszewski *et al.*, 2014) and in the properties of the reagent materials, e.g. particle size, surface area, material history, purity and contaminants present (Ellern, 1968).
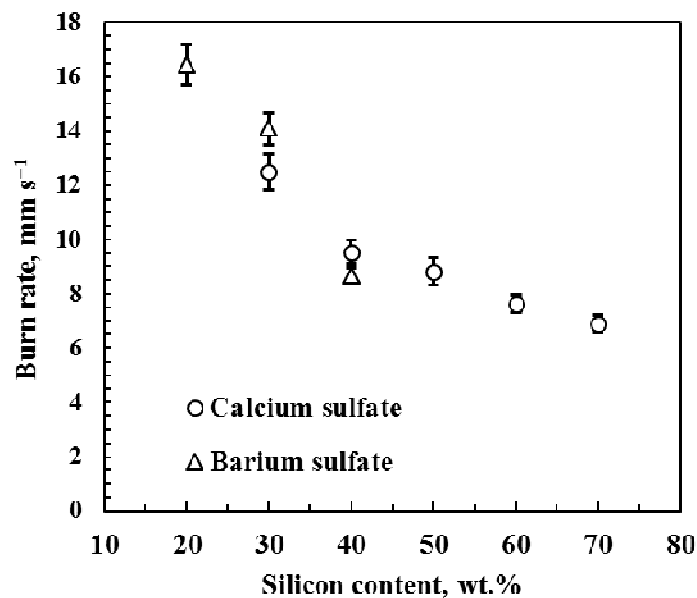
Figure 5-7   Effect of fuel content on the burn rate of Si-$BaSO_4$ and Si-$CaSO_4$ compositions

5.6   XRD Analysis of Reaction Products

Quantitative XRD analysis performed on the reaction products of the Si-$BaSO_4$ collected from the bomb calorimeter are reported in Table 5-3. The XRD diffractograms revealed a significant amount of an amorphous phase with quartz (SiO_2) and unreacted silicon as the only crystalline products. The presence of trace amounts of bismuth metal and bismuthinite (Bi_2S_3) is attributed to the proprietary bismuth oxide-based starter that was used for ignition. Similar observations were made for the Si-$CaSO_4$ compositions. No barium sulfate was detected, regardless of the initial composition. This was expected as the compositions were fuel rich.

Sulphur analyses of the solid reaction residues (Table 5-3) allowed determination of the sulphur content of the amorphous phase. Between 50 and 70% of the initial sulphur was retained in the amorphous phase, depending on the initial stoichiometry. If it is assumed that no impurities were present in the reactants and that SO_2 was the only gas formed, sulphur mass balances enable estimation of the amount of gas produced by the reaction (Table 5-3). Depending on the stoichiometry, the gas evolved at standard temperature and pressure ranged between 17.8 and 31.6 cm^3 g^{-1}. The corresponding SO_2 estimates for the $CaSO_4$ compositions ranged from 29.2 to 67.5 cm^3 g^{-1}(Tichapondwa *et al*., 2015). Thus both compositions released more than 10 cm^3 g^{-1} of gas, the value regarded as an upper limit for classification as a gasless composition (Charsley *et al*., 1980).

Table 5-3 Quantitative analysis of the reaction products identified from the Si-BaSO$_4$ pyrotechnic composition using XRD, as well as an analysis of the total sulphur content in the solid products

Phase	Formula	20	30	40	50	60
Silicon	Si	4.9	13.9	26.1	36.4	45.7
Quartz	SiO$_2$	8.0	7.1	11.9	11.4	5.4
Bismuth	Bi	2.1	1.9	2.7	2.7	1.7
Bismuthinite	Bi$_2$S$_3$	2.9	2.6	2.1	1.9	1.1
Amorphous		82.0	74.6	57.3	47.8	46.1
Sulphur analysis	wt.%	8.6	5.6	6.2	3.5	3.1
Gas evolved	cm^3 g^{-1} (STP)	20.1	31.6	16.6	25.3	17.8

5.7 Simulated Reaction Products

Figure 5-8 and Table 5-4 present equilibrium product spectra predicted by EKVI simulations of the Si-BaSO$_4$ system. The reaction in all compositions was essentially gasless. The exception is the 10 wt.% silicon composition where S$_2$ gas is predicted and unreacted solid BaSO$_4$ was expected. For compositions above 10 Si wt.% the solid phases predicted were SiO$_2$, BaS, BaSiO$_3$, SiS and unreacted silicon. Interestingly, SiS is formed and no BaS is found in the products of the 30 wt.% composition. Further analysis suggests that the formation of SiS is favoured when the reaction products end up in a molten state. Below its melting temperature, approximately 1 090 °C, SiS is not formed. The products predicted by the EKVI software are in accord with the experimental observations if BaS, BaSiO$_3$ and SiS form the detected amorphous phase.

Owing to the limited data on barium silicate phases available in the EKVI software, simulations of the Si-BaSO$_4$ reaction were also carried out using MTDATA software. Figure 5-9 and Table 5-5 show the predicted adiabatic reaction temperatures and product spectra. The barium silicate phases predicted were Ba$_2$Si$_3$O$_8$ and BaSi$_2$O$_5$, rather than the BiSiO$_3$ phase predicted by the EKVI software. All the other product compositions were similar to those predicted by the EKVI software, with the exception of SiS which was not present. A comparison of the adiabatic

76

reaction temperatures determined by the two software programs shows that they were nearly identical.
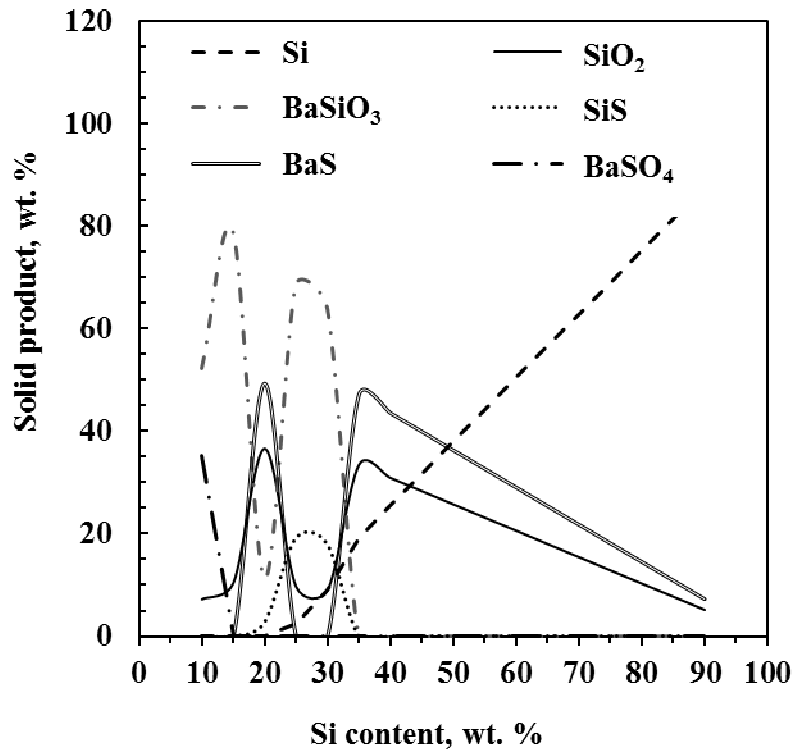
Figure 5-8 Solid products obtained during the combustion of the Si-BaSO$_4$ pyrotechnic composition predicted with the EKVI thermodynamics software

Table 5-4 Product spectrum and adiabatic temperature (T$_{ad}$) predicted with the EKVI thermodynamics code for the Si-BaSO$_4$ system

	10	20	30	40	50	60	70	80	90
S$_2$ (g)	5.3	-	-	-	-	-	-	-	-
BaSiO$_3$ (s)	52.3	11.4	64.0	-	-	-	-	-	-
SiO$_2$ (s)	7.2	36.6	9.0	30.9	25.7	20.6	15.4	10.3	5.2
SiS (s)	-	2.7	18.0	-	-	-	-	-	-
BaS (s)	-	49.3	-	43.5	36.3	29.0	21.8	14.5	7.3
Si (s)	-	-	8.9	25.6	38.0	50.4	62.8	75.2	87.6
BaSO$_4$ (s)	35.2	-	-	-	-	-	-	-	-
T$_{ad}$ (°C)	654	1262	1078	949	793	635	482	329	178
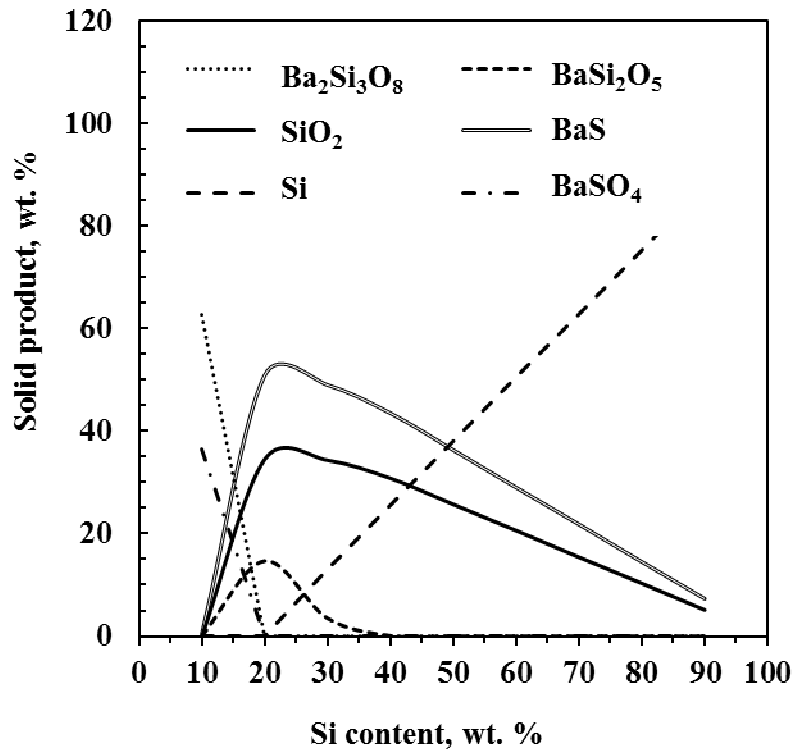
Figure 5-9 Solid products obtained during the combustion of the Si-BaSO$_4$ pyrotechnic composition predicted with the MTDATA thermodynamics software

Table 5-5 Product spectrum and adiabatic temperature (T_{ad}) predicted with MTDATA software for the Si-BaSO$_4$ system

	10	20	30	40	50	60	70	80	90
Ba$_2$Si$_3$O$_8$ (s)	62.7	-	-	-	-	-	-	-	-
BaSi$_2$O$_5$ (s)	-	14.6	3.5	0.1	-	-	-	-	-
SiO$_2$ (s)	-	34.5	34.3	30.8	25.7	20.6	15.4	10.3	5.1
BaS (s)	0.5	50.9	49.0	43.5	36.3	29.0	21.8	14.5	7.3
Si (s)	-	-	13.1	25.6	38.0	50.4	62.8	75.2	87.6
BaSO$_4$ (s)	36.5	-	-	-	-	-	-	-	-
T_{ad} (°C)	631	1214	1097	949	793	635	482	329	177

5.8   Sensitivity Testing

Knowledge of the sensitivity to impact, friction and ESD stimuli is important when processing, handling and transporting the compositions. These were evaluated for the two 30 wt.% silicon compositions (Table 5-6). No ignition was observed at the highest settings available for both the impact and friction testers (98 J for impact and 360 N for friction). Therefore, both compositions were classified as insensitive to impact and friction stimuli in accordance with the UN recommendations on the transportation of dangerous goods (2007). The calcium sulfate composition was more sensitive to ESD (118 ± 46 mJ) compared with the barium sulfate (145 ± 26 mJ). Both formulations were classified as insensitive to ESD given that the approximate maximum ESD energy developed by the average person at 200 pF and 25 kV is approximately 60 mJ (Kosanke *et al*., 2012). It should be noted that humans are capable of acting as conduits passing higher ESD energy from other objects.

Table 5-6   Sensitivity of the 30 wt.% silicon compositions of barium sulfate and calcium sulfate to impact, friction and ESD stimuli

	Impact (J)	**Friction (N)**	**ESD (mJ)**
Barium sulfate	> 98	> 360	145 ± 26
Calcium sulfate	> 98	> 360	118 ± 46

5.9   Discussion

Silicon dioxide and unreacted silicon were the only crystalline phases detected in the predominantly amorphous solid residue left by the $Si-BaSO_4$ reaction. Beck (1989) earlier reported that the residue is X-ray amorphous. Previous studies have established that the barium silicate system, $xBaO-(100 - x)SiO_2$, has a glass-forming region around $x = 25$–40 (Tyurnina *et al*., 2006; Rai and Mountjoy, 2014). In this study the composition of the amorphous phase was assessed based on the TGA and XRD results, sulphur analysis data, EKVI and MTDATA simulations, as well as a previously reported reaction mechanism (Tichapondwa *et al*., 2015). It is postulated that the amorphous phase is a composite mixture of any of the following phases: $BaSiO_3$, $Ba_2Si_3O_8$, $BaSi_2O_5$, BaS, SiO_2 and $BaSO_4$. The SiS predicted by EKVI was not considered as a component in the amorphous phase since the analysed residual material would have cooled to room temperature and the SiS should have transformed into a more stable form.

The unreacted silicon was also not considered as part of the amorphous phase as the crystalline amounts quantified by XRD were almost identical to those predicted by the software packages. Barium sulide accounted for most of the sulphur, with the balance present in the form of unreacted amorphous $BaSO_4$ (Hopwood and Mann, 1997). It should be noted that the barium silicate compounds are essentially combinations of SiO_2 and BaO units; this is a well-known system that has been extensively studied (Grebenshchikov and Toropov, 1962; Hesse and Liebau, 1980; Tyurnina *et al*., 2006; Rai and Mountjoy, 2014; Boulay *et al*., 2014). The combination of these two compounds in various mole ratios generates seven possible solid phases, i.e. Ba_3SiO_5, Ba_2SiO_4, $BaSiO_3$, $Ba_2Si_3O_8$, $Ba_5Si_8O_{21}$, $Ba_3Si_5O_{13}$ and $BaSi_2O_5$ (Figure 5-10) (Boulay *et al*., 2014).

Although barium sulfate is insoluble in water, its reaction with silicon has the potential to produce soluble reaction products. The barium-containing reaction products predicted by EKVI and MTDATA simulations are to a certain degree soluble in water. Barium sulfide has a solubility of ca. 9 g per 100 mL of water at 20 °C. Although barium silicates are not all stable in the presence of water and over time barium may leach, they undergo hydration reactions and may partially decompose to form free $Ba(OH)_2$ (Tashiro *et al*., 1976). The latter is soluble and toxic. The solid residue obtained after burning the various compositions was contacted with water. All the residues produced a distinct "rotten egg" smell which confirmed the presence of sulide compounds as these are known to release H_2S due to hydrolysis in water. Analysis of the resulting leachate using ICP-OES showed dissolved barium in the range of 50 to 140 mg per gram of barium sulfate reacted for the different compositions. Pure barium sulfate was also contacted with water and virtually no barium was detected in the resultant solution. This confirmed that the barium detected was due to the products formed. The degree of barium dissolution was generally low. This was thought to result from the barium sulfide being trapped within the glassy amorphous silicate phase. Although the amount of dissolved barium was relatively low, it should be noted that the maximum contaminant level (MCL) of barium in drinking water is 2 mg L^{-1} (WHO, 2004). Acute exposure at levels above this can potentially cause gastrointestinal disturbances and muscular weakness. Long-term exposure results in hypokalemia, which can lead to ventricular tachycardia, hypertension and/or hypotension, muscle weakness and paralysis (Jacobs *et al*., 2002).
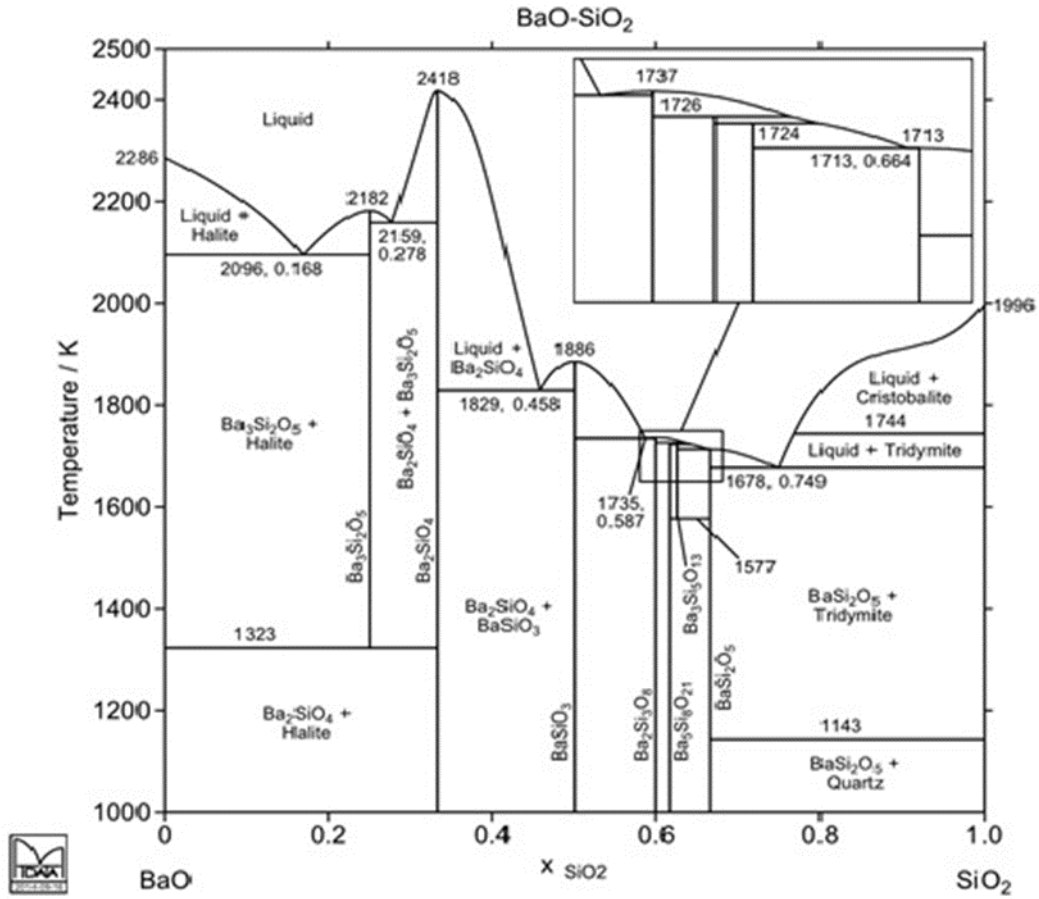
Figure 5-10   Phase diagram for the BaO-SiO₂ system produced using the MTDATA software

CHAPTER 6   RESULTS: THE EFFECT OF ADDITIVES ON THE BURN RATE OF THE SILICON-CALCIUM SULFATE DELAY COMPOSITIONS

6.1   Effect of Fuel Particle Size on the Si-CaSO₄ Pyrotechnic Reaction

6.1.1   Particle Size Distribution of Silicon Fuels

Figure 6-1 and Table 6-1 report the particle size distribution (PSD) and BET surface areas of the silicon fuels used to investigate the effect of particle size on the reactivity of the Si-$CaSO_4$ composition.
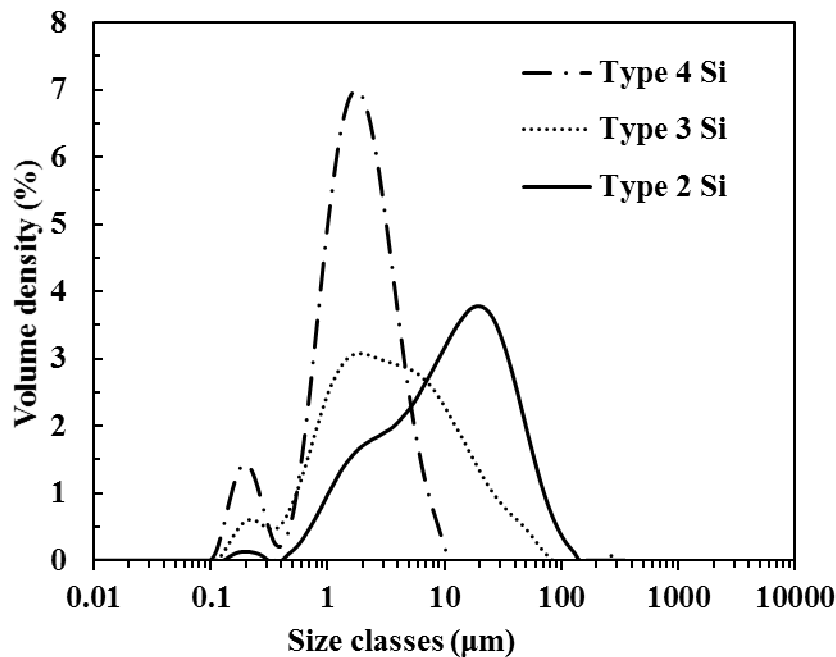
Figure 6-1   Particle size distribution of the Type 2, 3 and 4 silicon fuel powder

Table 6-1   Volume-based particle size distribution and BET surface areas of different silicon fuel powders

	D_{10} (µm)	D_{50} (µm)	D_{90} (µm)	BET ($m^2\,g^{-1}$)
Silicon Type 2	1.97	15.8	98.65	4.01
Silicon Type 3	0.83	5.02	65.43	10.46
Silicon Type 4	0.61	1.85	4.58	11.02

82

6.1.2 Thermal Stability of Reactants

Figure 6-2 shows the oxidation behaviour of silicon powders with different particle sizes. Types 3 and 4 silicon had similar thermogravimetric behaviour throughout the temperature range tested and attained similar mass gains. However, Type 2 silicon, which had larger particles with a smaller surface area, had a lower mass increase. The theoretical mass increase assuming total conversion was expected to be approximately 114%. However, this was not attained as SiO_2 has been shown to have some passivation properties (Dingemans *et al*., 2011; Tichapondwa *et al*., 2013). The thermal stability of calcium sulfate is also shown in Figure 6-2. The anhydrous $CaSO_4$ was stable beyond 1 000 °C, with the onset of decomposition being above 1100 °C.
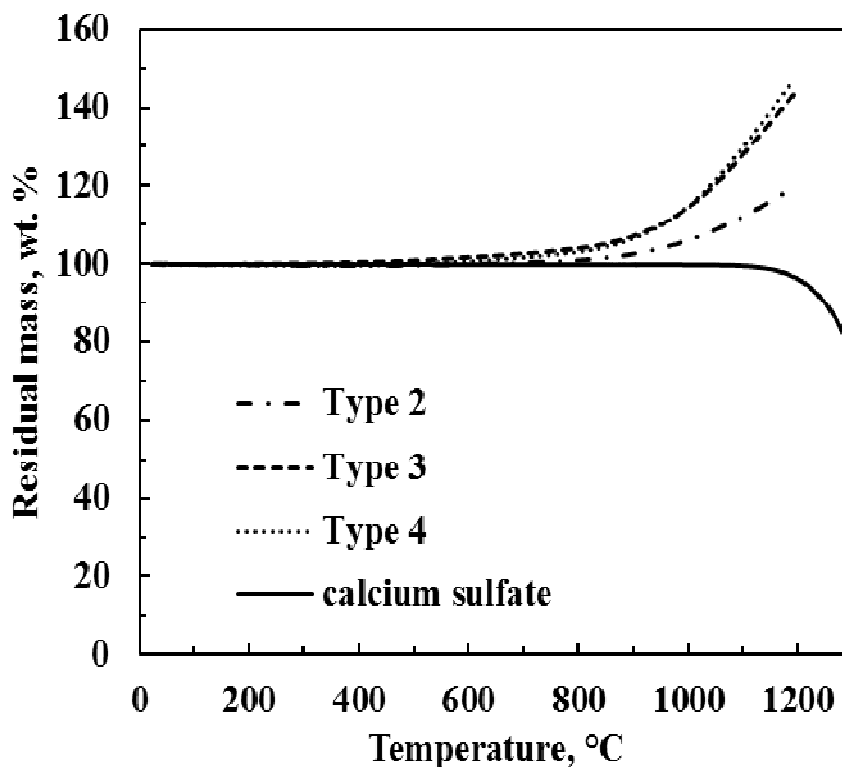
Figure 6-2 TGA results for silicon powders with different particle sizes in an oxygen atmosphere and that of calcium sulfate recorded in a nitrogen atmosphere

6.1.3 Effect of Particle Size on the Energy Output

The effect of the silicon stoichiometry and particle size on the energy output of Si-$CaSO_4$ compositions is shown in Figure 6-3. The general trend was that energy output decreased linearly with increase in Si content. The energy outputs for compositions with the same fuel

83

content but different particle sizes was almost similar. These results were analogous to observations made by Berger *et al*. (1996) who reported that the particle size of the reducing agent does not influence the heat of reaction. However, other researchers have recorded slight increases in heat of reaction for compositions with smaller particle sizes (Bernard *et al*., 1980; Kosanke *et al*., 2004).
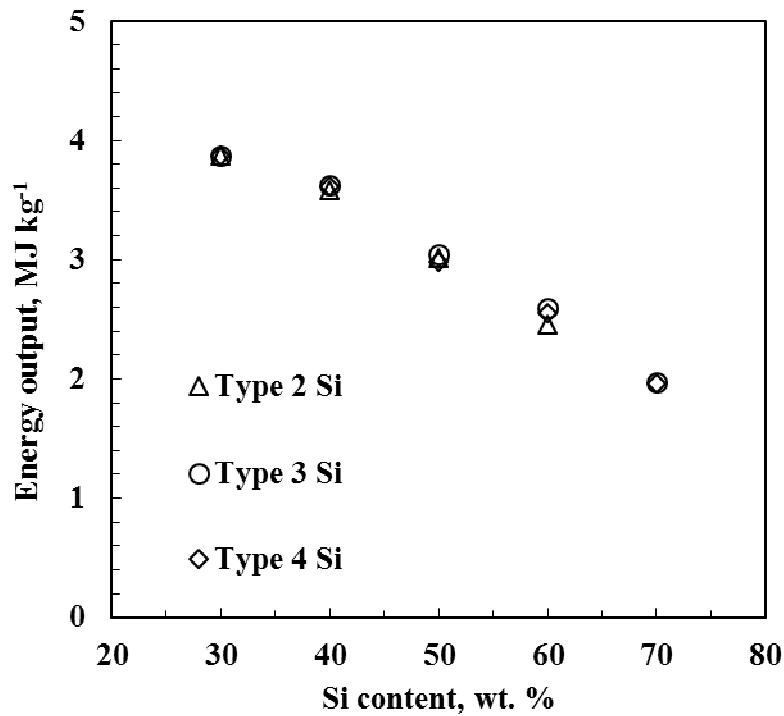
Figure 6-3   Energy outputs obtained with the bomb calorimeter in a helium atmosphere for Si-CaSO$_4$ compositions prepared using silicon powders with different particle sizes

6.1.4   Effect of Particle Size on the Pressure Response Time

The time-dependent changes in pressure, relative to the initially applied helium pressure of 3.0 MPa, for the 30 wt.% Si-CaSO$_4$ compositions prepared using silicon of varying particle sizes, are shown in Figure 6-4. Table 6-2 shows the parameters extracted from these profiles. There was a clear trend for the rate of pressure rise, as well as the maximum peak pressure, to increase with decreasing particle size. The time to reach maximum pressure increased with increase in particle size, with the Type 2 silicon taking 1.26 seconds and the Type 4 silicon 1.14 seconds. The increase in pressure for this system resulted primarily from a rise in temperature within the closed bomb system, rather than from the amount of evolved gas (Tichapondwa *et al*., 2015). Since the energy released by the three different particle sizes was almost comparable,

the marked difference in the pressure profiles was attributed to a variation in the rate of heat release.
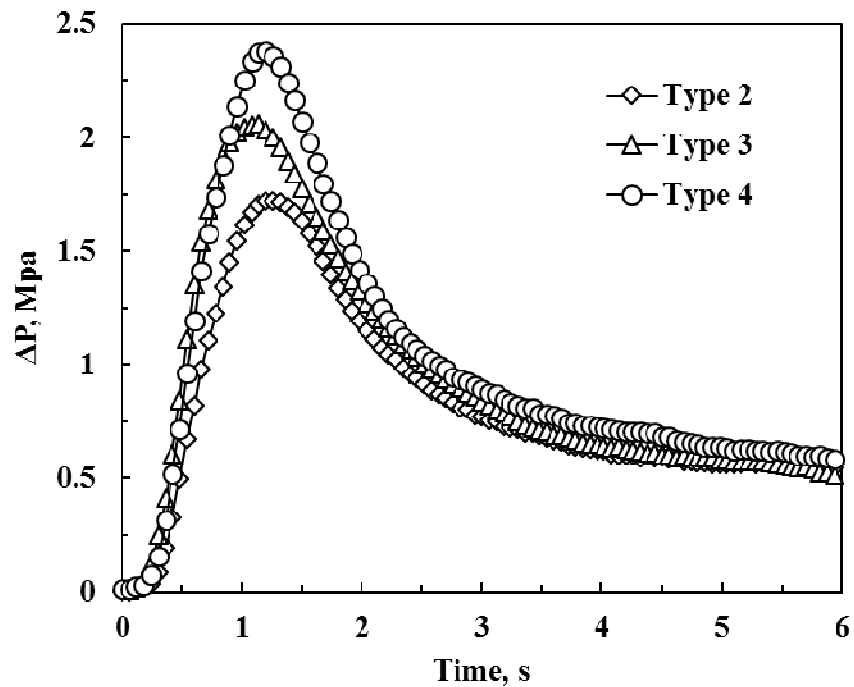
Figure 6-4 Comparison of increase in pressure with time for 30 wt.% Si-CaSO$_4$ compositions prepared using silicon with different particle sizes tested during the bomb calorimetry experiments in a helium atmosphere

Table 6-2 Energy output and peak pressures, times to reach the peak pressure and the maximum pressurisation rates extracted from the relative pressure–time profiles measured in the bomb calorimeter for 30 wt.% Si-CaSO$_4$ compositions

Silicon used	Type 2	Type 3	Type 4
P_{max} (MPa)	1.72	2.06	2.38
t_{max} (s)	1.26	1.20	1.14
dP/dt_{max} (MPa s^{-1})	3.04	4.45	4.62
Energy output (MJ kg^{-1})	3.87	3.87	3.87

6.1.5   Effect of Particle Size and Surface Area on the Burn Rates

The effect of particle size on the burn rate of the $Si-CaSO_4$ composition is shown in Figure 6-5. The composition prepared using the smallest particle size, Type 4 silicon ($d_{50} = 1.85$ µm), had the fastest burn rates (6.9–12.5 mm s^{-1}). Compositions prepared from Type 3 silicon ($d_{50} = 5.02$ µm) had slightly lower burn rates which ranged from 6.6 to 11.0 mm s^{-1}. However, compositions based on the coarser silicon Type 2 grade showed a decrease in burn rate by nearly a factor of two. Also, unlike the compositions prepared from the other two silicon samples which sustained burning in the range of 30 to 70 wt.% silicon, the Type 2 compositions only sustained burning for the 30 and 40 wt.% silicon, respectively. The decrease in burn rate was attributed to a decrease in the active surface area and the number of contact points within the particles of a given composition (Shimizu *et al*., 1990; Brown *et al*., 1998, Valliappan and Puszynski, 2003). The larger particles also required more energy over a longer time period to heat them up to the required reaction temperature compared with the smaller particles, which increases the activation energy and results in lower burn speeds (Kosanke *et al*., 2004). Figure 6-6 shows the effect of surface area on the burn rate for the 30 wt.% silicon composition. These results confirm that decreasing the fuel surface area increases combustion speed.
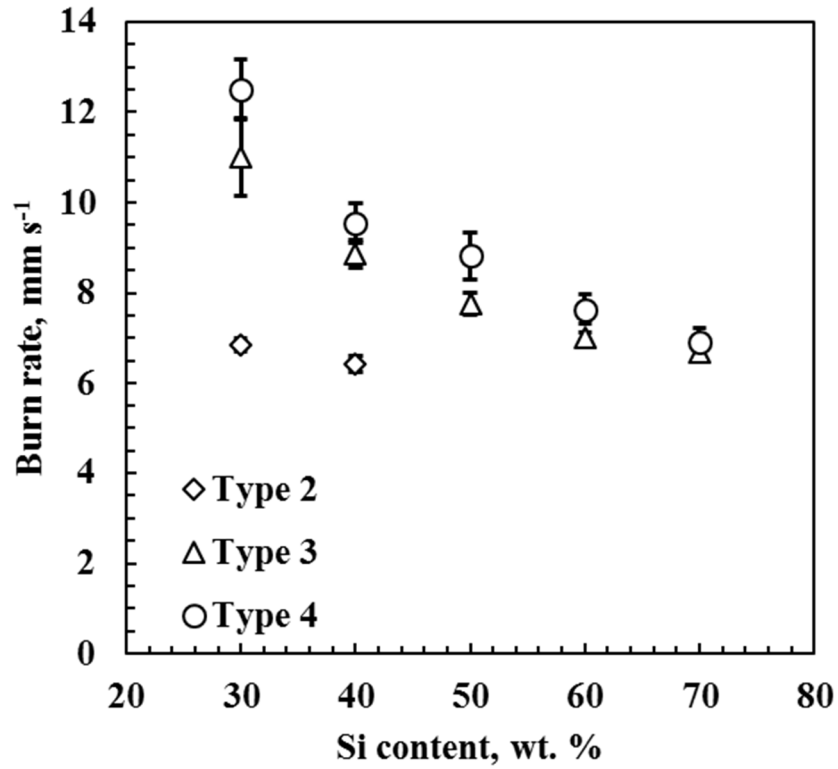
Figure 6-5 Effect of stoichiometry and particle size on the burn rate of Si-CaSO$_4$ compositions
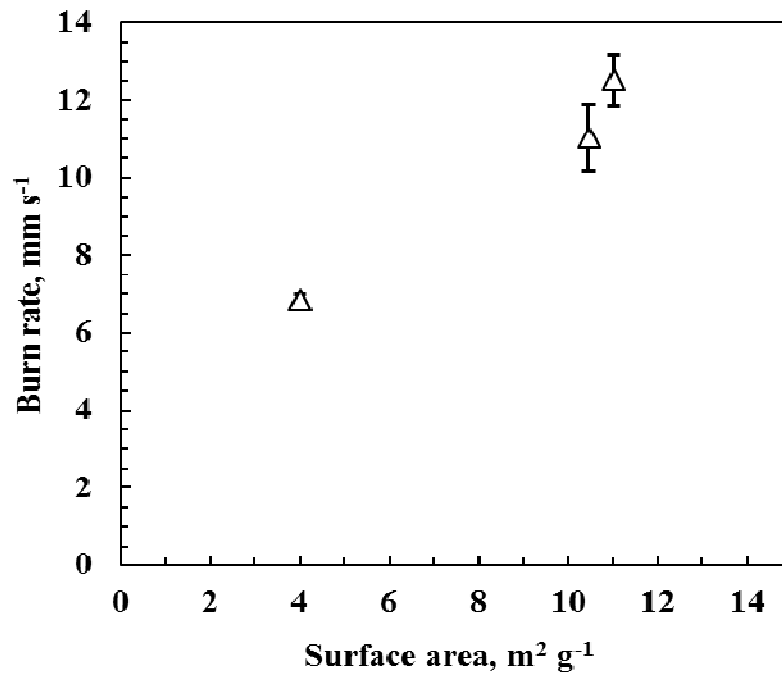
Figure 6-6 Influence of silicon surface area on the burn rate of the 30 wt.% Si-CaSO$_4$ compositions

6.2 Influence of Additives on the Si + CaSO₄ Pyrotechnic Reaction

6.2.1 Effect of Fuel Substitution on Burn Rate

Table 6-3 Effect of fuel additives on the burn rate and energy output of a 30 wt.% Si-CaSO₄ composition (25% Si + 5% fuel additive + 70% CaSO₄). The median particle size (d$_{50}$) and BET surface area properties of the fuels used are also indicated.

Fuel	Particle size d$_{50}$ (μm)	BET surface area (m^2 g^{-1})	Energy output (MJ kg^{-1})	Burn rate (mm s^{-1})
None (control)	-	-	3.8 ± 0.04	12.7 ± 0.7
B	2.1	6.7	3.9 ± 0.03	16.6 ± 1.7
Mn	23.4	0.3	4.1 ± 0.03	18.9 ± 1.3
Al	10.2	0.1	4.3 ± 0.13	31.8 ± 3.2
W	6.3	0.2	3.9 ± 0.08	#
S	–	4.2	4.1 ± 0.08	#
C	10.8	75.0	3.4 ± 0.08	#

$^{\#}$ Did not sustain burning in the aluminium tubes

The effect of substituting 5 wt.% of silicon with an alternative fuel on the burn rate and energy output of a 30 wt.% Si-CaSO₄ composition is shown in Table 6-3. All the compositions prepared ignited during bomb calorimetry in an inert helium atmosphere. The energy outputs for all the compositions (4.04 ± 0.16 MJ kg^{-1}) were slightly higher than the energy recorded for the binary control composition (3.87 ± 0.04 MJ kg^{-1}). The carbon-substituted composition, however, had a significantly lower energy output of 3.40 ± 0.01 MJ kg^{-1}. Substitution of silicon with alternative fuels increased the burn rate, with the highest burn rate recorded for the aluminium-substituted composition (31.8 mm s^{-1}). However, the formulations prepared using tungsten, sulphur and carbon did not propagate in the aluminium tubes. Carbon and calcium sulfate are known to undergo endothermic redox reactions at high temperatures (Van der Merwe *et al.*, 1999). It was postulated that addition of small amounts carbon black would reduce the burning rate by reducing the fraction of energy fed forward to the adjacent unreacted layers in the packed tubes.

Although tungsten has a higher thermal conductivity compared to silicon, it has a lower thermal diffusivity (Khaikin and Merzhanov, 1966). The tungsten therefore is less effective at transmitting the thermal energy, stifling propagation along the length of the tubes. Sulphur has a low melting temperature (115 °C) and was expected to act as a flux upon melting and possibly increase the burn rate. However, it also has a low vaporisation temperature (445 °C) which is lower than the ignition temperature of the composition; hence the fluxing effect is lost as sulphur sublimes and takes away energy from the system during the vaporisation (Conkling, 1985). The fast burn rates obtained with aluminium were attributed to the combined effect of the aluminium acting as a flux as it melts at 660 °C and increasing the overall thermal conductivity of the mixture.

6.2.2 Effect of Oxidiser Substitution on the Burn Rate

Table 6-4 reports the effect of replacing 5 wt.% of $CaSO_4$ with an equivalent amount of alternative oxidiser. The substitution did not have an appreciable effect on the energy output of the reaction, however, effects of the burn rate were noted. Substitution with V_2O_5, Sb_2O_3 and $CuSb_2O_4$ decreased the burn rate from 12.5 mm s^{-1} to 10.6, 10.9 and 11.4 mm s^{-1}, respectively. A faster burn rate of ca. 16.8 mm s^{-1} was recorded upon substitution with bismuth trioxide (Bi_2O_3). Compositions substituted with MnO_2 and CuO did not sustain combustion when pressed into aluminium tubes. The copper oxide has a high melting point (1326 °C) and it does not decompose or liberate gaseous oxygen below the melting temperature (Goswami and Trehan, 1957; Ren *et al*., 2002). It is likely that it acted by drawing heat from the main reaction, resulting in the stifling of the reaction. Beck and Flanagan (1992) patented the use of V_2O_5, which has a melting temperature of 600 °C, as a fluxing agent in the Si-BaSO$_4$ reaction. Their results showed comparable burn rates, regardless of the addition of V_2O_5. In addition, there are fewer failures with compositions containing V_2O_5. In the present results, the addition of V_2O_5 slightly increased the energy output but lowered the burn rate of the reaction. This implies that V_2O_5 did not participate in the reaction or alter its pathway. The lower burn rates are possibly due to some of the energy being used up in melting the V_2O_5, resulting in a lower fraction of energy being fed forward to the next layers.

89

Table 6-4   Effect of oxidiser additives on the burn rate and energy output of a 30 wt.% Si-CaSO$_4$ composition (30% Si + 65% CaSO$_4$ + 5% oxidiser). The median particle size (d$_{50}$) and BET surface area properties of these oxidisers are also shown.

Oxidiser	Particle size d$_{50}$ (μm)	BET surface area (m^2 g^{-1})	Energy output (MJ kg^{-1})	Burn rate (mm s^{-1})
None (control)	-	-	3.8 ± 0.04	12.7 ± 0.7
V$_2$O$_5$	10.1	5.5	4.0 ± 0.02	10.6 ± 1.5
Sb$_2$O$_3$	0.9	2.4	3.8 ± 0.04	10.9 ± 1.5
CuSb$_2$O$_4$	9.3	1.1	3.9 ± 0.06	11.4 ± 1.3
Bi$_2$O$_3$	8.8	0.8	4.0 ± 0.06	16.8 ± 0.9
MnO$_2$	8.3	13.6	4.2 ± 0.05	#
CuO	12.7	1.6	3.9 ± 0.07	#

$^{#}$ Did not sustain burning in the aluminium tubes

6.2.3   Effect of Addition of Diluents on the Burn Rate

Inert materials are deliberately added to a composition so as to slow down the burn rate to a desirable speed (McLain, 1980; Conkling, 1985; Beck and Brown, 1986). Ideally, these inert materials are not expected to participate in the pyrotechnic reaction. Rather they function as thermal insulators that retard the rate of layer-by-layer propagation within the composition. A fixed 5 wt.% of several inert materials was added to the 30 wt.% Si-CaSO$_4$ composition. All the compositions ignited in the bomb calorimeter and featured heats of reaction that were comparable to that of the control (Table 6-5). However, none of these compositions sustained burning when pressed into the aluminium elements. This includes the composition that had fumed silica added; it has previously been shown to either increase or maintain the burn rate in several compositions as it acts as a mixing aid (Ricco *et al*., 2004; Kalombo *et al*., 2007; Swanepoel *et al*., 2010). It was postulated that besides the thermal insulation effect of the inert materials, their addition also increases the activation energy of the composition, making it more difficult to ignite. The collective effect of these variables can be summarised using the Frank-Kamenetzky diagram (Figure 2-2) which defines the conditions necessary for a reaction to ignite and propagate (Merzhanov and Averson, 1971). According to this diagram, self-ignition

of a composition is only possible when the rate of heat generation within the material exceeds the rate at which heat is lost by radiation, convection and conduction to the surroundings. Since addition of inert material affected the thermal conductivity of the formulation and the rate of the reactions (owing to the separation of the reactants), it modified the position of the composition on the diagram and moved it to a position where propagation cannot take place.

Table 6-5 Effect of addition of 5 wt.% inert materials on the energy output and burn rate of the 30 wt.% Si-CaSO$_4$ composition (30% Si + 70% CaSO$_4$ + 5% inert material). The median particle size (d$_{50}$) and BET surface area properties of these additives are also shown.

Fuel	Particle size d$_{50}$ (μm)	BET surface area (m^2 g^{-1})	Energy output (MJ kg^{-1})
None (control)	-	-	3.8 ± 0.04
Fumed silica	-	-	3.7 ± 0.11
Vermiculite	10.7	15.8	3.8 ± 0.81
Silica	9.7	1.3	3.9 ± 0.10
Wollastonite	115	0.1	4.0 ± 0.05
Attapulgite	9.7	72.9	4.0 ± 0.05

6.2.4 Effect of Additive Content on the Burn Rate of the Stoichiometric Composition for Selected Additives

Based on the results reported in Tables 6-3, 6-4 and 6-5, Al, V$_2$O$_5$, Bi$_2$O$_3$ and fumed silica were chosen for further investigation. The fumed silica was included in this set of additives to ascertain that its effect on the composition was not a result of too much inert material having been added to the compositions reported in Table 6-5. In these tests, the amount of additive added to or substituted in the Si-CaSO$_4$ base composition ranged from 1 to 10 wt.%. Figure 6-7 reports the burn rates obtained. In the case of aluminium, the burn rate increased with increases in the amount added, with the 10 wt.% composition having a burn rate of 43 mm s^{-1}, i.e. a 244% increase in the burn rate. Substitution of CaSO$_4$ with Bi$_2$O$_3$ also resulted in an increase in the burn rate with increases in the amount of Bi$_2$O$_3$ substituted. This increase occurred until the 5 wt.% composition, after which the burn rate remained constant at ca. 17.4 mm s^{-1}. Vanadium pentoxide resulted in a decrease in the burn rate with increases in the amount added, i.e. from 12.5 to 8.7 mm s^{-1}. Increasing the amount from 7.5 to 10 wt.% did not result

91

in any further decrease. The addition of 1 wt.% of fumed silica stifled combustion in the aluminium tubes. This indicates that the Si-CaSO$_4$ composition is very sensitive to the presence of inert diluents.
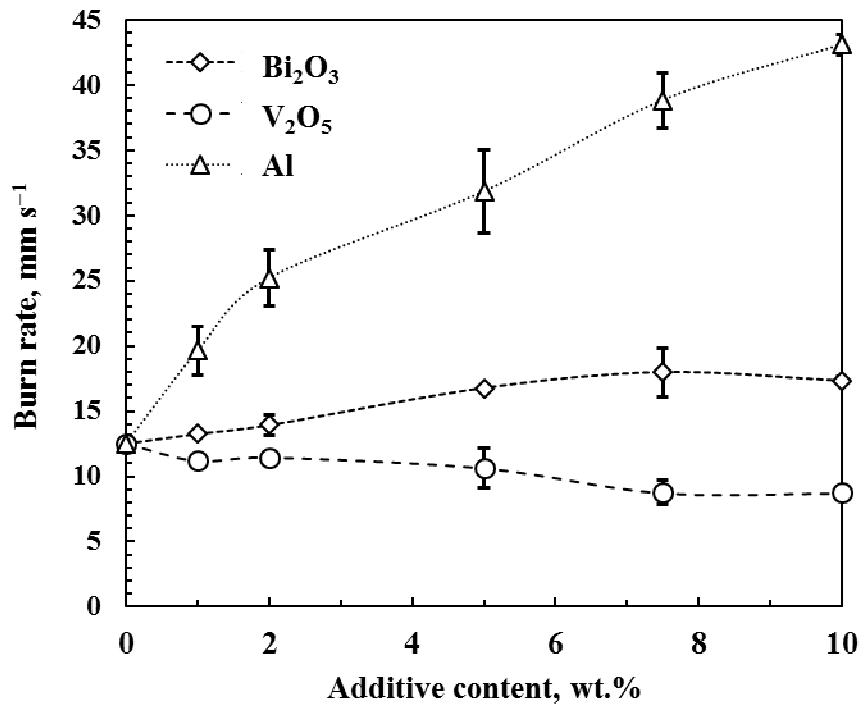
Figure 6-7   Effect of the amount of additive substituted on the burn rate of the 30 wt.% Si–CaSO$_4$ composition

6.2.5   5 wt.% Al Substitution of Si in the 30–70 wt.% Fuel Range

Figure 6-7 shows the burn rates obtained when 5 wt.% of the silicon fuel was substituted with an equal mass of aluminium powder in the 30–70 wt.% fuel range. The influence of the aluminium addition was more pronounced in the 30 and 40 wt.% fuel compositions. The burn rate for these two composition increased from 12.5 mm s^{-1} to 36.7 mm s^{-1} and 9.5 mm s^{-1} to 23.9 mm s^{-1}, respectively. The compositions with a fuel composition of 50 wt.% and above had comparable burn rates regardless of the Al addition. The influence of Si substitution with aluminium at different fuel stoichiometries on the energy output of the composition is shown in Figure 6-8. The energy outputs increased by approximately 0.31 MJ kg^{-1} for the all the fuel stoichiometries tested. This indicates that the aluminium participated in the reaction, which in turn altered the reaction mechanism. EKVI simulations of these compositions further support this assertion as they revealed product spectra (Table 6-6) that were different from those predicted for the base composition (Tichapondwa *et al*., 2015). The markedly lower burn rates

92

recorded for compositions at 50 wt.% fuel and beyond were thought to result from the absorption of energy by the excess fuel, thus taking heat away from the main reaction.
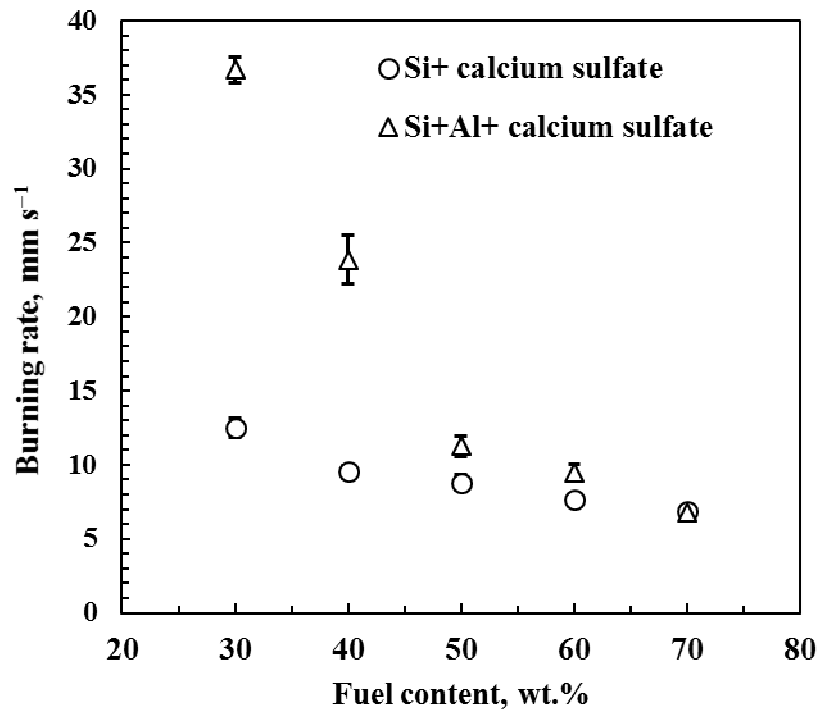
Figure 6-8   Effect of stoichiometry and 5 wt.% Si substitution with 5 wt.% Al on the burn rate of the Si-CaSO$_4$ composition

93

Table 6-6   Major solid reaction products of the Si-Al-CaSO$_4$ composition predicted using EKVI thermodynamics code under adiabatic conditions

Fuel (wt.%)	Si	Al	Al$_2$O$_3$	CaS	CaAl$_4$O$_7$	Ca$_2$SiO$_4$	CaAl$_2$Si$_2$O$_8$
10	-	-	-	2.9	67.5	29.2	0.4
20	0.9	-	41.5	25.8	-	8.2	23.7
30	14.5	-	39.5	26.6	-	-	19.2
40	26.5	-	42.6	24.4	-	-	6.4
50	36.3	2.0	40.3	21.6	-	-	-
60	44.4	6.3	32.2	17.1	-	-	-
70	52.4	10.6	24.2	12.8	-	-	-
80	60.5	14.9	16.1	8.6	-	-	-
90	68.6	19.1	8.1	4.3	-	-	-
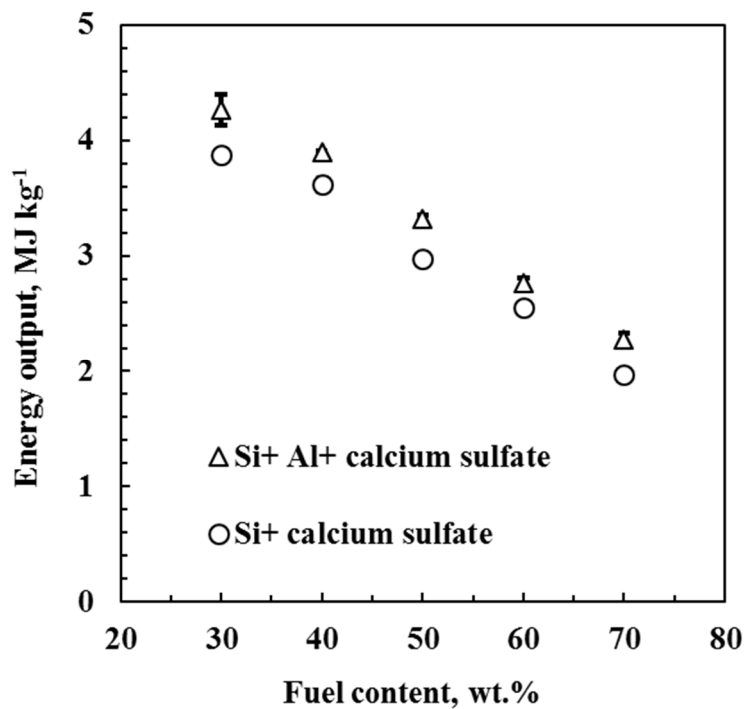
Figure 6-9   Effect of stoichiometry and 5 wt.% Si substitution with aluminium on the energy output of the Si-CaSO$_4$ composition

CHAPTER 7   CONCLUSIONS AND RECOMMENDATIONS

Calcium sulfate was shown to be a viable oxidant for silicon in slow to intermediate-burning time delay compositions. The energy outputs, pressure–time profiles and burn rate measurements all showed a general trend of decreasing with increasing silicon content. XRD analysis of the reaction products revealed that the products were a composite mixture of crystalline and amorphous phases. The fair agreement between the EKVI simulation results and the present experimental data suggested that the metal-oxidant reaction proceeded to form the thermodynamically favoured products. Both the reactants and the products of the composition tested are environmentally benign.

The Si-BaSO$_4$ composition was characterised and compared with that of silicon and calcium sulfate. Barium sulfate has a higher thermal degradation temperature than calcium sulfate. In both systems the energy output, the pressure generated, the amount of gas generated and the burn rate decreased with increasing silicon content. Except for the burn rates, these performance indices were lower with barium sulfate as the oxidant. The reaction residues for the BaSO$_4$ compositions were essentially XRD-amorphous, but minor amounts of crystalline SiO$_2$ and unreacted silicon were detected. EKVI and MTDATA thermodynamic simulations for the Si-BaSO$_4$ system provided insight into the possible composition of the amorphous phase. The solid reaction products formed by the Si-BaSO$_4$ compositions released soluble barium ions when contacted with water. Both systems were relatively insensitive to impact, friction and electrostatic discharge stimuli at a silicon content of 30 wt.%.

The influence of fuel particle size and the addition of various additives on the burn properties of the Si-CaSO$_4$ reaction was investigated. Differences in fuel particle size had no effect on the energy outputs of the reaction. However, the burn rates decreased with increasing particle size. It was also shown that the burn rate of the Si-CaSO$_4$ composition can be tuned to burn faster or slower using a wide range of additives. Fuel-based additives generally increased the combustion velocity, whereas oxidisers reduced it. An exception was noted for bismuth trioxide which increased the burn rate. The base composition was established to be sensitive to the presence of unreactive diluents, even at low concentrations, as the formulations tested did not ignite or propagate when pressed into aluminium tubes.

Spray drying of pyrotechnic formulations is used to produce well-mixed, free-flowing granules that are suitable for the automated element filling process. The spray drying process requires that the components of the composition be mixed in water to form slurries before spraying.

With this in mind, it is recommended that further tests be carried out on the Si-CaSO$_4$ composition in order to determine the effect that contacting the reactants with water has on the burn properties. It is recommended that the β-anhydrite that was used throughout this study be used for these tests as it has a lower possibility of rehydrating unlike the other calcium sulfate forms. In order to produce free-flowing spherical agglomerates that are mechanically sound and non-dusting after spray drying it is often necessary to add organic binders to the slurry solutions. These have the potential of modifying the burn behaviour of the composition. It is therefore further recommended that the effect of binder additives be investigated using the commercially available binders that are currently used in industry. Finally, the Si-CaSO$_4$ compositions were found to be highly sensitive to the presence of inert additives when using aluminium elements with an internal diameter of 3.6 mm. The geometry of the element is known to affect the propagation of pyrotechnic compositions. Therefore is also recommended that investigations be carried out using elements with wider internal diameters.

REFERENCES

AL-KAZRAJI, S. & REES, G. 1978. The fast pyrotechnic reaction of silicon and red lead. Part 1. Differential thermal analysis studies. *Combustion and Flame,* 31, 105-113.

AL-KAZRAJI, S. & REES, G. 1979a. Differential thermal analysis studies of the reactions of silicon and lead oxides. *Journal of Thermal Analysis and Calorimetry,* 16, 35-39.

AL-KAZRAJI, S. S. & REES, G. J. 1979b. The fast pyrotechnic reaction of silicon and red lead: heats of reaction and rates of burning. *Fuel,* 58, 139-143.

AL-KAZRAJI, S. S. 1982. Pyrotechnic reactions of silicon and lead oxides. *PhD Thesis*, Polytechnic of Wales, UK.

AL-KAZRAJI, S. S., DOULAH, M. S. & REES, G. J. 1980. Gas-less combustion reactions: a mathematical model for the analysis of the self-sustained combustion between silicon and red lead in a compressed form. *Fuel,* 59, 598-600.

ALDUSHIN, A. & KHAYKIN, B. 1975. Agency of the thermal physical characteristics on stability of stationary burning of off-gas systems. *Combustion Explosion and Shock Waves,* 1, 128-134.

AUBÉ, R. 2011. Delay compositions and detonation delay device utilizing same. *US Patent 8066832 B2*

BARTON, T. J., GRIFFITHS, T., CHARSLEY, E. L. & RUMSEY, J. 1982. The role of organic binders in pyrotechnic reactions. *8th International Pyrotechnics Seminar,* 12–16 July 1982, Steamboat Springs, CO, USA.

BAYLEY, A., CHAPMAN, D., WILLIAMS, M. & WHARTAN, R. 1992. The handling and processing of explosives. *Proceedings of the 18th International Pyrotechnics Seminar*, 13–17 July 1992, Breckenridge, CO, USA, pp 33-49.

BECK, M. 1989. *A preliminary investigation into the Si/BaSO₄ combustion mechanism.* Ardeer Site: ICI Explosives Group.

BECK, M. W. & BROWN, M. E. 1986. Modification of the burning rate of antimony/potassium permanganate pyrotechnic delay compositions. *Combustion and Flame,* 66, 67-75.

BECK, M. W. & FLANAGAN, J. 1992. Delay composition and device. *US Patent 5 147 476.*

BERGER, B. 2005. Parameters influencing the pyrotechnic reaction. *Propellants, Explosives, Pyrotechnics,* 30, 27-35.

BERGER, B., HAAS, B. & REINHARD, G. 1996. Influence of the particle size of the reducing agent on the reaction parameters of pyrotechnic redox systems. *27th International Annual Conference of the Fraunhofer ICT, Fraunhofer-Institut für Chemische Technologie Jahrestagung,* 25–28 June 1996, Karlsruhe, Germany.

BERNARD, M. L., ESPAGNAQ, A. & BRANKA, R. 1980. On the importance of thermochemical parameters in solid-solid pyrotechnic reactions. *7th International Pyrotechnics Seminar,* 14–18 July 1980, Vail, CO, USA.

BOBERG, T., CARLSSON, S., EKMAN, B.-M. & KARLSSON, B. 1997. A nontoxic, water-insoluble mixture comprising dibismuth trioxide oxidiser, silicon fuel. *US Patent 5654520.*

BODDINGTON, T., LAYE, P. G., MORRIS, H., ROSSER, C. A., CHARSLEY, E. L., FORD, M. C. & TOLHURST, D. E. 1975. A study of pyrotechnic reactions by temperature profile analysis and differential thermal analysis. *Combustion and Flame,* 24, 137-138.

BOULAY, E., NAKANO, J., TURNER, S., IDRISSI, H., SCHRYVERS, D. & GODET, S. 2014. Critical assessments and thermodynamic modeling of BaO–SiO₂ and SiO₂–TiO₂ systems and their extensions into liquid immiscibility in the BaO–SiO₂–TiO₂ system. *Calphad,* 47, 68-82.

BRAMMER, A. J., CHARSLEY, E. L., GRIFFITHS, T. T., ROONEY, J. J. & B., W. S. 1996. A study of the pyrotechnic performance of the silicon-bismuth oxide system. *22nd International Pyrotechnics Seminar,* 15–19 July 1996, Fort Collins, CO, USA.

BROWN, M. E. 2001. *Introduction to Thermal Analysis: Techniques and Applications.* Springer Science & Business Media.

BROWN, M. E., TAYLOR, S. J. & TRIBELHORN, M. J. 1998. Fuel–oxidant particle contact in binary pyrotechnic reactions. *Propellants, Explosives, Pyrotechnics,* 23, 320-327.

CALLISTER, W. D. & RETHWISCH, D. G. 2007. *Materials Science and Engineering: An Introduction.* Wiley, New York.

CASPARI, W. 1936. Calcium sulfate hemihydrate and the anhydrites. I. Crystallography. *Proceedings of the Royal Society of London. Series A, Mathematical and Physical Sciences,* 155, 41-48.

CHARSLEY, E., CHEN, C.-H., BODDINGTON, T., LAYE, P. & PUDE, J. 1980. Differential thermal analysis and temperature profile analysis of pyrotechnic delay systems: ternary mixtures of silicon, boron and potassium dichromate. *Thermochimica Acta,* 35, 141-152.

CONKLING, J. A. 1985. *Chemistry of Pyrotechnics, Basic Principles and Theory.* Marcel Dekker, Inc., New York.

CONKLING, J. A. 2001. Pyrotechnics. In: *Kirk-Othmer Encyclopedia of Chemical Technology*, Wiley Online Library.

CONKLING, J. A. & MOCELLA, C. 2010. *Chemistry of Pyrotechnics: Basic Principles and Theory.* CRC Press, Boca Raton, FL, USA.

CRAMER, R. 2012. Green energetic materials: An overview. *38th International Pyrotechnics Seminar*, 10–15 June 2012, Denver, CO, USA.

DANALI, S., PALAIAH, R. & RAHA, K. 2010. Developments in pyrotechnics (Review Paper). *Defence Science Journal,* 60, 152-158.

DAVIES, R., DINSDALE, A., GISBY, J., ROBINSON, J. & MARTIN, S. 2002. MTDATA-thermodynamic and phase equilibrium software from the National Physical Laboratory. *Calphad,* 26, 229-271.

DAVITT, A. L. & YUILL, K. A. 1983. Delay composition for detonators. *US Patent 4374686.*

DEAL, B. E. & GROVE, A. 1965. General relationship for the thermal oxidation of silicon. *Journal of Applied Physics,* 36, 3770-3778.

DINGEMANS, G., VAN DE SANDEN, M. & KESSELS, W. 2011. Excellent Si surface passivation by low temperature SiO_2 using an ultrathin Al_2O_3 capping film. *Physica Status Solidi (RRL)-Rapid Research Letters,* 5, 22-24.

DREIZIN, E. L. 2009. Metal-based reactive nanomaterials. *Progress in Energy and Combustion Science,* 35, 141-167.

DRENNAN, R. L. & BROWN, M. E. 1992. Binary and ternary pyrotechnic systems of Mn and/or Mo and BaO_2 and/or SrO_2. Part 2. Combustion studies. *Thermochimica Acta,* 208, 223-246.

DUBIN, J. 1949. Delay fuse compositions. *US Patent 2457860.*

DUNMEAD, S. D., READEY, D. W., SEMLER, C. E. & HOL, J. B. 1989. Kinetics of combustion synthesis in the Ti-C and Ti-C-Ni systems. *Journal of the American Ceramic Society,* 72, 2318-2324.

ELLERN, H. 1968. *Military and Civilian Pyrotechnics.* Chemical Publishing Company, New York.

FORDHAM, S. 2013. *High Explosives and Propellants*. Elsevier, Burlington, VT, USA.

GLADUN, V. & BASHAEVA, L. 1995. High-temperature synthesis of wollastonite and possibilities of its using in pyrotechnics. *21st International Pyrotechnics Seminar*, 11–15 September, Moscow, Russia.

GOLDSCHMIDT, H. 1908. Manufacture of thermic mixtures. *US Patent 906009.*

GOODFIELD, J. A. & REES, G. J. 1981. Pyrotechnic reaction of lead monoxide and silicon: Measurement of reaction temperature. *Fuel,* 60, 151-154.

GOODFIELD, J. A. & REES, G. J. 1985. Metal/oxidant combustion reactions: Variation of propagation rate with consolidation pressure. *Fuel,* 64, 1627-1630.

GOSWAMI, A. & TREHAN, Y. 1957. The thermal decomposition of cupric oxide *in vacuo*. *Proceedings of the Physical Society, Section B,* 70, 1005.

GREBENSHCHIKOV, R. & TOROPOV, N. 1962. New data on the barium oxide-silica phase diagram. *Bulletin of the Academy of Sciences of the USSR, Division of Chemical Science,* 11, 503-509.

HAARMANN, D. J. 1985. The few, the proud, the sulfates. *PGI Bulletin* 46.

HALE, G. C. 1931. Delay powder. *US Patent 1877127*.

HAND, R. 1997. Calcium sulfate hydrates: A review. *British Ceramic Transactions,* 96, 116-120.

HEDGER, J. 1983. Factors influencing the pyrotechnic reaction of silicon and red lead. *Propellants, Explosives, Pyrotechnics,* 8, 95-98.

HESSE, K.-F. & LIEBAU, F. 1980. Crystal chemistry of silica-rich barium silicates. *Zeitschrift für Kristallographie-Crystalline Materials,* 153, 3-18.

HILL, R., SUTTON, L., TEMPLE, R. & WHITE, A. 1950. Slow self-propagating reactions in solids. *Research,* 3, 569.

HOLT, B. D. & ENGELKEMEIR, A. 1970. Thermal decomposition of barium sulfate to sulphur dioxide for mass spectrometric analysis. *Analytical Chemistry,* 42, 1451-1453.

HOPWOOD, J. D. & MANN, S. 1997. Synthesis of barium sulfate nanoparticles and nanofilaments in reverse micelles and microemulsions. *Chemistry of Materials,* 9, 1819-1828.

ILUNGA, K., DEL FABBRO, O., YAPI, L. & FOCKE, W. W. 2011. The effect of Si-Bi_2O_3 on the ingnition of the Al-CuO thermite. *Powder Technology,* 205, 97-102.

JACOBS, I. A., TADDEO, J., KELLY, K. & VALENZIANO, C. 2002. Poisoning as a result of barium styphnate explosion. *American Journal of Industrial Medicine,* 41, 285-288.

JAKUBKO, J. 1999. Combustion of the silicon-red lead system. Temperature of burning, kinetic analysis and mathematical model. *Combustion Science and Technology,* 146, 37-55.

KALOMBO, L. 2005. Evaluation of Bi_2O_3 and Sb_6O_{13} as oxidants for silicon fuel in time delay detonators. *Master's Dissertation*, University of Pretoria, South Africa.

KALOMBO, L., DEL FABBRO, O., CONRADIE, C. & FOCKE, W. W. 2007. Sb_6O_{13} and Bi_2O_3 as oxidants for Si in pyrotechnic time delay compositions. *Propellants, Explosives, Pyrotechnics,* 32, 454-460.

KHAIKIN, B. & MERZHANOV, A. 1966. Theory of thermal propagation of a chemical reaction front. *Combustion, Explosion, and Shock Waves,* 2, 22-27.

KOCH, E. C. & CLEMENT, D. 2007. Special materials in pyrotechnics: VI. Silicon – an old fuel with new perspectives. *Propellants, Explosives, Pyrotechnics,* 32, 205-212.

KOSANKE, K., KOSANKE, B., STURMAN, B., SHIMIZU, T., WILSON, M., VON MALTITZ, I., HANCOX, R., KUBOTA, N., JENNINGS-WHITE, C. & CHAPMAN, D. 2004. *Pyrotechnic Chemistry*, Pyrotechnic Reference Series, No. 4. Huntingdon, UK, Journal of Pyrotechnics Inc. & CarnDu Ltd

KOSANKE, K. L., STURMAN, B. T., WINOKUR, R. M. & KOSANKE, B. 2012. *Encyclopedic Dictionary of Pyrotechnics (and Related Subjects)*. Huntingdon, UK, Journal of Pyrotechnics Inc. & CarnDu Ltd.

KRISHNAMOHAN, G., KURIAN, E. & RAO, H. Thermal analysis and inverse burning rate studies on silicon-potassium nitrate system. *Proceedings of the 8th International Pyrotechnic Seminar*, 12–16 July 1988, Steamboat Springs CO, USA.

LAYE, P. & CHARSLEY, E. 1987. Thermal analysis of pyrotechnics. *Thermochimica Acta,* 120, 325-349.

LEVENSPIEL, O. 1999. Chemical reaction engineering. *Industrial & Engineering Chemistry Research,* 38, 4140-4143.

LINZELL, H. K. 1947. Incendiary composition. *US Patent 2424937*.

MCINTYRE, F. L. 1978. Incident/Accident survey of pyrotechnic compositions. *Proceedings of the 6th International Pyrotechnic Seminar,* 17–21 July 1978, Estes Park, Denver CO, USA.

MCLAIN, J. H. 1980. *Pyrotechnics: From the Viewpoint of Solid State Chemistry,* Philadelphia, The Franklin Institute Press.

MCLAIN, J. H. & RUBLE, T. A. 1953. First fire charge composition. *US Patent 2643946*.

MELLOR, J. 1924. *A Comprehensive Treatise on Inorganic and Theoretical Chemistry.* Volume V. London, Longmans, Green and Company.

MERZHANOV, A. & AVERSON, A. 1971. The present state of the thermal ignition theory: An invited review. *Combustion and Flame,* 16, 89-124.

MEYERRIECKS, W. & KOSANKE, K. 2003. Color values and spectra of the principal emitters in colored flames. *Journal of Pyrotechnics,* 18, 1-22.

MIKLASZEWSKI, E. J., PORET, J. C., SHAW, A. P., SON, S. F. & GROVEN, L. J. 2014. Ti/C-3Ni/Al as a replacement time delay composition. *Propellants, Explosives, Pyrotechnics,* 39, 138-147.

MIL-STD-1751A 2001. *US Department of Defense Test Method Standard, Safety and Performance Tests for the Qualification of Explosives (High Explosives, Propellants, and Pyrotechnics).* US Department of Defense.

MOFFETT, D., SMITH, C., STEVENS, Y.-W., INGERMAN, L., SWARTS, S. & CHAPPELL, L. 2007. Toxicological profile for barium and barium compounds. US Department of Health and Human Services.

MOGHADDAM, A. Z. & REES, G. J. 1981. The fast pyrotechnic reaction of silicon with lead oxides: Differential scanning calorimetry and hot-stage microscopy studies. *Fuel,* 60, 629-632.

MOHAZZABI, P. & SEARCY, A. W. 1976. Kinetics and thermodynamics of decomposition of barium sulfate. *Journal of the Chemical Society, Faraday Transactions 1: Physical Chemistry in Condensed Phases,* 72, 290-295.

MORGAN, C. G. & RIMMINGTON, C. 2012. Manufacture of pyrotechnic time delay compositions. *US Patent 8118956.*

MOTT, N. 1993. *Conduction in Non-crystalline Materials*. Oxford, Oxford University Press (UK).

MU, J. & ZAREMBA, G. 1987. Effect of carbon and silica on the reduction of calcium sulfate. *Thermochimica Acta,* 114, 389-392.

NAKAHARA, S. 1961. Observations of thermal changes in delay powders. *Journal of the Industrial Explosives Society, Japan,* 22, 259.

NAKAHARA, S. & HIKITA, T. 1960. Studies on delay powders, 3, the mechanism of delay powder combustion. *Journal of the Industrial Explosives Society, Japan,* 21, 9.

NEWMAN, E. 1941. Behavior of calcium sulfate at high temperatures. *Journal of Research of the National Bureau of Standards (USA),* 27, 191-196.

OH, S.-T., SEKINO, T. & NIIHARA, K. 1998. Effect of particle size distribution and mixing homogeneity on microstructure and strength of alumina/copper composites. *Nanostructured Materials,* 10, 327-332.

OSORIO, J. G. & MUZZIO, F. J. 2015. Evaluation of resonant acoustic mixing performance. *Powder Technology*, 278, 46-56.

PANTOYA, M. L. & GRANIER, J. J. 2005. Combustion behavior of highly energetic thermites: Nano versus micron composites. *Propellants, Explosives, Pyrotechnics,* 30, 53-62.

PEACOCK, D. G., RICHARDSON, J. F. & Coulson, J. M. (Eds). 2012. *Chemical Engineering.* Volume 3: *Chemical and Biochemical Reactors & Process Control*, Elsevier Science & Technology.

PICKARD, J. M. 2002. Critical ignition temperature. *Thermochimica Acta,* 392, 37-40.

PIERCEY, D. G. & KLAPOETKE, T. M. 2010. Nanoscale aluminum-metal oxide (thermite) reactions for application in energetic materials. *Central European Journal of Energetic Materials,* 7, 115-129.

PORET, J. C., SHAW, A. P., CSERNICA, C. M., OYLER, K. D., VANATTA, J. A. & CHEN, G. 2013. Versatile boron carbide-based energetic time delay compositions. *ACS Sustainable Chemistry & Engineering,* 1, 1333-1338.

RAI, M. & MOUNTJOY, G. 2014. Molecular dynamics modelling of the structure of barium silicate glasses BaO–SiO$_2$. *Journal of Non-Crystalline Solids,* 401, 159-163.

REN, G., ZHANG, T., WANG, X., MA, H., GUO, X., LIU, J. & ZOU, G. 2002. The reactions of CuO at high pressure and high temperature. *Journal of Physics: Condensed Matter,* 14, 11177.

RICCO, I., FOCKE, W. & CONRADIE, C. 2004. Alternative oxidants for silicon fuel in time-delay compositions. *Combustion Science and Technology,* 176, 1565-1575.

RIPLEY, W. L. & LIPSCOMB, C. A. 1968. *A preliminary investigation of the reactivity of lead dioxide*. UK Defence Technical Information Centre document.

RUGUNANAN, R. A. 1992. Intersolid pyrotechnic reactions of silicon. *PhD Thesis*, Grahamstown, Rhodes University, South Africa.

RUGUNANAN, R. A. & BROWN, M. E. 1993a. Combustion of binary and ternary silicon/oxidant pyrotechnic systems. Part I: Binary systems with Fe$_2$O$_3$ and SnO$_2$ as oxidants. *Combustion Science and Technology,* 95, 61-83.

RUGUNANAN, R. A. & BROWN, M. E. 1993b. Combustion of binary and ternary silicon/oxidant pyrotechnic systems. Part II: Binary systems with Sb$_2$O$_3$ and KNO$_3$ as oxidants. *Combustion Science and Technology,* 95, 85-99.

RUGUNANAN, R. A. & BROWN, M. E. 1994. Combustion of binary and ternary silicon oxidant pyrotechnic systems. Part 3: Ternary-Systems. *Combustion Science and Technology,* 95, 101-115.

SEUFERT, S., HESSE, C., GOETZ-NEUNHOEFFER, F. & NEUBAUER, J. 2009. Quantitative determination of anhydrite III from dehydrated gypsum by XRD. *Cement and Concrete Research*, 39, 936-941.

SHIDLOVSKIY, A. 1997. *Principles of Pyrotechnics*. Dingmans Ferry, PA, USA, American Fireworks News.

SHIMIZU, A., SAITOU, J. & HAO, Y.-J. 1990. Effect of contact points between particles on the reaction rate in the $Fe_2O_3 \cdot V_2O_5$ system. *Solid State Ionics,* 38, 261-269.

SMIT, K. J., DE YONG, L. V. & GRAY, R. 1995. Time resolved FTIR spectroscopy of silicon based pyrotechnics. *21st International Pyrotechnics Seminar*, 11–15 September, Moscow, Russia.

SPECTOR, M., SURIANI, E. & STUKENBROEKER, G. 1968. Thermite process for fixation of high-level radioactive wastes. *Industrial & Engineering Chemistry Process Design and Development,* 7, 117-122.

SPICE, J. & STAVELEY, L. 1949. The propagation of exothermic reactions in solid systems. Part II: Heats of reaction and rates of burning. *Journal of the Society of Chemical Industry,* 68, 348-355.

STEINHAUSER, G. & KLAPÖTKE, T. M. 2008. "Green" pyrotechnics: A chemists' challenge. *Angewandte Chemie, International Edition,* 47, 3330-3347.

STERN, K. & WEISE, E. 1966. *High temperature properties and decomposition of inorganic salts. Part 1. Sulfates.* UK Defence Technical Information Centre document.

SUBRAHMANYAM, J. & VIJAYAKUMAR, M. 1992. Self-propagating high-temperature synthesis. *Journal of Materials Science,* 27, 6249-6273.

SWANEPOEL, D., DEL FABBRO, O., FOCKE, W. W. & CONRADIE, C. 2010. Manganese as fuel in slow-burning pyrotechnic time delay compositions. *Propellants, Explosives, Pyrotechnics,* 35, 105-113.

TASHIRO, C., YAMADA, H., AKIBA, T. & NAWATA, S. 1976. Study on the hydration of $2BaO \cdot SiO_2$. *Cement and Concrete Research,* 6, 633-640.

TICHAPONDWA, S. M., FOCKE, W. W., DEL FABBRO, O. & MULLER, E. 2013. Suppressing hydrogen evolution by aqueous silicon powder dispersions by controlled silicon surface oxidation. *Propellants, Explosives, Pyrotechnics,* 38, 48-55.

TICHAPONDWA, S. M., FOCKE, W. W., DEL FABBRO, O. & KELLY, C. 2015. Calcium sulfate as a possible oxidant in "green" silicon-based pyrotechnic time delay compositions. *Propellants, Explosives, Pyrotechnics*, 40, 518-525.

TRIBELHORN, M. J. 1995. Reactions of iron-and zinc-fuelled pyrotechnic systems. *PhD Thesis*, Grahamstown, Rhodes University, South Africa.

TRUNOV, M. A., SCHOENITZ, M. & DREIZIN, E. L. 2005. Ignition of aluminum powders under different experimental conditions. *Propellants, Explosives, Pyrotechnics,* 30, 36-43.

TUUKKANEN, I. M., CHARSLEY, E. L., LAYE, P. G., ROONEY, J. J., GRIFFITHS, T. T. & LEMMETYINEN, H. 2006. Pyrotechnic and thermal studies on the magnesium-strontium nitrate pyrotechnic system. *Propellants, Explosives, Pyrotechnics,* 31, 110-115.

TYURNINA, Z., LOPATIN, S., SHUGUROV, S. & STOLYAROVA, V. 2006. Thermodynamic properties of silicate glasses and melts. I. System $BaO-SiO_2$. *Russian Journal of General Chemistry,* 76, 1522-1530.

UMBRAJKAR, S. M., SCHOENITZ, M. & DREIZIN, E. L. 2006. Control of structural refinement and composition in $Al-MoO_3$ nanocomposites prepared by arrested reactive milling. *Propellants, Explosives, Pyrotechnics*, 31, 382-389.

UNITED NATIONS 2007. *UN Recommendations on the transportation of dangerous goods. Model regulations,* 15th ed. United Nations, New York, Geneva.

VALLIAPPAN, S. & PUSZYNSKI, J. A. 2003. Combustion characteristics of metal-based nanoenergetic systems. *Proceedings of the South Dakota Academy of Science*, 82, 97-101.

VAN DER MERWE, E., STRYDOM, C. & POTGIETER, J. 1999. Thermogravimetric analysis of the reaction between carbon and $CaSO_4 \cdot 2H_2O$, gypsum and phosphogypsum in an inert atmosphere. *Thermochimica Acta,* 340, 431-437.

WARD, C. R. & FRENCH, D. 2006. Determination of glass content and estimation of glass composition in fly ash using quantitative X-ray diffractometry. *Fuel,* 85, 2268-2277.

WEBB, R. 2004. Using thermodynamic codes to simulate pyrotechnic reactions. *1st Workshop on Pyrotechnic Combustion Mechanisms,* 10 July 2004, Fort Collins, CO, USA.

WHO (World Health Organization) 2004. *Barium in drinking-water: Background document for development of WHO Guidelines for Drinking-water Quality.* WHO/SDE/WSH/03.04/76.

WILHARM, C. K., CHIN, A. & PLISKIN, S. K. 2013. Thermochemical calculations for potassium ferrate (VI), K_2FeO_4, as a green oxidiser in pyrotechnic formulations. *Propellants, Explosives, Pyrotechnics*, 39(2), 173-179.

YANAGISAWA, F. & SAKAI, H. 1983. Thermal decomposition of barium sulfate-vanadium pentoxide-silica glass mixtures for preparation of sulphur dioxide in sulphur isotope ratio measurements. *Analytical Chemistry,* 55, 985-987.

YANG, L., GUAN, B., WU, Z. & MA, X. 2009. Solubility and phase transitions of calcium sulfate in KCl solutions between 85 and 100 °C. *Industrial & Engineering Chemistry Research,* 48, 7773-7779.

YEN, N. H. & WANG, L. Y. 2012. Reactive metals in explosives. *Propellants, Explosives, Pyrotechnics,* 37, 143-155.

YETTER, R. A., RISHA, G. A. & SON, S. F. 2009. Metal particle combustion and nanotechnology. *Proceedings of the Combustion Institute,* 32, 1819-1838.

YOGANARASIMHAN, S. & JOSYULU, O. 2014. Reactivity of the ternary pyrotechnic system red lead-silicon-ferric oxide. *Defence Science Journal,* 37, 73-83.

ZHENG, D., LU, H., SUN, X., LIU, X., HAN, W. & WANG, L. 2013. Reaction mechanism of reductive decomposition of FGD gypsum with anthracite. *Thermochimica Acta,* 559, 23-31.

PUBLICATIONS

Journal Articles

Tichapondwa, S.M., Focke, W.W., Gisby, J., Del Fabbro. O. and Kelly, C. (2015). A comparative study of Si-BaSO$_4$ and Si-CaSO$_4$ pyrotechnic time delay compositions. *Journal of Energetic Materials* (Accepted).

Tichapondwa, S.M., Focke, W.W., Del Fabbro, O. and Kelly, C. (2015). Calcium sulfate as a possible oxidant in "green" silicon-based pyrotechnic time delay compositions. *Propellants Explosives and Pyrotechnics*, 40, 518-525.

Tichapondwa, S.M., Focke, W.W. and Del Fabbro, O. The effect of additives on the burning rate of the silicon-calcium sulfate pyrotechnic delay compositions. Target journal: *Propellants, Explosives, Pyrotechnics* (Manuscript in preparation).

Conference Papers Presented

Tichapondwa, S.M., Focke, W.W., Del Fabbro, O. and Kelly, C. Calcium sulfate as a possible oxidant in "green" silicon-based pyrotechnic time delay compositions. *40th International Pyrotechnics Seminar*, 13–18 July 2014, Colorado Springs, USA.

APPENDICES

Appendix A: XRD Spectra
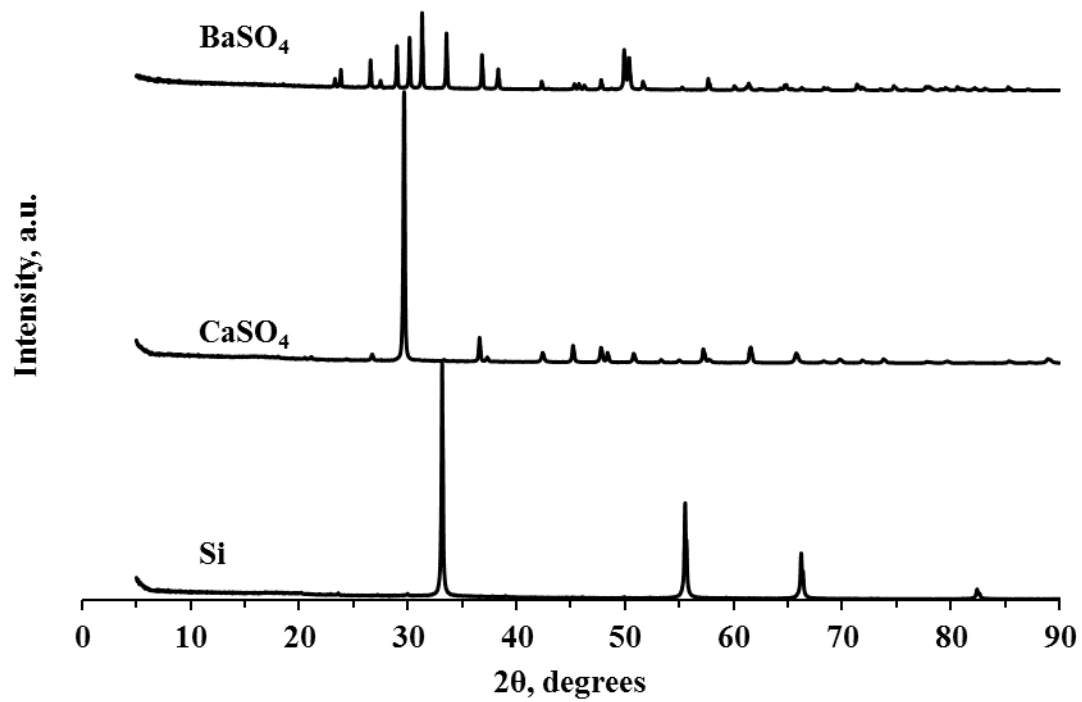
Figure A-1   XRD spectra of the main reactant materials used
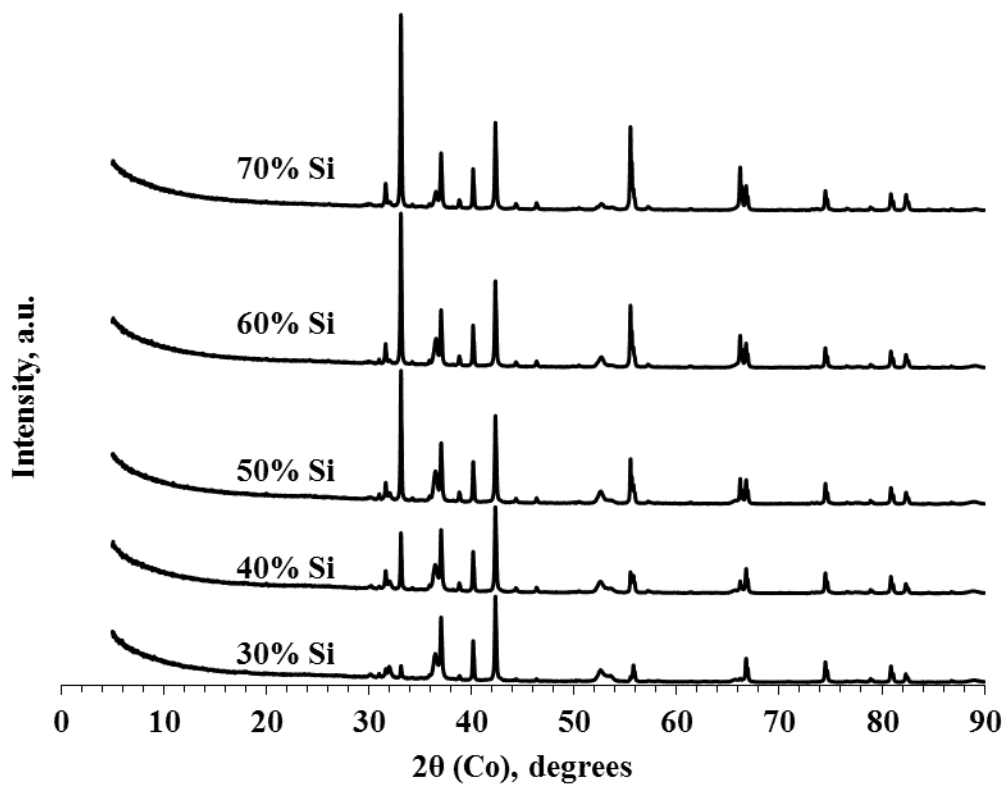
Figure A-2   XRD spectra of the reaction products formed when various stoichiometries of the Si-CaSO$_4$ composition were combusted in a helium atmosphere in a bomb calorimeter

113
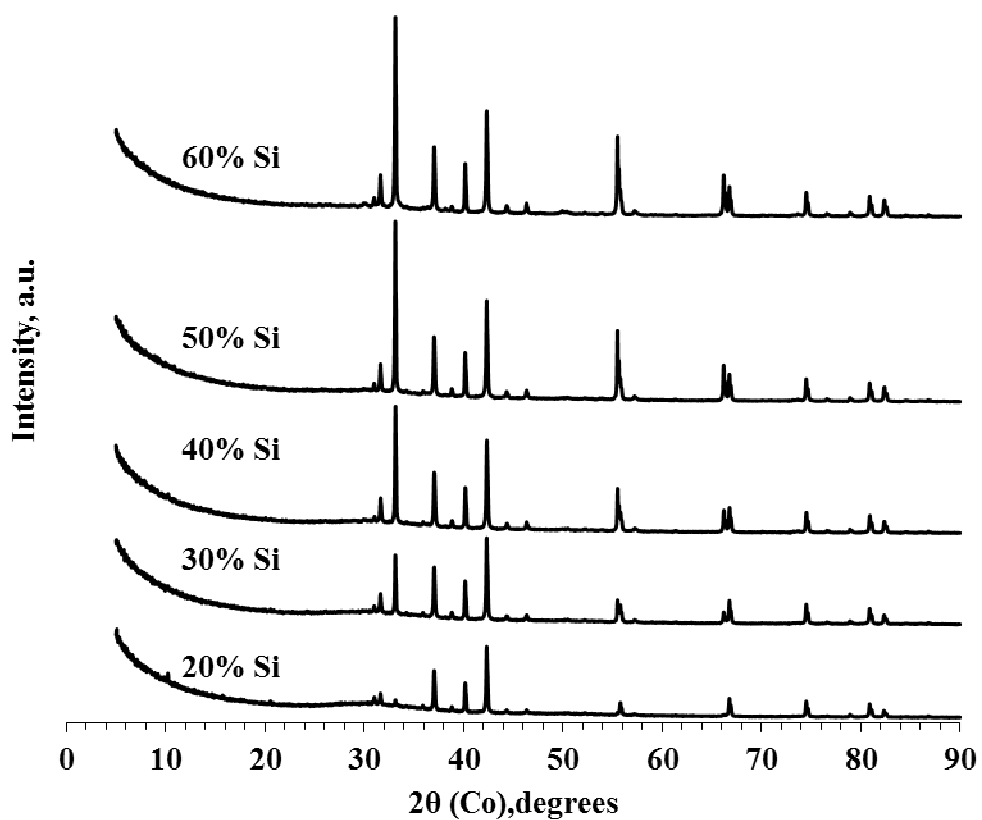
Figure A-3 XRD spectra of the reaction products formed when various stoichiometries of the Si-BaSO$_4$ composition were combusted in a helium atmosphere in a bomb calorimeter

114

Appendix B: XRF Analysis

Table B-1   XRF analysis of the main reactant material used

Sample	Type 4 Si	$BaSO_4$	$CaSO_4$	Calibration standard 12/76	
				Certified	**Result**
SiO_2	99.01	0.41	0.31	**45.42**	45.52
TiO_2	0.0089	<0.01	<0.01	**1.54**	1.55
Al_2O_3	0.248	0.34	0.23	**16.62**	17.08
$Fe_2O_{3\,(t)}$	0.394	0.01	0.02	**9.73**	10.01
MnO	0.043	0.008	0.001	**0.180**	0.176
MgO	0.113	0.01	0.12	**8.15**	7.78
CaO	0.091	0.05	38.24	**10.93**	10.57
Na_2O	<0.01	1.10	0.37	**3.65**	3.69
K_2O	<0.01	0.10	0.02	**0.70**	0.70
P_2O_5	<0.01	0.004	0.005	**0.259**	0.260
CoO	<0.001	<0.001	<0.001		0.005
Cr_2O_3	0.045	<0.001	0.010	**0.074**	0.073
CuO	<0.001	0.007	<0.001		0.002
NiO	<0.01	<0.001	0.002		0.012
PbO	<0.001	<0.001	0.001		<0.001
SO_3	0.0132	34.70	60.25		<0.001
V_2O_5	<0.01	0.003	<0.001		0.055
BaO	0.036	64.14	0.068		0.063
ZnO	<0.001	<0.001	<0.001		<0.001
ZrO_2	<0.01	0.169	0.026		0.018
SrO	0.002	0.438	0.136		0.043

Appendix C: Mass Balance Calculations

Example of mass balance calculations for a 40% Si + CaSO₄ composition
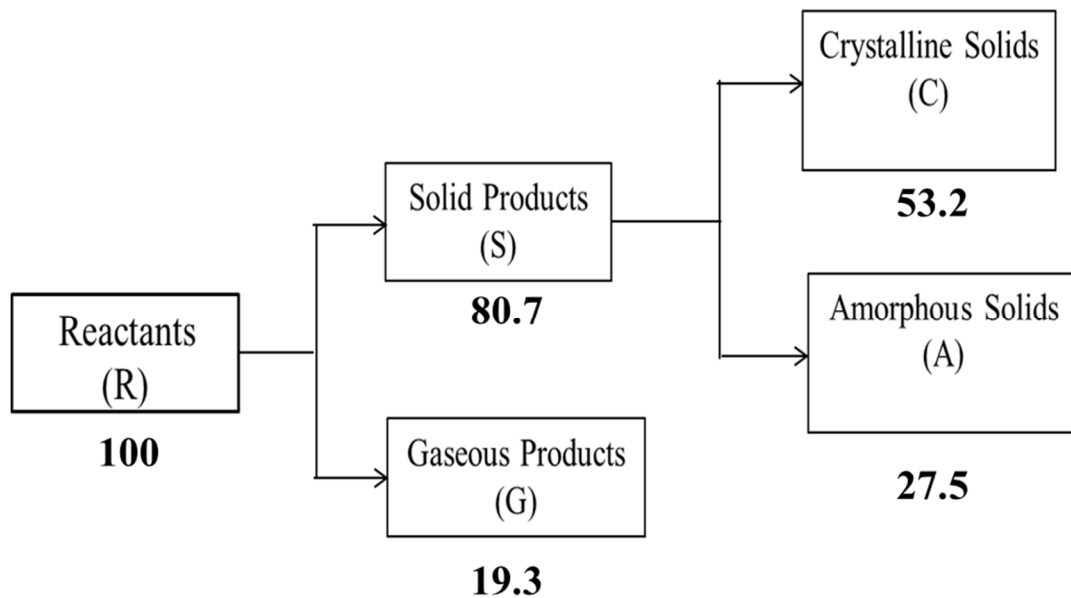
Figure C-1. Block diagram used as guide for the mass balance calculations

Basis: 100 g of total reactants

Overall mass balance

$$R = S+G = 100 \qquad (1)$$

$$S = C+A \qquad (2)$$

Component balance for sulfur

$$100\, w_i = Sw_f + Gw_g \qquad (3)$$

Where:

w_i = weight fraction of sulfur in the reactants

w_f = weight fraction of sulfur in the solid products

w_g = weight fraction of sulfur in the gaseous products

Using a basis of 100 g of reactants for a 40% Si-CaSO$_4$ composition, then

Mass of Si = 40 g

Mass of CaSO$_4$ = 60 g

Sulfur Balance

Determining the weight fraction of sulfur in the reactants

Molar mass S = 32.065 gmol^{-1}

Molar mass CaSO$_4$ = 136.08 gmol^{-1}

Sulfur in CaSO$_4$ = (32.065 / 136.08)*100 = 23.56%

Therefore mass of sulfur in 60 g CaSO$_4$ = 0.2356 x 60g = 14.1g

Weight fraction of sulfur in the reactants (w_i) = 0.141

Weight fraction of sulfur in gaseous products

Assuming that SO$_2$ will be the only gas formed, the mass fraction of sulfur in the gaseous products (w_g) equals molar mass S / molar mass SO$_2$ = 32.065 / 64.065 = 0.5

Weight fraction of sulfur in the solid reaction products (w_f)

This parameter was experimentally determined using sulfur analysis of the solid reaction products. Table 4-4 shows the results obtained. In the case of the 40% Si-CaSO$_4$ composition w_f is 0.055.

Determining the fraction of sulfur in the crystalline products

This calculation makes use of the XRD results presented in Table 4-4.

The sulfur containing compounds include:

117

CaS = 14.4%

Bi$_2$S$_3$ = 1.9%

Amorphous = 34.1%

Based on their molar masses, the amount of sulfur in CaS and Bi$_2$S$_3$ is 44.4 and 18.7%, respectively.

Basis: 100 g solid reaction products,

The mass of sulfur due to CaS = 14.37 g x 0.444 = 6.38 g

The mass of sulfur due to Bi$_2$S$_3$ = 1.9 g x 0.187 = 0.355 g

The total amount of crystalline solids = Total solid products – amorphous solids products

$$= 100g - 34.1g = 65.9 \text{ g}$$

Therefore the fraction of sulfur in the crystalline phase = (6.38 + 0.355)/65.9 = 0.1022

Determining the actual total amount of solid and gaseous products produced by the reaction

The actual amount of solid and gaseous products produced by reacting 100 g of reactants can be determined by combining equations (3) and (4)

100 w_i = Sw_f + Gw_g

But G = 100-S

The combination these equations yields,

100 w_i = Sw_f + (100-S)w_g

S= 100(w_i - w_g)/(w_f - w_g)

Substituting the mass fractions

S= 100*(0.141 – 0.5)/(0.055- 0.5) = 80.67 g

Therefore mass of solid products = 80.67g

Mass of gas produced = 100 g – 80.67 g = 19.33 g

Mass of amorphous phase (Based on XRD results) = 0.341 x 80.67 g = 27.51 g

Since S = C + A

The mass of the crystalline phase is 80.67 g – 27.51 g = 53.16 g

Having established the various masses, it is then possible to determine the amount of sulfur in these components.

Mass of sulfur in the reactants   = 100 g x 0.1411 = 14.11 g

Mass of sulfur in the solid products   = 80.67 g x 0.055 = 4.44 g

Mass of sulfur in the gaseous product = 19.33 g x 0.5 = 9.665 g

Mass of sulfur in the crystalline solid = 53.16 g x 0.1022 = 5.43 g

Mass of sulfur in the amorphous solid = Mass of S in the solid products - Mass of S in the crystalline solid

Mass of sulfur in the amorphous solid = 4.44 g - 5.43 g = -0.99 g

Note that although a negative number was obtained from the mass balance, the result indicates an absence of sulfur in the amorphous phase with all the sulfur being accounted for in the CaS. The discrepancy can be attributed to the combined effects of experimental errors in the XRD and sulfur analyses.

Gas evolved calculations

The total mass of gas evolved was 19.33 g. It was assumed that the only gas produced during the reaction was SO_2.

Therefore:

Moles of SO_2 = 19.33 g / 64.065 gmol^{-1} = 0.3 moles

At standard room temperature and pressure 1 mole of gas = 22400 cm^3

The volume of SO_2 released per gram of reactant = (0.3 moles x 22400 cm^3 mol^{-1}) / 100g

$$= 67.6 \text{ cm}^3 \text{ g}^{-1}$$

Calcium Balance

Determining the weight fraction of calcium in the reactants

Molar mass Ca = 40.078 gmol^{-1}

Molar mass $CaSO_4$ = 136.08 gmol^{-1}

Calcium in $CaSO_4$ = (40.078 / 136.08)*100 = 29.45%

Therefore mass of calcium in 60 g $CaSO_4$ = 0.2945 x 60g = 17.67 g

Weight fraction of calcium in the reactants (w_i) = 17.67 g / 100 g = 0.1767

Determining the fraction of calcium in the crystalline products

This calculation makes use of the XRD results presented in Table 4-4.

The calcium containing compounds include:

CaS = 14.4%

$Ca_3(SiO_3)_3$ = 25.47%

Amorphous = 34.1%

Based on the molar masses, the weight % of calcium in CaS and $Ca_3(SiO_3)_3$ is 55.6 and 34.5%, respectively.

Basis: 100 g of solid reaction products,

The mass of calcium due to CaS = 14.37 g x 0.556 = 7.99 g

The mass of calcium due to $Ca_3(SiO_3)_3$ = 25.4 g x 0.345 = 8.79 g

Therefore the fraction of calcium in the crystalline phase = (7.99 + 8.79)/65.9 = 0.254

The mass of calcium in the reactants and product phases can then be calculated as shown below.

Mass of calcium in reactants = 100 g x 0.1767 = 17.67 g

Mass of calcium in crystalline solids = 53.16 g x 0.254 = 13.55 g

Mass of calcium in the amorphous solid = 17.67 g – 13.55 g = 4.12 g

Silicon Balance

Determining the weight fraction of silicon in the reactants

Since 40 wt.% of silicon was used, the fraction of initial Si was 0.4

Determining the fraction of silicon in the crystalline products

This calculation makes use of the XRD results presented in Table 4-4.

The silicon containing compounds include:

$Ca_3(SiO_3)_3$ = 25.4%

SiO_2 = 4.02%

Amorphous = 34.1%

Unreacted Si = 17.72%

Based on their molar masses, the weight % of silicon in $Ca_3(SiO_3)_3$ and SiO_2 is 24.2 and 46.7%, respectively.

Basis: 100 g of solid reaction products,

The mass of silicon due to $Ca_3(SiO_3)_3$ = 25.4 g x 0.2418 = 6.16 g

The mass of silicon due to SiO_2 = 4.02 g x 0.4674 = 1.88 g

Unreacted silicon accounts for 17.72 g

Therefore the fraction of silicon in the crystalline phase   = (6.16 + 1.88 + 17.72)/65.9

$$= 0.391$$

The mass of silicon in the reactants and product phases can then be calculated as shown below.

Mass of silicon in reactants = 100 g x 0.4= 40 g

Mass of silicon in crystalline solids = 53.16 g x 0.391 = 20.8 g

Mass of silicon in the amorphous solid = 40 g – 20.8 g = 19.2 g

Oxygen Balance

Determining the mass of oxygen in the reactants

Molar mass Ca = 15.99 gmol^{-1}

Molar mass $CaSO_4$ = 136.08 gmol^{-1}

Oxygen in $CaSO_4$ = ((15.99 x 4) / 136.08)*100 = 47%

Therefore mass of oxygen in 60 g $CaSO_4$ = 0.47 x 60 g = 28.21 g

Determining the mass of oxygen in the gaseous products

Assuming that SO_2 is the only gas formed, the weight fraction of oxygen in SO_2 is 0.5. It has already been shown that the mass of gas formed for this composition is 19.33 g for every 100 g of composition reacted.

Therefore the mass of oxygen in the gas phase = 19.33 g x 0.5 = 9.665 g

Determining the fraction of oxygen in the crystalline products

This calculation makes use of the XRD results presented in Table 4-4.

The oxygen containing compounds include:

$Ca_3(SiO_3)_3 = 25.47\%$

$SiO_2 = 4.02\%$

Amorphous = 34.1%

Based on their molar masses, the weight % of oxygen in $Ca_3(SiO_3)_3$ and SiO_2 is 41.3% and 53.3%, respectively.

Basis: 100g of solid reaction products,

The mass of oxygen due to $Ca_3(SiO_3)_3$ = 25.4 g x 0.413 = 10.49 g

The mass of oxygen due to SiO_2 = 4.02 g x 0.533 = 2.14 g

Therefore the fraction of oxygen in the crystalline phase   = (10.49 g + 2.14 g) / 65.9 g

= 0.192

The mass of oxygen in the solid product phases can then be calculated as shown below:

Mass of oxygen in the solid products = mass of oxygen in the reactants - mass of oxygen in the gas phase

= 28.21 g - 9.665 g

= 18.545 g

Mass of oxygen in crystalline solids = 53.16 g x 0.192 = 10.21 g

Mass of oxygen in the amorphous solid = 18.545 g – 10.21 g = 8.34 g

Summary

Conversion of the mass of the different elements to moles yields the results shown in Table C-1. Also indicated in the table are the Si to Ca ratios of the reactants and various product phases.

Table C-1. Summary of the elemental mass balance in moles for the reaction of a 40% Si-$CaSO_4$ composition

	Reactants	Gas products	Solid products	Crystalline products	Amorphous products
Si	1.42		1.42	0.74	0.68
Ca	0.44	-	0.44	0.34	0.10
S	0.44	0.30	0.14	0.17	-0.03
O	1.76	0.60	1.16	0.64	0.52
Si/Ca mole ratio	3.23	-	3.23	2.47	6.8

Appendix D: Sensitivity Tests

The friction tests for the 30 wt.% Si compositions of both calcium sulfate and barium sulfate were conducted using standard BAM weights. No ignition was recorded at the maximum loading which used weight number B9 at notch number 6 and is equivalent to 360N (Table D-1).

Table D-1   Standard friction load BAM weights conversion table

Friction Load - Standard BAM weights (N)						
Weight No.	Notch No.					
	1	2	3	4	5	6
B1	5	6	7	8	9	10
B2	10	12	14	16	18	20
B3	20	24	28	32	36	40
B4	30	36	42	48	54	60
B5	40	48	56	64	72	80
B6	60	72	84	96	108	120
B7	80	96	112	128	144	160
B8	120	144	168	192	216	240
B9	180	216	252	288	324	360

Table D-2   Impact test measurements for the 30% Si-BaSO$_4$

No.	Height (cm)	1	2	3	4	5	6	7	8	9	10	11	12	13	14	15	16	17	18	19	20	21	22	23	24	25	26	27	28	29	30
8																															
7																															
6																															
5																															
4																															
3																															
2																															
1	100.0	M	M	M	M	M	M	M	M	M	M	M	M	M	M	M	M	M	M	M	M	M	M	M	M	M	M	M	M	M	M

* M represents a misfire.

Table D-3   Impact test measurements for the 30% Si-CaSO$_4$

No.	Height (cm)	1	2	3	4	5	6	7	8	9	10	11	12	13	14	15	16	17	18	19	20	21	22	23	24	25	26	27	28	29	30
8																															
7																															
6																															
5																															
4																															
3																															
2																															
1	100.0	M	M	M	M	M	M	M	M	M	M	M	M	M	M	M	M	M	M	M	M	M	M	M	M	M	M	M	M	M	M

* M represents a misfire.

126

Table D-4   Conversion table used to interpret the impact sensitivity data

Log Scale step	Log Value	Height (cm)	Impact Energy (J) Weight Mass (kg)				
			0.50	1.0	2.0	5.0	10.0
0	1.00	10.0	0.49	0.98	1.96	4.90	9.80
1	1.05	11.2	0.55	1.10	2.20	5.50	11.00
2	1.10	12.6	0.62	1.23	2.47	6.17	12.34
3	1.15	14.1	0.69	1.38	2.77	6.92	13.84
4	1.20	15.8	0.78	1.55	3.11	7.77	15.53
5	1.25	17.8	0.87	1.74	3.49	8.71	17.43
6	1.30	20.0	0.98	1.96	3.91	9.78	19.55
7	1.35	22.4	1.10	2.19	4.39	10.97	21.94
8	1.40	25.1	1.23	2.46	4.92	12.31	24.62
9	1.45	28.2	1.38	2.76	5.52	13.81	27.62
10	1.50	31.6	1.55	3.10	6.20	15.50	30.99
11	1.55	35.5	1.74	3.48	6.95	17.39	34.77
12	1.60	39.8	1.95	3.90	7.80	19.51	39.01
13	1.65	44.7	2.19	4.38	8.75	21.89	43.77
14	1.70	50.1	2.46	4.91	9.82	24.56	49.12
15	1.75	56.2	2.76	5.51	11.02	27.55	55.11
16	1.80	63.1	3.09	6.18	12.37	30.92	61.83
17	1.85	70.8	3.47	6.94	13.88	34.69	69.38
18	1.90	79.4	3.89	7.78	15.57	38.92	77.84
19	1.95	89.1	4.37	8.73	17.47	43.67	87.34
20	2.00	100.0	4.90	9.80	19.60	49.00	98.00

Table D-5   ESD test results for the 30% Si-CaSO₄ composition

AEL Mining Services Ltd

ESD 2008 Testing Protocol /Up & Down Method — Pg. No.: 1

Sample:	30% Si + CaSO4		Operator:		AMB	
Date:	########	Temperature (°C): 22	Humidity (%): 24		Job:	UP
Capacity C (nF):	3.376	Capacity of discharge circuit Ck (pF): 0		**D** Energy step [mJ]		5.94
U_{min} (kV)	7.8	E_{min} (mJ) 102.70	U_{max} (kV) 9.8		E_{max} (mJ)	162.12

Interval i	Energetic level E_i (mJ)	Frequency of events n_i +	Frequency of events n_i −
7	144.29	2	
6	138.35	2	2
5	132.41	3	1
4	126.47	1	2
3	120.53	2	
2	114.58	3	2
1	108.64	3	3
0	102.70		3

$N^{+}=\Sigma n_i$ 16 $N^{-}=\Sigma n_i$ 13

j	Ej [mJ]	Uj [kV]
10	162.12	9.80
9	156.18	9.62
8	150.24	9.43
7	144.29	9.25
6	138.35	9.05
5	132.41	8.86
4	126.47	8.66
3	120.53	8.45
2	114.58	8.24
1	108.64	8.02
0	102.70	7.80

TABLE Up & Down (X - activation, O - no activation)

U_j (kV)	1	2	3	4	5	6	7	8	9	10	11	12	13	14	15	16	17	18	19	20	21	22	23	24	25	26	27	28	29
9.80																													
9.62																													
9.43																													
9.25		x											x																
9.05	o		x						o		x																		
8.86				x		x		o				x																	
8.66					o		o							x															
8.45															x										x				
8.24																x		x				o		x					o
8.02																	x		o		x		o				x	o	
7.80										o																o			
Trial No:	1	2	3	4	5	6	7	8	9	10	11	12	13	14	15	16	17	18	19	20	21	22	23	24	25	26	27	28	29

L	102.7	A=Σnᵢ.i	32	E_{50} (mj)	117.555	S/D	7.74198
N=Σnᵢ	16	B= Σnᵢ . i²	140	S (mj)	46.0028	0.5 < S/D < 2.0	

128

Table D-6   ESD test results for the 30% Si-BaSO₄ composition

AEL Mining Services Ltd

ESD 2008 Testing Protocol /Up & Down Method — Pg. No.: 1

Sample:	30% Si + BaSO4		Operator:		AMB	
Date:	########	Temperature (°C): 20	Humidity (%):	30	Job:	UP
Capacity C (nF):	3.376	Capacity of discharge circuit Ck (pF): 0	D Energy step [mJ]			5.94
U_{min} (kV)	7.8	E_{min} (mJ) 102.70	U_{max} (kV) 9.8	E_{max} (mJ)		162.12

Interval i	Energetic level E_i (mJ)	Frequency of events n_i +	−
7	162.12	3	
6	156.18	1	3
5	150.24	2	1
4	144.29	3	2
3	138.35	3	3
2	132.41	1	4
1	126.47		2
0	120.53		1

j	Ej [mJ]	Uj [kV]
10	162.12	9.80
9	156.18	9.62
8	150.24	9.43
7	144.29	9.25
6	138.35	9.05
5	132.41	8.86
4	126.47	8.66
3	120.53	8.45
2	114.58	8.24
1	108.64	8.02
0	102.70	7.80

$N^+ = \Sigma n_i$ 13 $N^- = \Sigma n_i$ 16

TABLE Up & Down (X - activation, O - no activation)

U_j (kV)	1	2	3	4	5	6	7	8	9	10	11	12	13	14	15	16	17	18	19	20	21	22	23	24	25	26	27	28	29
9.80							x		x		x																		
9.62						o		o		o		x																	
9.43					o								x						x										
9.25				o										x					o		x								x
9.05			o												x	x		o				x					o		
8.86		o															o		o				x		o				
8.66		o																						o					
8.45	o																												
8.24																													
8.02																													
7.80																													

L	120.5	A=Σnᵢ.i	60	E_{50} (mJ)	144.98	S/D	4.4181
N=Σnᵢ	13	B= Σnᵢ . i²	312	S (mJ)	26.2524	0.5 < S/D < 2.0	

129

Appendix E: Determining the Amount of Dissolved Barium

Table E-1 Concentration of dissolved barium detected after contacting the combustion products of the Si-BaSO$_4$ pyrotechnic composition with water for one month. The theoretical concentration assuming that all the barium is dissolved based on a 2 g pyrotechnic mixture is also given. Finally the percentage of dissolved Ba as a ratio to the maximum theoretical possible is also reported.

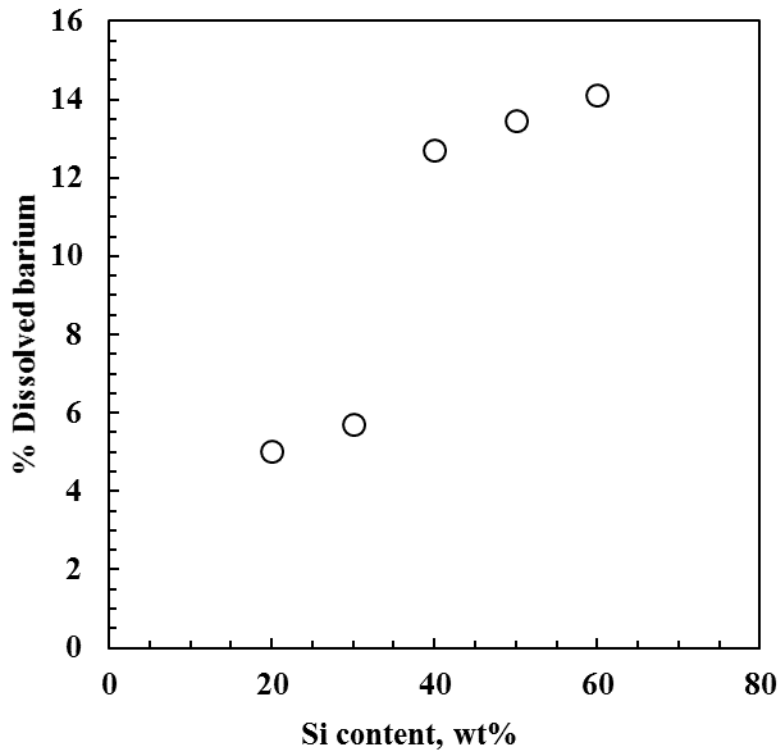| Residue from composition with x% Si	0.5 ml made up to 50 ml	Actual Ba concentration		Theoretical Ba based on 2 g mixture	% dissolved Ba
x	mg L^{-1}	mg L^{-1}	g L^{-1}	g L^{-1}	-
20	47.27	4727	4.73	94.15	5.02
30	47.08	4708	4.71	82.38	5.72
40	89.78	8978	8.98	70.61	12.72
50	79.17	7917	7.92	58.84	13.45
60	66.41	6641	6.64	47.07	14.11

Figure E-1 Percentage of dissolved Ba as a ratio of the theoretical maximum Ba assuming that it all dissolves after contacting the combustion products of the Si-BaSO$_4$ pyrotechnic composition with water for one month

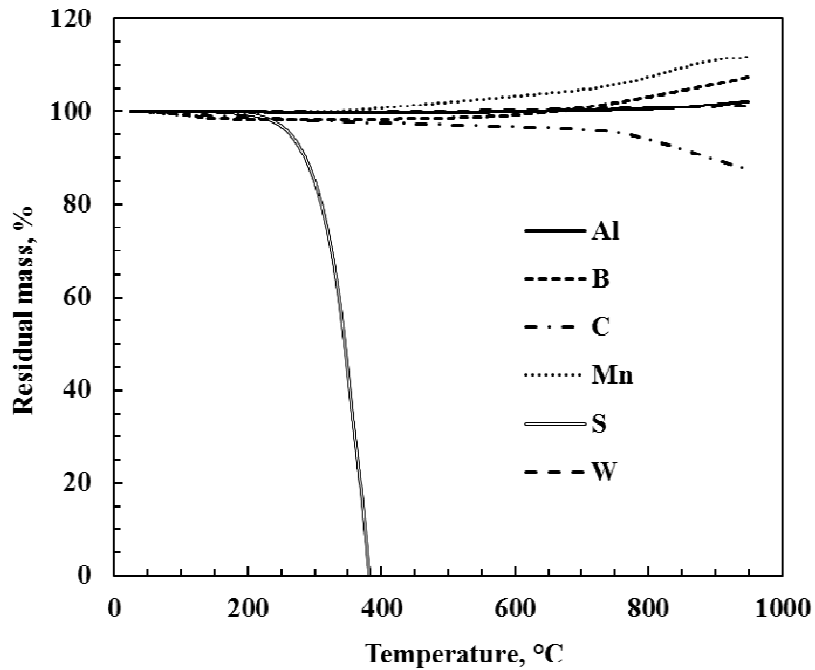**Appendix F: TGA Curves of Various Additives Recorded in Nitrogen Atmosphere**

Figure F-1 TGA results of the fuel additives added to the Si-CaSO$_4$ composition recorded in nitrogen atmosphere
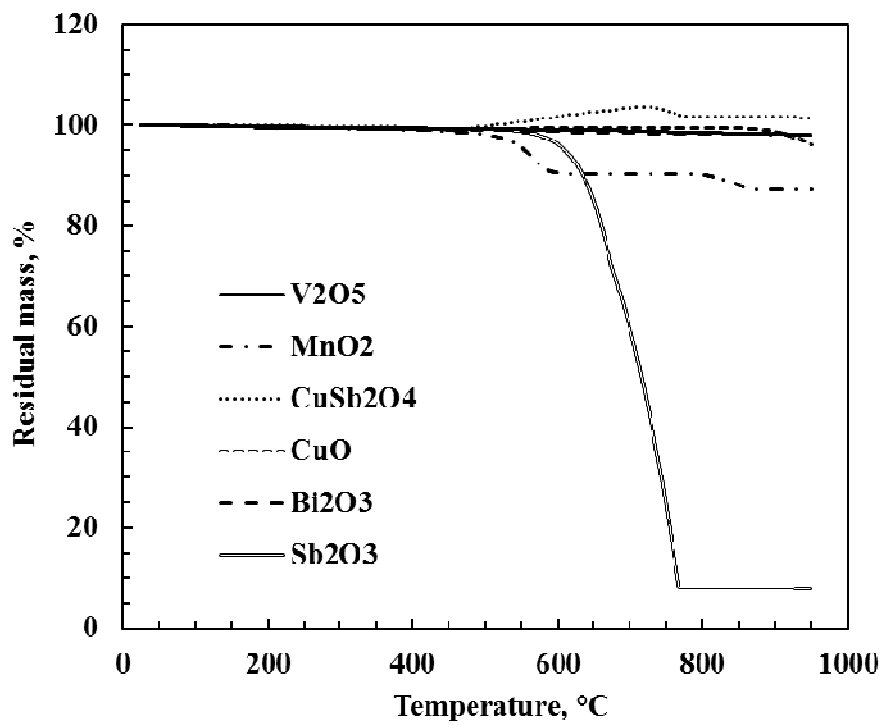

Figure F-2 TGA results of the oxidiser additives added to the Si-CaSO$_4$ composition recorded in a nitrogen atmosphere
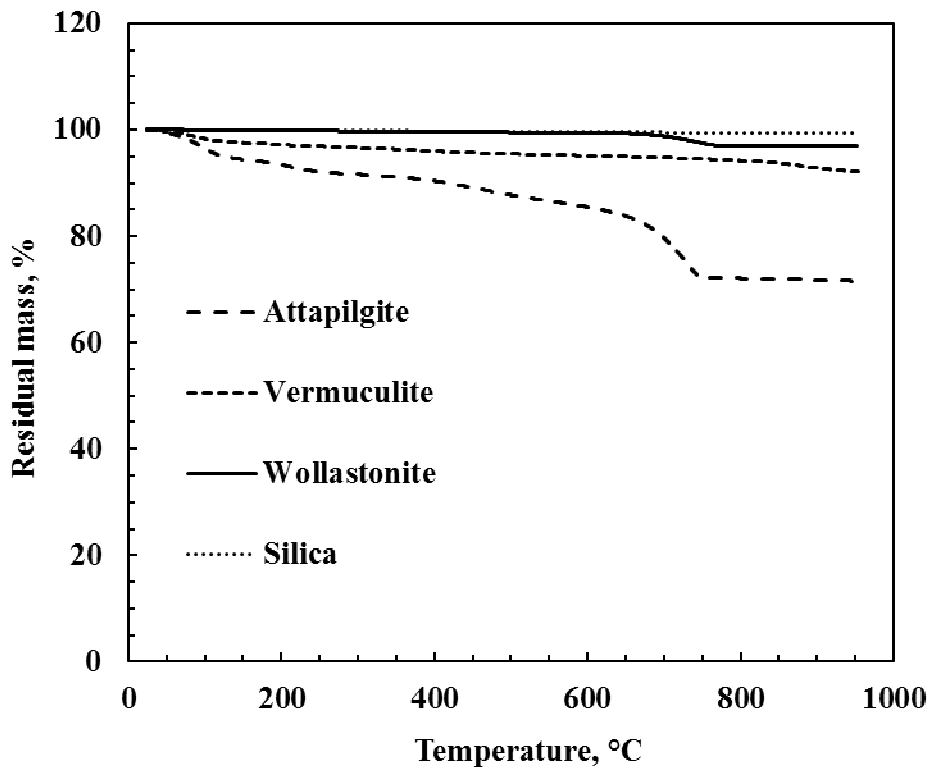
132

Figure F-3   TGA results of the inert additives added to the Si-CaSO$_4$ composition recorded in a nitrogen atmosphere